3D Printed Hydraulic Actuation

Design and Evaluation of a 3D Printed Hydraulic Actuation System, Applied in an Upper Limb Prosthesis

J.J. Tiel Groenestege

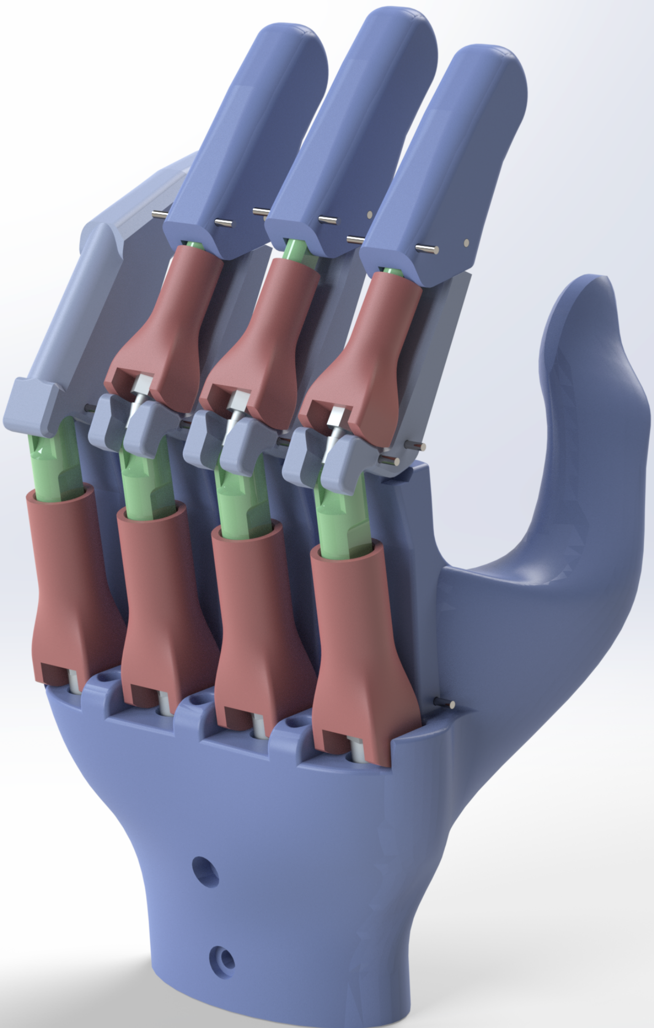

TU Delft

3D Printed Hydraulic Actuation

Design and Evaluation of

a 3D Printed Hydraulic Actuation System, Applied in an Upper Limb Prosthesis

by

J.J. Tiel Groenestege

in partial fulfilment of the requirements for the degree of Master of Science
at the Delft University of Technology,
to be defended on Thursday January 14, 2021 at 10:00 AM.

Course code:	ME51032	
Student number:	4323653	
Thesis committee:	Prof. dr. ir. P. Breedveld,	TU Delft
	Dr. ir. G. Smit,	TU Delft, supervisor
	Dr. C. Della Santina,	TU Delft

This thesis is confidential and cannot be made public until January 14, 2023.

An electronic version of this thesis is available at `http://repository.tudelft.nl/`.

TU Delft

Abstract

Objective The objective of this study was to develop and evaluate a 3D printed hydraulic actuation system, applied in a multi-articulate upper limp prosthesis. The prosthesis was designed to produce sufficient pinch force to be competitive with comparable devices ($\geq 30\,\mathrm{N}$), and weigh less than a human hand ($< 0.43\,\mathrm{kg}$). The actuator should function at a high operating pressure ($> 1.4\,\mathrm{MPa}$) and be compact, such that it fits within the mechanism of the hand.

Method The prosthesis was designed according to a modified V-model design methodology. A prototype was made that embodies the index finger, thumb, and part of the palm. The structural parts were printed using FDM. The actuators were printed in a single step using SLA, requiring only cleaning and curing. To evaluate the performance of the actuators, a set of measurements was carried out, measuring geometrical accuracy, static pressure, and friction in the cylinder. The prototype was tested on pinch force, closing time and weight.

Results Cylinders that are printed at an angle of 90° with respect to the build plate, have a higher roundness that cylinders that are printed at 45°. The actuators were tested at pressures of up to 4.5 MPa, showing no signs of plastic deformation, and have a theoretical maximum pressure of up to 5.9 MPa. While lifting a mass of 6.49 kg, a cylinder friction force of 25.7 N was measured, which is higher than expected. The prototype could reliably deliver a pinch force of 30 N, with a maximum measured value of 41 N. When operating at high pressures, leakage through the piston O-ring seal was not prevented.

Conclusion This study presents the first hydraulic actuation system that is fabricated entirely with 3D printing. A prototype was built to demonstrate that the prosthetic hand that is designed, is able to produce a pinch force of $> 40\,\mathrm{N}$, showing that it can compete with similar devices. Its mass (0.35 kg without pump and battery) is less than that of a human hand. Controlling friction and leakage remains a serious concern due to the geometrical accuracy of 3D printing. Future possibilities are increased customization and reduced fabrication cost of hydraulically actuated mechanical systems.

Preface

Before you lies my Master's Thesis on 3D Printed Hydraulic Actuation, which presents the design and evaluation of an upper limb prosthesis with hydraulic actuation, which is entirely 3D printed. It has been written to fulfil the graduation requirements for the degree of Master of Science in Mechanical Engineering. I was engaged in researching and writing this thesis during the most remarkable year of my time as a student in Delft. In January 2020, I started with the prospect of working from the Faculty of 3mE, surrounded by fellow students. Now, I look back at this crowning piece of my studies, which was largely carried out from home. Nonetheless, it has been a positive experience that I will never forget.

This project was carried out with supervision from within the department of BioMechanical Engineering. It started with the idea of Gerwin Smit to investigate printing elements of a hydraulic actuation system such as used in the Delft Cylinder Hand, which he developed. The entire design of the prosthesis presented in this paper, was carried out be me and was inspired by the Delft Cylinder Hand. Fabricating the prototype was challenging and was carried out at home, the Faculty of 3mE and the Science Cente in Delft.

I would like to thank my supervisor Gerwin Smit for his sharp questions and helpful ideas. I would also like to thank Nabi Kambiz for his help with 3D printing, Jos van Driel for helping me set up the measurements, and Jan van Frankenhuyzen for his helpfulness in the Robotlab. Finally, I am grateful for support from my roommates, family, and friends, and their contribution to my happiness during these strange times.

J.J. Tiel Groenestege
Rotterdam, January 2021

Contents

Nomenclature

ΔL Elongation of the spring [m]

ΔP Pressure difference [MPa]

η_{force} Force efficiency [-]

σ Stress [MPa]

$\sum M$ Sum of the moments around the joint [Nm]

$a_{actuator}$ Moment arm of the actuator around the joint [m]

$A_{cylinder}$ Cross sectional area of the cylinder [m^2]

a_{spring} Moment arm of the spring around the joint [m]

A_{th} Shear area of threaded connection [m^2]

ADL Activity of Daily Living

AM Additive Manufacturing

D_{cross} Cross sectional diameter of the O-ring [m]

d_{obj} Diameter of the pinched object [m]

D_{out} Outer diameter of the O-ring [m]

d_{pitch} Pitch diameter of a thread [m]

DCH Delft Cylinder Hand

DIP Distal interphalangeal

F_0 Initial spring force [N]

$F_{actuator}$ Force exerted by the actuator [N]

F_{axle} Load force on the axle of a joint [N]

$F_{friction}$ Friction force [N]

F_{pinch} Pinch force [N]

F_{spring} Force exerted by the springs [N]

FDM Fused Deposition Modeling

h_{pitch} Pitch hight of a thread [m]

L_e Length of engagement [m]

MCP Metacarpophalangeal

P Pressure in the actuator [MPa]

P_{atm} Atmospheric pressure [MPa]

P_{work} Operating pressure [MPa]

P_{yield} Pressure at yield [MPa]

PGD Piston Groove Diameter [m]

PIP Proximal interphalangeal

PLA Polylactic acid

Q_p Flow rate in the hydraulic circuit of the prototype [m^3/s]

R Transmission ratio [-]

$r_{cylinder}$ Radius of the cylinder bore [m]

r_{sq} Squeeze ratio [-]

ROM Range of motion

s Wall thickness or the cylinder [m]

Sf Safety factor [-]

SLA Stereolithography

$T_{actuator}$ Torque resulting from the actuator force [Nm]

T_{MCP} Torque around the MCP joint [Nm]

T_{pinch} Torque resulting from the pinch force [Nm]

T_{PIP} Torque around the PIP joint [Nm]

t_p Closing time of the prototype [s]

$T_{springs}$ Torque resulting from the spring force [Nm]

V_p Volume of the hydraulic circuit of the prototype [m^3]

1

Introduction

1.1. Developments in hydraulic actuation

Hydraulic actuators are known for their high power density. This high power density is attained by the high pressures that can be generated [74]. For example, hydraulic cylinders in excavators operate at pressures of up to 35 MPa [65]. Hydraulic actuators with low-velocity and high-force are especially suitable for heavy duty equipment used in construction and manufacturing [56, 75]. As they are robust and have a high power capacity, hydraulic actuators are also used in robotics, both in walking devices as well as in end effectors [38]. For example, Ko et al. developed a humanoid robotic hand with five degrees of freedom and an output force of 300 N [41]. The field of hydraulics could be considered to be mature. Actuators that are used in industry have seen minimal changes over the past decades and design parameters have been optimized [46]. However, there are still research challenges to be solved: improving energy efficiency and reliability, and increasing compactness [41]. For example, Yong et al. presented a hydraulic cylinder that aims to improve energy efficiency, by means of adjustable effective piston area [76]. Recently, there have been efforts to develop hydraulic actuators made from alternative materials, i.e. composites and plastics. Solazzi successfully reduced the weight of an actuator for an excavator, by using composite material [65]. Stryczek et al. developed a hydraulic actuator largely made from plastic and have demonstrated how using plastics yields multiple advantages, including a reduced weight, possibility of complex shaped components, and a shorter and less expensive production process [67]. Xia and Durfee investigated the scalability of hydraulic systems and emphasized the recent interest in portable, wearable devices, including powered orthotics [74]. They concluded that at an output of $\leq$ 100 W, hydraulic systems are lighter than electromechanical alternatives, as long as they operate at high pressures, preferably $\geq$ 3.5 MPa. There is a need for small hydraulic components that operate at high pressures (> 1.4 MPa), as argued by Xia and Durfee [74]. However, currently, tiny off-the-shelf hydraulic components do not exist [19].

1.2. Hydraulics in prosthetic hands

Hydraulics have also been implemented in prostheses and orthotics [47, 55]. Similar technical challenges exist in the actuation of powered prosthetics and orthotics: the actuation system should be lightweight and compact, yet have a sufficient power output [19]. Hydraulic actuation can offer a suitable solution as its key advantages are a high force-to-weight and force-to-volume ratio [19]. Moreover, efficient energy transmission can potentially be achieved using hydraulics. There have been various attempts to use hydraulics as a means of actuation or transmission in an upper limp prosthesis, several before 1980 [11, 63]. In more recent years, Kargov et al. have developed a hydraulically actuated hand prosthesis that allows for multiple grip patterns [39]. The fingers of the hand are actuated using hydraulic bellow actuators, operating at a pressure of 0.6 MPa. The design shows that it is possible to integrate a pump and reservoir into the limited space of a hand prosthesis. Smit was the first to successfully implemented hydraulic actuation in a hand prosthesis that meets basic user requirements [64]. The result is the Delft Cylinder Hand (DCH), a lightweight device with efficient energy transmission (Figure 1.1). The multi-articulate hand is underactuated, such that the fingers can adapt to the shape of the object. A disadvantage is that the system is complex and has a lot of parts, which makes fabrication time consuming and expensive.

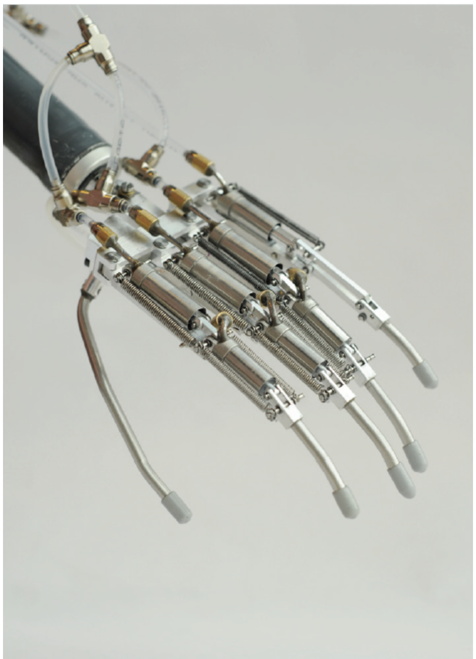

Figure 1.1: The Delft Cylinder Hand, a body powered upper limp prosthesis using hydraulic actuation [64].

1.3. The combination with additive manufacturing

When making a hydraulic actuator from an alternative material, additive manufacturing (AM) could be considered. Additive manufacturing, the technique of layer-by-layer production of parts by selectively depositing or solidifying small volumes of material, has been used for pneumatic piston-cylinder actuators. For example, Krause presented a linear pneumatic actuator with integrated sensors for force and position control and has demonstrated that it is less expensive than off-the-shelf alternatives [44]. Boland et al. developed a smaller system: a pneumatic stepper motor using four pistons that is suitable to operate in an MRI environment [8]. However, there does not exist any 3D printed, hydraulic piston-cylinder system in current literature. The concept of 3D printing actuators is relatively new, despite its potential benefits for hydraulic actuators [44]. Additive manufacturing would enable customization and allow for complex design geometries, without losing the advantage of a high force-to-weight ratio. Moreover, it could potentially reduce the cost of fabrication by reducing the number of parts and eliminating assembly. The use of plastics could result in reduced weight and size [68].

1.4. Problem definition

There has been a recent interest in the development of wearable devices including exoskeletons, orthotics and prostheses [74]. Hydraulic actuators are especially suited for such devices as they fit the requirements of being lightweight and compact, and having a high power output [19]. However, off-the-shelf, small hydraulic systems do not exist [19]. Additive manufacturing could provide a solution. 3D printing of hydraulic actuators offers multiple possible benefits, including customization, increased design freedom and possibly a reduction of fabrication cost. However, there does not exist any 3D printed, hydraulic piston-cylinder system in current literature. The feasibility and performance of a hydraulic actuator that is fully 3D printed, are unknown. Challenges in the production of such a system include achieving the required level of geometrical accuracy to prevent leakage. Moreover, the surface quality of the cylinder should be sufficient such that friction does not become predominant. The force output should not be compromised for the actuator to be competitive with conventionally fabricated devices. This could be achieved by using a high operating pressure (> 1.4 MPa) [74], which all elements of the hydraulic circuit should be able to withstand.

1.5. Objective

The objective of this study is to develop and evaluate a 3D printed hydraulic actuation system, applied in a multi-articulate upper limp prosthesis. The prosthesis should produce sufficient pinch force to be competitive with comparable devices (≥ 30 N), and weigh less than a human hand (< 0.43 kg). The actuator should function at a high operating pressure (> 1.4 MPa) and be compact, such that it fits within the mechanism of the hand. The prosthesis is designed to require a minimum number of fabrication and assembly steps, to explore the benefits of additive manufacturing.

1.6. Outline

The design and evaluation of the prosthetic hand, was structured according to a modified version of the V-model design methodology, depicted in Figure 1.2. The V-model is a method in which complex systems are divided into subsystems [78]. Both systems and subsystems are evaluated according to their requirements. In this study, one subsystem is considered: the actuator. In chapter 2, the requirements are discussed and the method is described for the design, fabrication and evaluation. In chapter 3, the results of the design methods are elaborated on, together with a visualization of the detailed design. The design verification, results, and evaluation of the requirements are discussed in chapter 4. Finally, the conclusion is given in chapter 5.

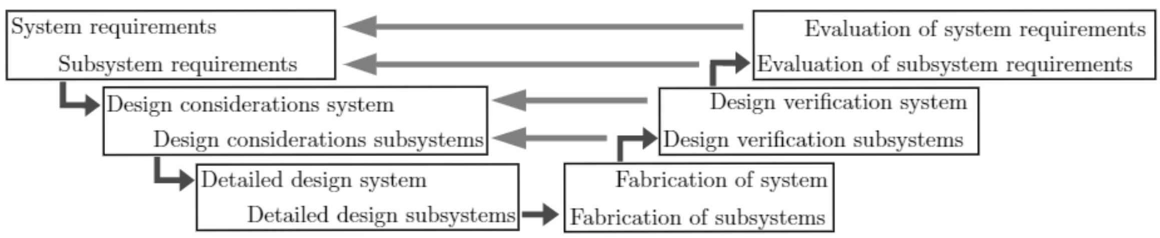

Figure 1.2: Visualisation of the design method, based on the V-model design methodology.

2 Method

2.1. Determining requirements

2.1.1. Hand

Mass The abandonment rate of upper limp prosthetics is 20% and is largely caused by a lack of comfort or functionality of the device [6]. Increasing the comfort through weight improvement, is of the highest importance according to individuals using a prosthesis [7]. Current 3D printed upper limb prostheses weigh 546 g on average, with the majority between 240 g and 450 g, based on available data [69]. As the prosthesis is experienced as an external load, it is desirable that it weighs less than a human hand (426 ± 63 g [64]). Therefore, the hand is required to weigh less than 426 g. This is lighter than most existing comparable 3D printed devices.

Functionality The prosthesis should be useful for activities of daily living (ADLs). Therefore, the hand should allow for grip types that are used frequently for ADLs. In a study by Resnik et al., the most used grip types of individuals who used a DEKA hand prosthesis at home, were a power grip, a pinch grip, and a lateral pinch grip using the thumb [58]. The hand should at least be able to perform a power grip and a pinch grip, making it useful for ADLs, while having a passive thumb. It was decided to use one input signal, similar to the Delft Cylinder Hand [64], to simplify the control of the hand. The actual control of the hand is outside the scope of this study. To achieve a power grip, the fingers must be multiarticulate. As there is only one input signal, the hand is underactuated: it has more independent degrees of freedom than controlled inputs. The principle of under actuation has the benefit that the fingers can adapt to the shape of the object [42]. This allows grasping of objects with irregular shapes and facilitates larger contact area between the hand and the object, which results in stable grasping at a lower force [40]. Also, the hand should be able to achieve a stable pinch grip. The force produced by the prosthesis should be sufficient for a wide variety of activities. Some hydraulic upper limp prostheses produce a pinch force of as low as 8 N [55]. Smit considered a pinch force of 30 N sufficient for the DCH for a broad functional range, which is higher than most body powered devices (~ 15 N) [64]. Based on this, the hand is required to pinch at least 30 N, as stated in the objective. The prosthesis should be suited for activities of daily living and should have high cosmetic value, therefore, the range of motion should be similar to that of a human hand. The closing time is required to be similar to the state of the art. Therefore the closing time of the hand should be 0.25 – 1.0 seconds [51, 64].

Cosmesis Excellent cosmetic value is a part of the basic user requirements for prosthetic devices [54]. A high level of anthropomorphism is needed, in terms of size and weight, but also shape and colour [6]. This can be achieved by employing the device inside a cosmetic glove. The mechanism should be designed to have an anthropomorphic shape and should fit in the cosmetic glove.

Fabrication The goal of using additive manufacturing, is to reduce the number of fabrication and assembly steps. Fabrication steps are limited by designing the system in such a way that a minimal number of post processing steps is necessary. Using 3D printing to fabricate the prosthesis, opens up design possibility as more complex shapes can be produced without significant extra cost. This added design freedom can be explored by designing a modular system and aiming to minimize the number of parts. This reduces the assembly time and thus the cost of fabrication. Moreover, the damaged or imperfect parts can easily be replaced during maintenance. Conclusively, the system is designed to have a minimal number of parts and assembly steps.

2.1.2. Actuator

Working principle The objective is to develop a hydraulic actuation system as hydraulics have shown to be especially suited when the actuation should be lightweight and compact, and have sufficient power output [19]. Nevertheless, it is important to justify the choice for hydraulics and elaborate on its benefits over other types of actuation. First of all, in small scale applications, a hydraulic solution will often be lighter than the electromechanical equivalent. Xia et al. performed an analysis on small scale hydraulic systems and concluded that using hydraulics can offer a significant weight advantage, provided that the system operates at high pressures, preferably 3.5 – 6.9 MPa [74]. A disadvantage of using electric motors, is that they require transmission. Secondly, pneumatics could also be considered as a means of actuation. However, hydraulics has significant advantages over pneumatics. Higher forces can be achieved using liquids as it is a stiffer medium [55]. Most importantly, a hydraulic system requires less energy to deliver a certain pinch force than a similar pneumatic system. This is caused by the difference in compressibility of air and oil. Pylatiuk et al. showed that the compression energy for oil can often be neglected, which is not the case for air [55]. Finally, hydraulic transmission is favourable over a cable-pulley transmission, as it has a higher stiffness. Smit showed that a hydraulic piston-cylinder system requires significantly less energy than an alternative using cables, as it has a higher system stiffness [63].

Force and pressure The actuator should generate enough force for the prosthesis to pinch with at least 30 N. The pinch force relates to the actuator force through the dimensions of the system and the energy efficiency. An estimation of the required actuator force can be made by omitting the friction and other losses in the calculation. The actual force is higher as energy losses due to friction and elasticity that have to be overcome. The operating pressure of the actuator should be at least 1.4 MPa, following the objective. The actuator force depends on the operating pressure and the piston diameter. As the diameter is constraint by the size of the prosthesis, the operating pressure will be the driving factor in the amount of force the actuator can generate. The cylinders, and all parts of the actuation system, should be able to withstand a sufficiently high pressure to assure that the actuators can operate at the desired operating pressure.

Dimensions Following the requirement for cosmesis, the device should fit inside a silicone glove. This limits the diameter of the cylinder as both actuator and structural parts of the prosthesis should fit in a finger of the glove. The length of the actuator is also governed by the dimensions of the glove. The actuator should have a large enough stroke to realise the desired range of motion around the joints of the finger. This depends mostly on the structural dimensions of the prosthesis.

Fabrication The objective of this study is to fabricate both the actuator and the structural elements of the prosthesis through additive manufacturing, limiting the number of production steps. It is important for the actuator to have a high surface quality to minimize both friction and leakage between the piston and the cylinder [53]. If sufficient surface quality cannot be guaranteed through single step fabrication, additional post processing steps might be necessary. This is undesirable as it lengthens the fabrication process. Therefore, the actuators are required to be fabricated without extensive post processing, such as machining. The fabrication method should produce parts with sufficient geometrical accuracy. The gap between the piston and the cylinder is closed by a seal. For the seal to work properly, the distance should be constant, therefore the roundness of the cylinders should be maximized. Any distortions in the parts that occur during printing are undesirable.

Sealing The sealing in a piston-cylinder system makes sure that the working fluid is contained in the desired volume. A proper seal is crucial for the systems performance as leakage causes loss of pressure and contamination of the environment of the actuator [18]. The friction due to the seal should be minimized avoid energy loss through heat production.

2.2. Design and fabrication method

2.2.1. Hand design

Working principle The structure of the mechanism of the prosthesis was based on the anatomy of the human hand. Each finger of the prosthesis consists of two slender bodies that can rotate with respect to each other (see Figure 2.1). The first slender body represents the proximal phalanx. The second body represents the middle and the distal phalanges. These are fixated with respect to each other to simplify the mechanism. The distal interphalangeal joint (DIP joint) was fixated at a 15° angle, this is in accordance with the recommended angle in the medical practice of fixating joints (arthrodesis) [36]. The proximal phalanx is connected with a hinge to the palm on one side and to the middle-distal phalanx on the other side. The thumb that is connected to the palm, is fixed. A fixated thumb is enough to realise a pinch and a power grip. The fingers are actuated with two hydraulic piston-cylinder actuators each. The first creates a torque around the metacarpophalangeal joint (MCP joint), as shown in Figure 2.3b, rotating the proximal phalanx. The second one creates a torque around the proximal interphalangeal joint (PIP joint), rotating the middle-distal phalanx. All cylinders are connected to the same pressure source and are essentially in contact with each other. This means that there is one input signal: the pressure across the system. As there is only one control signal and multiple degrees of freedom, the system is underactuated. The hand is closed by increasing the pressure in the actuators. To open the hand, there are springs incorporated in the system that create a torque around the joints, in the opposite direction of the actuators. Also, the pump is reversed during the opening of the hand. The working principle of the prosthesis was based on that of the Delft Cylinder Hand [64]. Figure 2.1 shows the working principle of one finger.

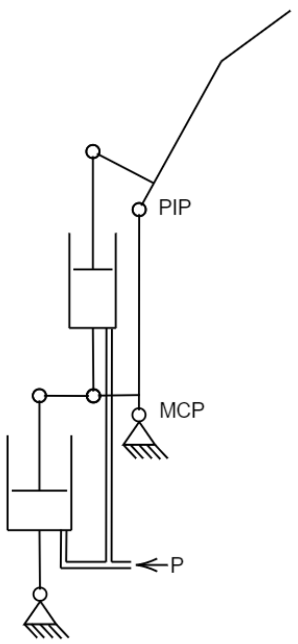

Figure 2.1: Working principle of a finger of the Delft Cylinder Hand, a body powered upper limp prosthesis using hydraulic actuation [64].

Dimensions Phalanges The prosthesis should have a high cosmetic value, as discussed in section 2.1.1. A convenient way to achieve this, is to cover the mechanism with an anthropomorphic cosmetic glove. This gives the prosthesis the appearance of a human hand. Preferably, the glove should be made from silicone. Silicone gloves have proven to require and dissipate less energy when flexing a joint, than PVC gloves [62]. In practice, the selection of a specific model glove is based on the dimensions of the sound hand [57]. For the purpose of this study, a hypothetical hand was assumed with dimensions similar to that of an average Dutch male. These dimensions were determined using DINED, an anthropomorphic database created by the TU Delft. The mechanism of the prosthesis was designed to fit inside the selected glove. The model of the glove only prescribes global hand dimensions, such as the total length of each finger. Therefore, the dimensions of the individual hand segments are yet to be determined. For this purpose, a paper was used that focuses on finding a pattern of length correlation of metacarpals and phalanges [13]. Buryanov and Kotiuk described the relative distances between the joints of the finger with respect to the external finger dimensions, for a group of 66 adult males. The soft tissue on the tip of the finger and the height of the web in between the fingers, was also considered. The length of the phalanges of the prosthesis were determined by using the length of the fingers of the glove and the relations described by Buryanov. The dimensions of the palm and the thumb followed from the size of the glove. While closing and opening the hand, the fingers should be able to move without making contact to prevent friction. To achieve this, there should be sufficient spacing between the MCP joints, that connect the fingers to the palm. Finally, the structural elements of the hand should be stiff [63]. As the hand pinches an object, the fingers start to elastically deform. They act as springs that store a large amount of energy. Minimizing this elastic energy reduces the required input energy. Therefore, the system was designed for stiffness, such that the stored elastic energy is minimized. As an example, the stiffness of a cantilever beam that is constraint on one end, and loaded on the other, can be determined using the following expression [12]:

$$K = \frac{3EI}{L^3} \tag{2.1}$$

Here, E is the elastic modulus of the material, I the moment of inertia of the beam and L the length of the beam. This relation shows that a larger moment of inertia of a beam results in a higher stiffness. The phalanges have a cross section that is similar to that of a square beam. This way, they can be printed without support material, in multiple orientations as there are multiple flat surfaces that can be placed on the build plate of the printer. The moment of inertia of a hollow rectangular beam, such as shown in Figure 2.2, can be determined using the following expression [71]:

$$I = \frac{BH^3}{12} - \frac{bh^3}{12} \tag{2.2}$$

Based on this expression, it can be concluded that if more material is placed near the outside perimeter of a hollow beam, the moment of inertia increases.

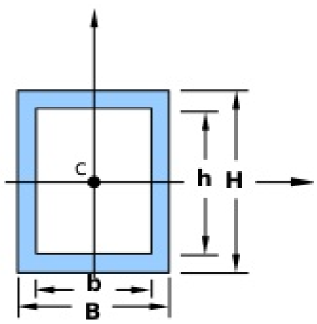

Figure 2.2: Cross section of a hollow beam, with the dimensions used to calculate its moment of inertia.

Moment arm and cylinder dimensions As mentioned, the prosthesis is underactuated as it has more independently moving fingers and phalanges than it has actuators. However, the hand should also be able to perform both a pinch grip and a power grip. Kragten et al. described how an underactuated hand can differentiate between these grip types in a purely mechanical way [42]. To describe this process, the closing of the hand around an object is considered. When the system is pressurised, the fingers rotate around the MCP joint. The PIP remains extended due to the spring. As soon as a finger makes contact with the object, a reaction force is applied on the finger at the point of contact. This force creates a reaction torque around

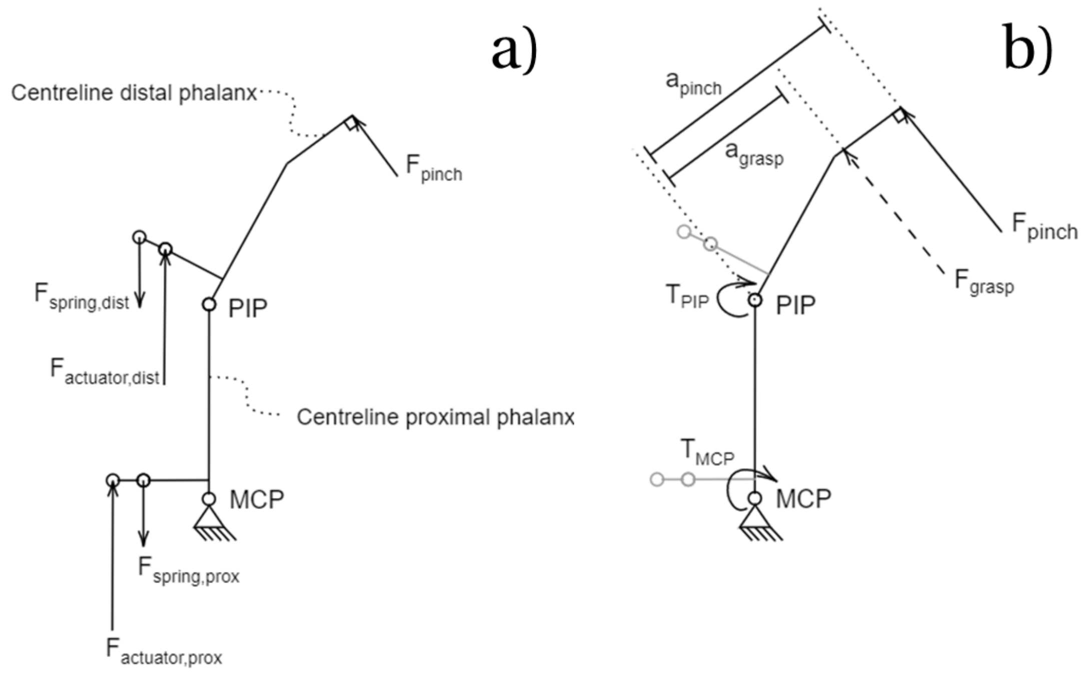

Figure 2.3: Schematic side view of the finger mechanism with a) the forces and b) torques acting it.

the PIP joint and the MCP joint. If the initial contact with the object is at the fingertip, the PIP joint should remain extended such that the finger acts as a rigid body and rotates around the MCP joint. This is achieved if around the PIP joint, the reaction torque of the object is larger than the actuator torque. This way, a precision grip is realised. However, if the initial contact with the object is not at the fingertip, the moment arm of the reaction force is smaller and therefore the reaction torque is smaller (see Figure 2.3b). Now, around the PIP joint, the reaction torque is smaller than the actuation torque, and the middle-distal phalanx flexes. In this case, the object is pushed towards the palm and enclosed by the fingers; a power grip is achieved. There are certain geometrical constraints on the mechanism to grasp according to the elaborated process. Primarily, to establish equilibrium of the fingers in both a precision grip and a power grip, the transmission ratio R should be considered. This is the ratio between the actuation torque $T_{actuator,PIP}$ around the PIP joint and $T_{actuator,MCP}$ around the MCP joint, described by [43]:

$$R = \frac{T_{actuator,PIP}}{T_{actuator,MCP}} \tag{2.3}$$

For the mechanism to establish both a stable pinch grip and a power grip, the transmission ratio should fulfill the folowing constraints, as described by Kragten et al.:

$$\frac{2\left(M - L_0^2\right)\left(M + (L_0 - L_1)^2\right)}{4M\left(L_0^2 + M\right)} \leq R \leq \frac{(L_0 - L_1)\left(M + (L_0 - L_1)^2\right)}{M\,(L_0 - 2L_1) + L_0\,(L_0 - L_1)^2} \tag{2.4}$$

For the mechanism of the hand, L_1 is equal to the length of the proximal phalanx. L_0, that describes the distance between the MCP joint and the thumb, is approximated using $\frac{1}{2} \cdot L_1$. M is defined as:

$$M = \frac{1}{4}\left(d_{\text{obj}} - 2t\right)^2 \tag{2.5}$$

In this expression, t is the distance from the centreline between the joints and the side of the phalanx near the object, d_{obj} is the diameter of the object that is grasped. Using the dimensions of the phalanges, this equation can be used to determine the required transmission ratio. The actuation torque applied by the proximal and distal actuators can be calculated as follows:

$$
\begin{aligned}
T_{actuator} &= a_{actuator} \cdot F_{actuator} \\
&= a_{actuator} \cdot P \cdot A_{cylinder} \\
&= a_{actuator} \cdot P \cdot \pi \cdot r_{cylinder}^2
\end{aligned}
\tag{2.6}
$$

In which $a_{actuator}$ is the moment arm of the actuator, P the pressure in the actuators and $A_{cylinder}$ the surface area of the cylinder.

Substituting this in equation 2.3 for the transmission ratio, results in:

$$
R = \frac{a_{actuator,distal} \cdot r_{cylinder,distal}^2}{a_{actuator,proximal} \cdot r_{cylinder,proximal}^2} \tag{2.7}
$$

This equation shows that the transmission ratio of the fingers depend on the radius of the cylinders and the moment arm of the actuator. The radius of the cylinder and the moment arm of each actuator should be chosen such that the transmission ratio complies with the constraints set by equation 2.4. Additionally, the dimensions of the glove impose a second constraint on the actuator dimension. The actuators and phalanges should fit inside the glove, both in extended and flexed configuration. The cross sections of the fingers of the glove was approximated to be a circle. Hence, the radius of the fingers could be calculated using the outside perimeter given by the manufacturer of the glove. Finally, the radius of the cylinder and the moment arm are not independent as the radius of the cylinder is constraint by the moment arm, as seen in Figure 2.4. Assuming there is material of the proximal phalanx located at the centerline between the PIP and MCP joint, for the moment arm of the cylinder holds:

$$
a_{actuator} \geq r_{cylinder} + s \tag{2.8}
$$

Here, s is the wall thickness of the cylinder. To achieve the highest possible pinch force, the actuation torque should be maximized. The actuation torque scales quadratically with the cylinder radius and linearly with the moment arm, as seen in equation 2.6. Therefore, the radius should be maximized while still complying with the aforementioned constraints. The inner radius should be a round number such that the cylinder is compatible with a commercially available O-ring, as was discussed in section 2.2.2.

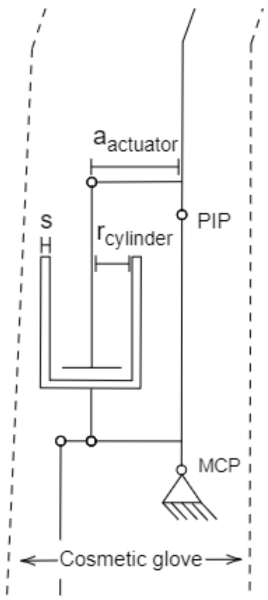

Figure 2.4: Schematic side view of the proximal phalanx and the distal cylinder within the cosmetic glove.

Springs The function of the springs in the mechanism is to open the hand. The springs apply a torque around the MCP joint and PIP joint that is opposite to the actuation torque. When the power to the pump is turned down, or if the pump is reversed, the pressure drops and the actuation torque decreases, the springs drive back the pistons such that the finger is extended. When at rest, the springs keep the phalanges against the extension stop such that the fingers are in equilibrium. The spring torque depends on the spring characteristics, the elongation and the points of engagement on the phalanges. The points of engagement at which the springs are attached to the phalanges, are chosen based on the available space in the mechanism. Then, the desired spring torque can be achieved by choosing springs with the appropriate characteristics. The resulting spring torque can be calculated using equations 2.15 and 2.16. The spring torque should be sufficient to drive back the piston and open the hand when the pump is reversed. In a study on 3D printed cylinders, the friction force $F_{friction}$ between an O-ring seal and an unreamed SLA printed cylinder, was determined to be $\sim 15\,\mathrm{N}$ at a pressure of 1.1 MPa [50]. This gives the order of magnitude of the friction force in the cylinder, which is estimated to be 10-20 N. To drive back the piston, the drive back force from the springs $F_{driveback,springs}$ should be larger than the friction force, such that: $F_{driveback,springs} > F_{friction}$. There is some contribution of the reversing of the motor during opening, which creates a partial vacuum in the cylinder. The maximum driveback force this causes to be applied on the piston, can be be calculated as follows:

$$\begin{aligned} F_{vacuum} &= P_{atm} \cdot A_{cylinder} \\ &= 0.1013\,\mathrm{MPa} \cdot 78.5\,\mathrm{mm}^2 \\ &= 7.96\,\mathrm{N} \end{aligned} \tag{2.9}$$

The spring force reduces the maximum pinch force as the spring torque is opposite to the actuation torque. Therefore, the spring force should be limited. Moreover, the transmission ratio should still comply with the constraints expressed in paragraph *Moment arm and cylinder dimensions*, section 2.2.1. Adding the spring torque to the equation for the transmission ratio, equation 2.3 becomes:

$$R = \frac{T_{actuator,PIP} - T_{springs,PIP}}{T_{actuator,MCP} - T_{springs,MCP}} \tag{2.10}$$

Joints In this paragraph, the design considerations for the joints of the mechanism are considered. Each finger consists of six bodies: two phalanges and two sets of a piston and a cylinder (Figure 2.5). The bodies are connected with six joints. The function of the joints is to constrain all undesired degrees of freedom. There are three main requirements for the joints; they should allow for easy assembly, add little extra parts to the device and the friction should be limited. To determine the best joint type for each joint, first they were divided in three categories based on their characteristics. Per category, different optional joint types and how well they meet the requirements, are discussed. The joint type used in the final design was chosen based on this discussion. The joints are labelled A to D, MCP and PIP, as shown in Figure 2.5. The first classification step was made based on how the joints are loaded. The joints between the phalanges, the MCP and PIP joint, are loaded in multiple directions as the hand is operated. Contrarily, the joints from the actuators, A to D, are only loaded in compression. Both parts connected in each of these four joints are always pressed against each other, due to the spring force designed to open the hand. A second classification step was made based on the range of motion (ROM) of the joints. The MCP and PIP joints have a similar range of motion. Joints A and C also have a ROM of about 90 degrees. However, the joints at the cylinders, B and D, only rotate for approximately 5 degrees. Now, the joints with similar characteristics were divided in groups 1, 2 and 3, as shown in Table 2.1. The possible joint types per group were based on a paper on joint types used in instruments for minimally invasive surgery [37]. Belted joints or joints based on bending were not considered, as these require additional parts or a multi material structure, increasing the complexity of fabrication considerably. The first joint type that was considered, is the sliding hinge joint, or a pin joint, schematically displayed in Figure 2.6a. The joint can take loads in all directions, constraining five degrees of freedom. Since the number of parts is to be minimized, the joint is assumed to be fabricated without an additional bearing. Then, the joint can be designed to consist of two or three parts, depending on the use of a separate or integrated pin. Some assembly effort is required either way. During rotation, the friction in the joint results is a friction torque acting on the pin. This friction torque can be calculated using the following equation [16]:

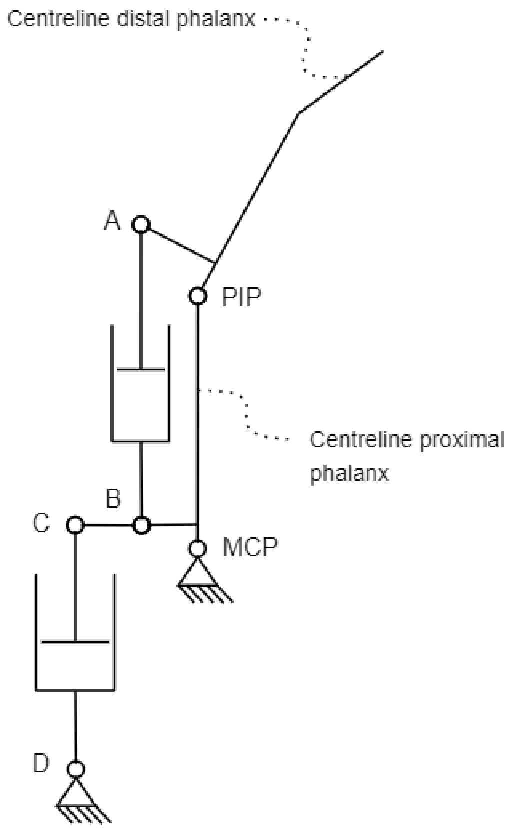

Figure 2.5: Schematic side view of the joints within the finger mechanism.

$$T_{friction} = f \cdot F_{axle} \cdot \frac{d}{2} \tag{2.11}$$

Here, f is the friction coefficient and F_{axle} is the load. To minimize the friction moment, the pin diameter d should be minimized. The entire joint can be 3D printed. Then, minimizing the pin diameter becomes challenging as small 3D printed structures tend to be brittle and the joint should be able to carry the required load to pinch 30 N. A paper presenting a 3D printed hand prosthesis with fully 3D printed joints, states that any parts that carry a load should have a sufficient cross sectional area to prevent the risk of material failure [17]. This prosthesis shows that the MCP joint requires considerable space when fully 3D printed, even when designed to pinch with 6 N. The second joint that was considered, is the sliding curved joint (Figure 2.6b). A benefit of this joint is that it can easily be assembled, and fabricated out of two parts. A disadvantage is that can not support loads that separate the two surfaces, meaning it should be loaded under compression. The friction can be approximated using equation 2.11, substituting the diameter of the joint surface for the pin diameter d. The third option is a rolling friction joint, schematically depicted in Figure 2.6c.

Table 2.1: Classification of the joints based on the load direction and ROM.

	Group 1	Group 2	Group 3
Joints	MCP, PIP	A, C	B, D
Load direction	Multiple	Compressive	Compressive
ROM	~ 90°	~ 90°	~ 5°
DOF	1	1	1
Possible joint types	Sliding hinged joint	Sliding hinged joint, sliding curved joint, rolling friction joint, rolling toothed joint	Sliding hinged joint, sliding curved joint, rolling friction joint, rolling toothed joint

Similar to the sliding curved joint, it has the benefits of easy fabrication and assembly, and can only be loaded in compression. Additionally, any transverse forces should be minimized as this can cause the convex part of the joint to slip or break away. The losses in a rolling joint are due to the deformation of the surfaces and depend on the normal load [45]. The surface roughness of the materials only has a minor contribution to the energy loss. Any plastic deformation of the surfaces would increase the energy loss dramatically. This should be considered in the design, especially if the joint is 3D printed and materials with a low yield strength are used. Finally, the rolling toothed joint could be used (Figure 2.6d). This joint type has similar characteristics as the rolling friction joint. However, the toothed surface make it more resistant to forces parallel to the contact plane of the joint. Fabricating such a joint using 3D printing, is challenging. Small scale 3D printed gears could fracture and the fracture behaviour of 3D printed materials has shown to be dramatically different compared to conventional materials [77]. Finally the range of motion of the joints is discussed. As stated in the requirements, the fingers should have a ROM similar to that of a human finger. Literature shows that the ROM of the MCP joint ranges from -19 degrees extension to 90 degrees flexion. For the PIP joint, this is -7 degrees extension to 101 degrees flexion [4]. However, the functional range of motion, the ROM needed to perform tasks of daily living, is significantly smaller. The functional ROM is 48% and 59% of the ROM of the MCP joint and the PIP joint, respectively. An extension stop and a flexion stop can be implemented to constrain the motion of the finger to a ROM that is similar that of a human finger.

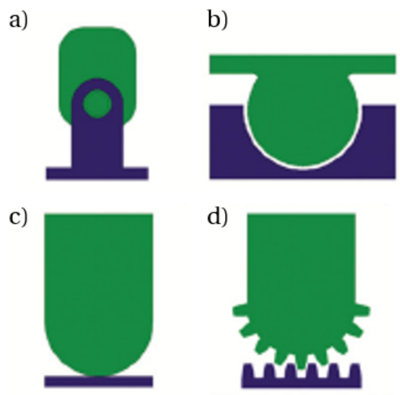

Figure 2.6: Graphical description of the joint types that were considered: a) Sliding hinged joint, b) sliding curved joint, c) rolling friction joint, d) rolling toothed joint. The schematic visualisation are used from Jelínek 2014 [37].

2.2.2. Actuator design

Force and pressure To design the actuators, it was necessary to determine the required pressure in the cylinders. The force that each of the cylinders delivers and the pressure P can be calculated using the following equation:

$$F_{actuator} = P \cdot A_{cylinder}$$
$$P = \frac{F_{actuator}}{A_{cylinder}} \tag{2.12}$$

The area of the cylinder $A_{cylinder}$ follows from its radius. The radius of both cylinders was determined based on the constraints on the transmission ratio, as described in section 2.2.1. The requirements state that the hand should be able to pinch 30 N. During pinching, there is only flexion at the MCP joint, as described in section 2.2.1. The required force can be calculated by using the required pinch force of 30 N and evaluating the equations of rotational equilibrium around the MCP joint:

$$\sum M_{mcp} = 0 \tag{2.13}$$

Considering the MCP joint, the sum of the moments is equal to the sum of the torques around the joint. Equation 2.13 then becomes:

$$-T_{actuator} + T_{springs} + T_{pinch} = 0 \tag{2.14}$$

$T_{springs}$ is the torque applied by the springs that open the hand, T_{pinch} is the reaction force caused by the pinching force. Counter clockwise rotation is defined as positive. First the required actuator toque $T_{actuator}$ was determined. Then the actuator force was calculated and finally, the required pressure. To solve equation 2.14, the following assumptions were made: The hand is pinching an object between the tip of the distal phalanx and the tip of the thumb. The bodies are in equilibrium such that the hand remains in a pinching configuration and does not convert to a power grip, as described in section 2.2.1. In this configuration the PIP joint is at 0 degrees flexion and the middle phalanx is against the extension stop. The hand is pinching an object of negligible thickness, such as a piece of paper. Inspection of the design shows that pinching a slightly larger object requires less force as the moment arm of the proximal actuator increases. The reaction force that the object exerts on the finger is assumed to be perpendicular to the centreline of the distal phalanx and is applied exactly at the tip of the distal phalanx. In reality, the exact point of application and direction of the force will vary as the tip is rounded and a wide range of objects can be handled. Using the furthest point on the centreline of the distal phalanx (see Figure 2.3), provides a margin to overcome these uncertainties as the actual reaction torque by the pinch force can only be smaller. The springs apply a positive torque around the MCP and PIP joints. It was assumed that each spring is linear such that the force is proportional to its elongation. The torques were calculated using the following formulae:

$$T_{springs} = 2 \cdot F_{spring} \cdot a_{spring} \tag{2.15}$$

With a_{spring} being the moment arm of the spring. The force of a single spring F_{spring} can be calculated as follows:

$$F_{spring} = c_{spring} \cdot \Delta L + F_0 \tag{2.16}$$

Substituting the spring torque T_{spring} and the reaction torque from the pinch force T_{pinch} into equation 2.14 and rewriting, yields an expression for $T_{actuator}$. The required pressure $P_{required}$ can be determined by solving this expression for $T_{actuator}$ and using the following relationship:

$$\begin{aligned} T_{actuator} &= a_{actuator} \cdot F_{actuator} \\ &= a_{actuator} \cdot P_{actuator} \cdot A_{cylinder} \end{aligned} \tag{2.17}$$

Finally, in the pinching configuration, the PIP joint is at 0 degrees flexion and the middle-distal phalanx was assumed to be pressed against the extension stop. To test this assumption, the equilibrium equations were evaluated around the PIP joint using the required actuator pressure $P_{actuator}$ found using equation 2.17.

$$\sum M_{pip} = -T_{actuator,proximal} + T_{springs,proximal} + T_{pinch,proximal} - T_{extensionstop} = 0 \tag{2.18}$$

As the pressure is known, $T_{actuator,proximal}$ can be evaluated using equation 2.17. Substituting the torques in the equilibrium equation gives the toque delivered by the extension stop $T_{extensionstop}$. If this torque is in opposite direction of $T_{springs,proximal}$, the phalanx is pressed against the extension stop and the assumption is justified. It should be noted that the calculated pressure $P_{actuator}$ is only an estimation of actual cylinder pressure required to pinch with 30 N. In addition to the geometrical simplifications, the phalanges were assumed to be infinitely stiff. Moreover, any friction was omitted and the hydraulic efficiency of the cylinders was assumed to be 100%.

Cylinder dimensions The function of the actuators is to deliver the force that is required for the hand to pinch 30 N. The actuator consists of three main elements: the piston, the cylinder and the tubing. It operates as a single acting piston cylinder system, meaning that the pressure acts on one side of the piston. The piston is driven back by the springs. In this section, the design considerations for the cylinder are discussed. There are three requirements from the actuator that are relevant for the cylinder: it should safely operate at the working pressure, it should fit within the mechanism of the phalanges and the cosmetic glove, and it should allow for easy assembly of the actuator. In section 2.1 it was emphasised how the actuators are to be fabricated without extensive post processing such as machining or using a reamer. Firstly, following the requirements for easy assembly of the actuators, the cylinder was designed as a single part such that it can be printed in a single step. A tube connector is to be mounted on this cylinder body to allow the tubing to be connected and disconnected from the cylinder. The bottom of the cylinder body should allow it to rotate with respect to the phalanx it is mounted on; this side is part of the joint as described in paragraph *Joints* in section 2.2.1. Secondly, the cylinder should fit within the mechanism and the cosmetic glove which poses constraints on its dimensions. Moreover, the inner radius of the cylinder was already determined based on the restrictions on the transmission ratio elaborated on in paragraph *Moment arm and cylinder dimensions* in section 2.2.1. Finally, it is essential that the actuation system can safely withstand the pressure required to operate the hand. Moreover, it should be robust enough to withstand any external impact or unexpected peak pressures. For the cylinders this means that the wall thickness should be sufficient to withstand the pressure. Generally, cylinders are divided into two groups, based on their geometry: thin walled and thick walled cylinders. For thin walled cylinders, it can be assumed that the stresses are uniformly distributed through the wall. This simplifies the stress calculations significantly [73]. For thick walled cylinders, it can no longer be assumed that the stresses are uniformly distributed through the wall. The problem becomes more complicated as not only equilibrium equations must be considered, but also the compatibility equations. To determine if the cylinder can be considered thin walled, a common international convention is used whereby a cylinder is thin walled if [73]:

$$\frac{s}{d_i} \leq \frac{1}{20} \tag{2.19}$$

The inner radius of the proximal and the distal cylinders of the design are known. For the designed cylinders to be considered thin-walled, the wall thickness should be:

$$\begin{aligned} Proximal: \quad s_p &= \frac{10\,\text{mm}}{20} = 0.50\,\text{mm} \\ Distal: \quad s_d &= \frac{7\,\text{mm}}{20} = 0.35\,\text{mm} \end{aligned} \tag{2.20}$$

These thicknesses seemed to be insufficient for the cylinder to be robust and able handle pressures of > 1.4 MPa. Therefore, for design purposes, the cylinders were assumed to be thick walled. This assumption was reflected on as the detailed design is finished. Furthermore, the material was assumed to be homogeneous. This makes the stress calculations significantly less complicated. This assumption is to be discussed as its validity depends on the material and fabrication method. To determine the required wall thickness of the cylinder, the stress caused by the internal pressure was considered. The stress in the wall can be divided into three principle stresses: the radial stress σ_r, the transverse stress σ_t and the axial stress σ_a. The radial stress is the stress in the direction of the radius. The transverse stress is always perpendicular to the radius and lies in the plane perpendicular to the central axis of the cylinder. The axial stress is parallel to the central axis of the cylinder. The multiaxial stress state as described, can be approached by transforming the stress tensor into a single equivalent stress σ_e. This equivalent stress can be treated as a tensile stress and thus compared with the material's yield strength [73]. However, the equivalent stress in itself is not of interest as the wall thickness is to be determined. To do this, the equivalent stress was equated to the allowable material stress, and then solved for the wall thickness s. This resulted in the following expression, taken from "Circular Cylinders and Pressure Vessels" by Vincent Vullo [73]:

$$s = r_i \left(\sqrt{\frac{\sigma_w + p_i}{\sigma_w - p_i}} - 1 \right) \tag{2.21}$$

Here, σ_w is the yield strength of the material of the cylinder wall. Equation 2.21 can be used to determine the minimum wall thickness for the cylinders to withstand the operating pressure calculated according to the paragraph *Force and pressure* in section 2.2.2. A safety factor was used such that the actuator can withstand unexpected peak pressures. This safety factor is defined as:

$$Sf = \frac{P_{yield}}{P_{work}} \tag{2.22}$$

The internationally used ASME standard requires a safety factor of 3.5 for pressure vessels [14]. Other sources state that a safety factor of 3.5 to 6 is common practice in the design of pressure vessels [22]. For the purpose of this study, a safety factor of 4 was used. Practically, this means that the cylinder was designed such that it can withstand a pressure of four times the operating pressure without failure.

Piston and sealing The piston has the function to transfer the pressure in the cylinder to a force applied on the phalanx it is connected to. The end of the piston that drives the phalanx is part of a joint that was designed according to paragraph *Joints* in section 2.2.1. The other end of the piston slides trough the cylinder. A seal between the piston and the cylinder prevents the working fluid to leak from the desired volume. In this section, the design considerations are discussed for the seal and the piston rod. The seal is a critical element of the actuator as it prevents leakage which can cause pressure loss in the cylinder [18]. The first requirement for the seal as described in section 2.1 is that the seal should minimize leakage. Secondly, the seal should be designed to have minimal friction to avoid heat production and thus energy loss. Various types of seal design are possible, however, contact seals such as O-rings or lipseals are most common in hydraulic applications [18]. O-ring seals can operate at a wide range of pressures and are cost-effective [53]. A one-component O-ring seal was chosen as it requires the least amount of space. Also, both the number of parts and the assembly steps is minimal. O-rings can be mounted in series, however, the first one always carries the full load. Moreover, adding a second O-ring to a piston of a certain length, significantly decreases the possible stroke. An O-ring seal consists of two elements: the O-ring and the gland in which it resides. To design the most optimal seal, the Parker O-ring handbook is used [53]. The outer diameter of the O-ring follows from the diameter of the cylinder, its cross-sectional diameter and material are determined based on literature. An important parameter in O-ring seal design, is the squeeze ratio. This is a measure of the degree at which the ring is squeezed between the piston and the cylinder wall. One of the reasons an O-ring seal works is that it has the tendency to return to its original shape [53]. The seal was designed to have a squeeze ratio r_{sq} of 10%, which is in accordance with literature and the recommendation of a manufacturer [25, 53]. The following formula was used to determine the piston groove diameter to achieve the desired squeeze ratio:

$$PGD = D_{out} - 2 \cdot D_{cross,squeezed} \tag{2.23}$$

As shown in Figure 2.7, PGD is the piston groove diameter, D_{out} the outer diameter of the O-ring and $D_{cross,squeezed}$ is the cross-sectional diameter when squeezed. The squeezed cross-section diameter can be calculated using the following equation:

$$D_{cross,squeezed} = (1 - r_{sq}) \cdot D_{cross} \tag{2.24}$$

Finally, the design of the piston rod is considered. The piston rod forms the connection between the joint at the end of the piston and the side with the O-ring seal that slides though the cylinder. The rod should withstand the high compressive forces without buckling. Moreover, the axis of the piston and the axis of the cylinder should be collinear to prevent asymmetrical loads and friction.

Tubing and connectors The tubes connect the pump to the cylinders. The tube connectors that are mounted on the cylinders allow the actuators to be disconnected from the system. The most important requirement for these components, is that they can operate without leakage at sufficiently high pressures. Furthermore, the dimensions should be such that the tubing and the connectors fit within the mechanism and the glove. The tubing and the connectors were selected to be compatible and modular with respect to each other, such

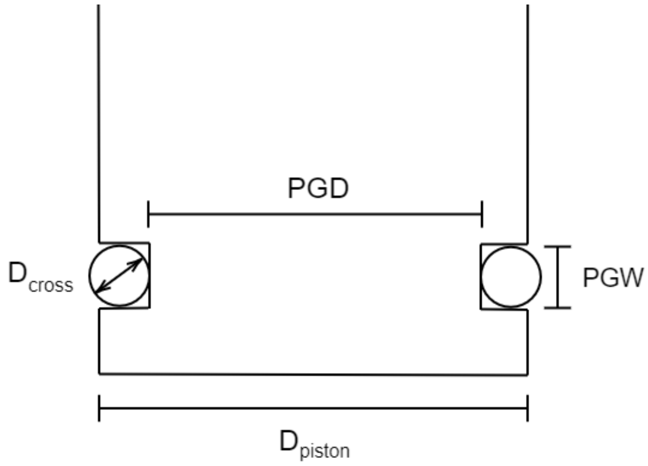

Figure 2.7: Cross section of the gland of the O-ring seal. Key dimensions are indicated.

that the prosthesis can be disassembled and parts can be replaced. The size of the tube connectors are constraint by the available space within the glove and the mechanism. Preferably the connector has a locking sleeve that can be slid over the tube and locked on the hose insert. Generally, such connectors are used at higher pressures and a locking sleeve can prevent leakage [48]. The tube connectors are mounted on the cylinders through a threaded connection. This connection should withstand the load caused by cylinder pressure, without leakage. To determine the pressure at which the threaded connection fails, it was assumed that the failure mode is thread stripping of the female thread. This assumption is based on the difference in yield strength of the metal tube connector and the 3D printed polymer cylinder in which a thread is tapped. For example, the ultimate yield strength for polyamide is 85 MPa, for steel it is 400 MPa [21]. The maximum operating pressure was determined by calculating the shear force at failure, using the following formula:

$$F_{fail} = \sigma_{shear} \cdot A_{th} \tag{2.25}$$

Here, A_{th} is the total thread shear area. The shear strength σ_{shear} can be approximated using the following relation, based on the Von Mises criterium: $\sigma_{shear} = 0.577 \cdot \sigma_{tensile}$. The shear area was calculated using a geometrical relation, cited by multiple sources [20, 23]:

$$A_{th} = 0.5 \cdot \pi \cdot d_{pitch} \cdot L_e \tag{2.26}$$

Where d_{pitch} is the pitch diameter of the thread and the length of engagement is $L_e = n_{threads} \cdot h_{pitch}$.

Pump and electrical components The function of the pump is to convert kinetic power into hydraulic power. Two main requirements apply on the pump, based on the requirement for the prosthesis as described in section 2.1. Firstly, the pump should generate the pressure necessary to achieve a pinch force of 30 N, namely P_{work}. Secondly, the mass of the pump and motor together, should be less than half of that of the prosthesis. This was based on an estimate of the contribution of different elements to the total mass of the prosthesis, which should be < 426 g (section 2.1). Concisely, the weight of the pump should be minimal while still generating sufficient pressure, therefore, the mass over pressure ratio was minimized. Various pump types are used in the field of hydraulics, ranging from gear pumps to piston pumps. A study performed in 2019 by Mark van Dort compared commercially available pumps based on their mass and their output pressure difference [72]. Based on this comparison, it was concluded that an external gear pump is the only type of pump that complies with the requirements. Commercially available internal gear pumps, axial and radial piston pumps, and vane pumps were found to be too heavy for this application. External gear pumps are generally known for their compactness, low cost and relatively high efficiency [32]. Two pumps were considered to be used, hereafter Pump A and Pump B. Pump A is the pump with the lowest mass to generated pressure ratio included in the study by Mark van Dort. Secondly Pump B, a small external gear pump that was not included in the study, has a similar generated pressure to mass ratio. Table 2.2 shows a comparison of the specifications of both pumps. It was decided to use Pump B based on the generated pressure and generated pressure over mass ratio. The hydraulic oil that is recommended by the retailer of Pump A was used as the hydraulic fluid.

Table 2.2: Pump characteristics of the two pumps that were considered. Pump B was selected.

	Pump A [49]	Pump B [66]
Generated pressure	2.0 MPa	4.5 MPa
Mass	30 g	66 g
Pressure/mass ratio	15.0	13.2
Geometry (lxbxh) [mm]	27x26x17	30x30x25
Retail price	€ 64.99	€ 46.43
Retailer	Magom HRC	Top-Gun RC Store

The pump is powered by a brushless electric motor. The motor that came attached to the pump is used and is assumed to be appropriate for this application. A disadvantage of the selected pump is that the motor specifications were not disclosed.

The rotational velocity of the motor is controlled using an electronic speed controller (ESC). This device also controls the rotational direction. An ESC is connected directly between the motor and the power source. It controls the motor through pulse width modulation (PWM). PWM is a technique that creates a signal consisting of variable width pulses to create an analog signal with a certain amplitude. For example, a 5V PWM signal consists of alternating periods of 5 V and 0 V. If the line is 'open' 50% of the time, the average output voltage delivered to the motor is 2.5 V. There are two requirements for the ESC: it should allow for bi-directional rotation of the motor and it should support the current going through the motor. The retailer of the motor that is used, recommends a 40A ESC. Based on this information, it was decided to use the Aerostar RVS 40A ESC [34]. It can be used in combination with a microcontroller such as an Arduino.

Finally, a power source was selected to complete the set of electronic components. It is important to note that the power source was not considered in the weight of the prosthesis as it can be placed outside of the hand and elsewhere on the body without drastic design implications. The ESC is compatible with LiPo (lithium polymer) and NiMH (nickel metal hydride) batteries [34]. LiPo batteries are generally lighter as they have a higher volumetric- and specific energy density [24]. Moreover, the power output of a LiPo battery is said to be more steady throughout the discharge compared to NiMH batteries [26]. A LiPo battery consist of one or more cells, connected in series. Each cell has a nominal voltage of 3.7 V [61]. This means that the total voltage is: $V_{nominal} = 3.7 \cdot n_{cells}$. The motor is advised to be used with a 11.1 V 3 cell battery [66]. The battery that was selected for the purpose of this study, is an 11.1 V LiPo battery pack with a capacity of 1300 mAh [15].

2.2.3. Fabrication

Structural elements As discussed in the requirements, both the hand and the actuators are to be 3D printed. In this section the fabrication method is discussed, first for the structural elements of the hand, then for the actuators. The first requirements that relate to the fabrication of the structural elements, is that the system should weigh less that a human hand, at 426 ± 26 g. Secondly, fabrication should be possible in a single step and with a minimal number of post-processing steps. Finally, the structural elements should be stiff as to reduce the stored elastic energy in the fingers and the required input energy, as discussed in section 2.2.1. The

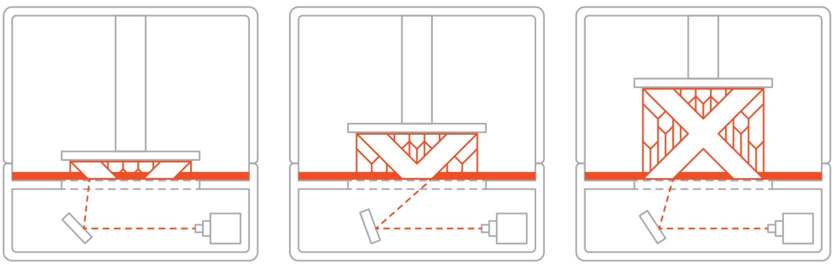

Figure 2.8: Schematic description of Stereolithography (SLA) [10].

two printing techniques that were considered, were chosen based on their availability to the writer. Additionally, these methods are among the most used methods of additive manufacturing and are widely adopted [60]. The first is Stereolithography (SLA), which is based on selective solidification of photocurable resin. Each additional layer of the printed part is added by tracing a pattern with a laser which locally polymerizes the resin. Figure 2.8 schematically shows a resin basin out of which a part is printed, while slowly lifting the build plate, as a part is printed using SLA. One of the advantages of SLA, is the high surface quality [60]. The second option that was considered, is Fused Deposition Modelling (FDM). FDM is a technique in which parts are created layer-for-layer by depositing a string of thermoplastic material that is extruded through a nozzle. The process is depicted schematically in Figure 2.9. Some of the benefits of FDM are that the process is cost effective and the parts require little post-processing [33]. Shown in Table 2.3, the techniques were compared based on the following properties of the printed material: density, stiffness, cost per mm^3 and ultimate yield strength. The materials that were used for this comparison give a reasonable representation of the material properties that can be expected from parts made with these print techniques. Considering the requirements, the higher stiffness, and considerably lower cost of PLA, FDM was chosen as the fabrication method for the structural parts. The slightly higher density of PLA with respect to the Formlabs Clear resin is of less concern since FDM printed parts generally have an infill ratio of <100% [5]. The orientation in which the parts are printed, depends on the geometry of the parts. Therefore, this will be elaborated on after the detailed design is discussed.

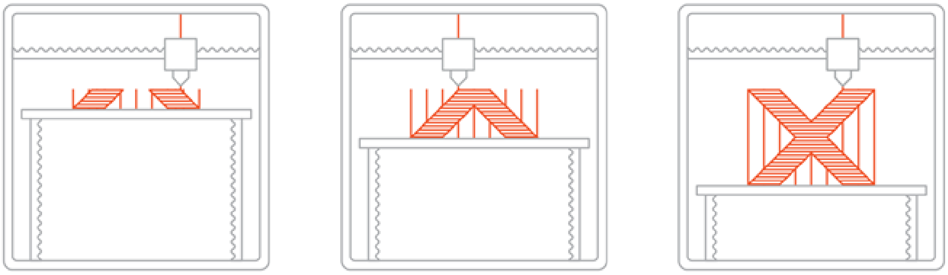

Figure 2.9: Schematic description of Fused Deposition Modeling (FDM) [9].

Table 2.3: Properties of materials printed with Steriolithography (SLA) and Fused Deposition Modeling (FDM)

	SLA		FDM	
Material	Resin (Formlabs Clear 03)		PLA	
Density	1.15-1.20 g/cm^3	[31]	1.25 g/cm^3	[35]
Young's Modulus	1.6-2.8 GPa	[30]	3.5 GPa	[35]
Cost	125.9 €/liter	[28]	25 €/liter	[1]
Ultimate Yield Strength	38-65 MPa	[30]	35 MPa	[35]

Actuators The requirements that concern the fabrication of the actuators are different than for the structural elements. The primary requirement for the actuators is that the cylinders should have a high surface quality to minimize friction and leakage between the piston and the cylinder wall, as discussed in section 2.1. It was emphasised how the actuators are to be fabricated without extensive post processing such as machining or using a reamer. Secondly, the fabrication method should yield parts with a high dimensional accuracy and repeatable mechanical performance. Finally, the weight of the cylinders should be minimized to increase the force to weight ratio, and the cylinders should be able to withstand the operating pressure P_{work}. Similarly as done for the structural elements, both FDM and SLA were considered as a fabrication method for the actuators. SLA is known for its high surface quality and the surface quality of FDM printed parts is known to be low [33]. Moreover, the print accuracy and resolution of SLA is higher than that of FDM, according to an established manufacturer of 3D printers [29]. Finally, the Formlabs Clear 03 resin has a lower density and a higher yield strength, as shown in table 2.3. Considering the requirements and the specifications of both the fabrication method and the material, SLA was chosen as the fabrication method for the actuators. The Clear 03 resin is compatible with the working fluid, hydraulic oil, which can act as a solvent [28]. The orientation of the part with respect to the build plate during printing, possibly has an effect on the surface finish and texture of the cylinder. This means that the friction between the piston and the cylinder possibly depends on the print orientation. To test this hypothesis, the friction was measured in cylinders that are printed in different orientations. This experiment is elaborated on in section 2.3.

2.3. Evaluation method

2.3.1. Evaluation parameters

A prototype was made to test the performance of the prosthesis. All the fingers of the hand have the same operating principle and similar dimensions. The proximal and distal actuators that were used, are equal in each finger. Consequently, the performance of one finger was presumed to be representative for the other digits. Therefore, the prototype embodies the index finger, the thumb and part of the palm, as to save time and resources. The design was evaluated by determining how well it complies with the requirements. A set of evaluation parameters was used to make a quantitative comparison between the prototype and the requirements. The evaluation parameters for the actuators and the prototype are, respectively:

I Actuators

- Geometrical accuracy
- Static pressure
- Friction in the cylinder
- Weight

II Prototype

- Pinch force
- Closing time
- Weight

These parameters are determined through a set of experiments. In this section, the goal, setup and protocol of the experiments are discussed. Notably, the results from the experiments also function as a substantiation of design choices and validation of certain assumptions.

2.3.2. Actuator - Geometrical accuracy

Goal The goal of this experiment was to determine the dimensions of a set of SLA printed cylinders. The inner diameter, the wall thickness and the roundness were of interest. The set of cylinders consisted of proximal and distal actuators. Variations are made in both the print angle and the designed wall thickness. The aim was to compare the results and gain insight in any influence these parameters have on the geometrical accuracy of the printed parts.

Setup Eight cylinders were tested, all fabricated through SLA printing. Their design and fabrication parameters are shown in Table 2.4. Each cylinder was placed in a vice after being cleaned with a dry paper towel. A three point internal micrometer (Tesa S.A.) was used to perform the internal measurements (see Figure 2.10b). This device has a resolution of 1 µm. The outside diameter was measured using a micrometre with a resolution of 10 µm.

Protocol First, the internal diameter was determined in the middle of the cylinder, at approximately 14 mm from the top brim. This was done by performing a set of four measurements, each with the measurement tool rotated 90 degrees, in the horizontal plane, with respect to each other. The resulting contact points between the micrometer and the cylinder are visualized in Figure 2.10a. Secondly, the diameter at the top is the cylinder was determined, at approximately 4 mm from the brim. This was done in the same way as for the middle. Finally, the outside diameter was determined at both the middle and the top, at approximately the same height as the internal diameter. At both heights, two measurements were performed, each at rotated 90 degrees with respect to each other. Each value that was read from the micrometre was noted in Microsoft Excel.

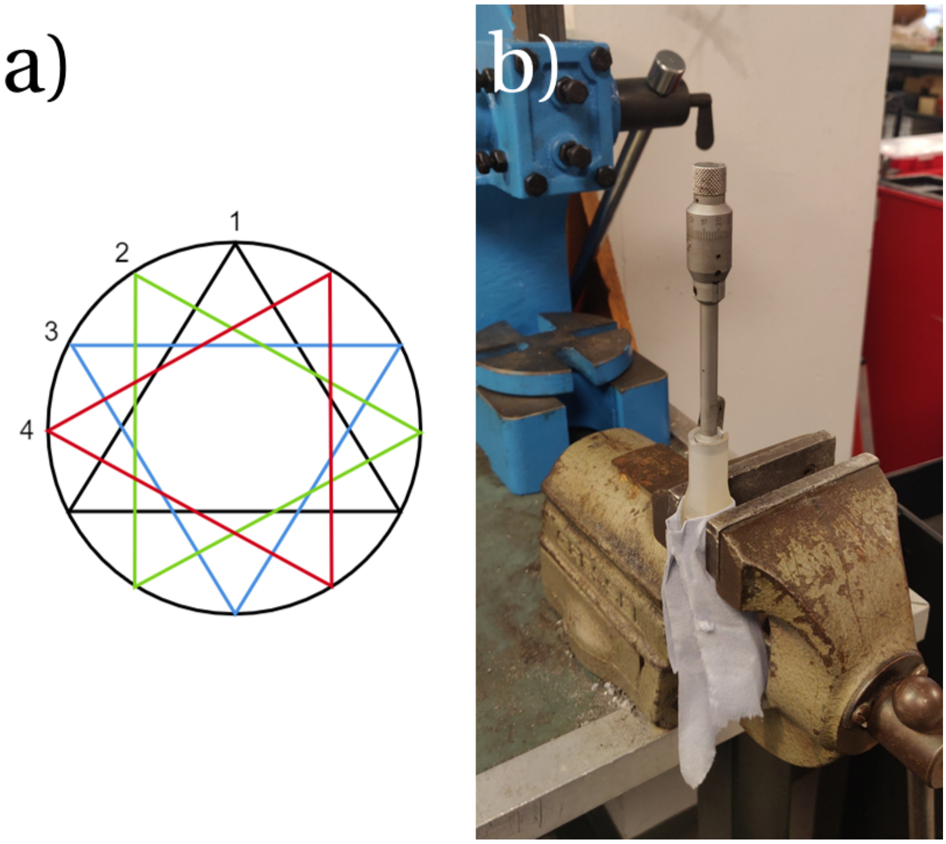

Figure 2.10: a) Visualization of the contact points between the micrometer and the cylinder when measuring the cylinder diameter. Each triangle represents one of the 4, 3-point measurements that was performed, rotated 90° with respect to each other,indicated with numbers 1-4. b) Picture of the internal micrometer in one of the cylinders. The cylinder is placed in a vice.

Table 2.4: Design and fabrication parameters of cylinders printed for measurements on geometry, pressure and friction. Cylinder code: the first number stands for the order of the cylinders, the letter for the wall thickness and the last two numbers denote the print angle.

	Cylinder code	Designed D_{in} [mm]	Designed s [mm]	Print angle [deg]
Proximal	1A90	10.3	1.65	90
	2A90	10.3	1.65	90
	3A45	10.3	1.65	45
	4A45	10.3	1.65	45
	5B90	10.3	1.18	90
	6C90	10.3	0.75	90
Distal	7D90	7.3	1.16	90
	8D45	7.3	1.16	45

2.3.3. Actuator - Static pressure

Goal The goal of this experiment was to determine what pressures the actuators can withstand and if pressurization leads to any plastic deformation. As discussed in section 2.2.2, the cylinders were designed to have a safety factor $Sf = 4$. The safety factor is defined in equation 2.22 as the ratio of the yield pressure P_{yield} over the estimated required operating pressure P_{work}. However, several assumptions were made in designing the actuators. If the actuator would fail, the pressure at which the actuator fails could be used to determine the actual safety factor. Secondly, by measuring the wall thickness and inside diameter of the cylinders before and after pressurisation, any plastic deformation could be observed. Three variations of the proximal actuator were used, each with a different wall thickness s. The cylinders each have a different safety factor: 2, 3 and 4, respectively. The cylinders that are used, are all printed at a 90 degree angle from the build plate.

Setup The actuator was clamped between a vertical press using two FDM printed clamping attachments. A 4x2.5 polyamide tube was connected to the tube connector of the cylinder. The other and of the tube was connected to a pressure sensor that measures up to 10 MPa (ATM/Ex Analog Pressure Transmitter, STS Sensor Technik). A data acquisition system (USB-6002 12-Bit DAQ, National Instruments) was used to connect the sensor to a laptop that runs LabVIEW 2018 to collect the data. Water was used as the working fluid. A schematic overview of this setup is depicted in Figure 2.11. A picture taken during the measurements is shown in Figure 2.12.

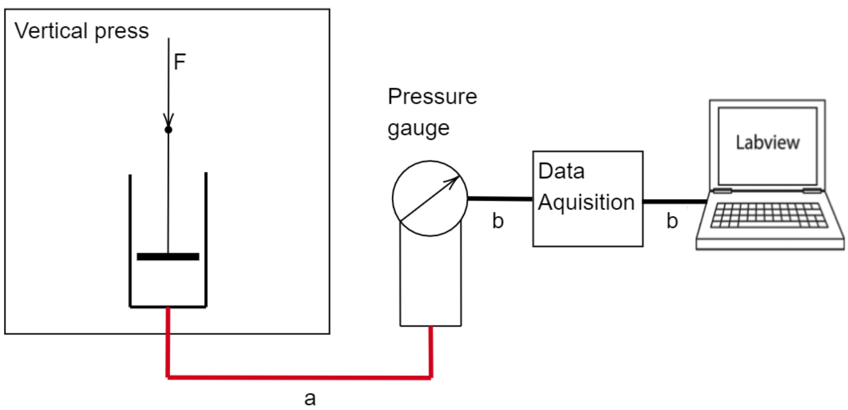

Figure 2.11: Schematic test setup of the pressure measurements. The tubes are denoted with an a, the wires with b.

Protocol The same experiment wass performed with each of the three cylinders, according to the following protocol:

1. The dimensions of the cylinder are measured using an internal micrometer, following the complete protocol as described in section 2.3.2.

2. The cylinder is placed vertically in the press. The initial pressure is zero. Turning the handle on the press, the pressure is increased from zero to approximately 1 MPa. After holding the handle of the vertical press at the same level for a few seconds, the pressure is relieved gradually.
3. The dimensions of the cylinder are measured, in the same manner as at step 1.
4. The cylinder is placed vertically in the press. The initial pressure is zero. Turning the handle on the press, the pressure is increased from zero to 3.5 MPa, or until failure occurs. The pressure is relieved gradually.
5. The dimensions of the cylinder are measured, in the same manner as at step 1.
6. The cylinder is placed vertically in the press. The initial pressure is zero. Turning the handle on the press, the pressure is increased from zero to 4.5 MPa or until failure occurs. The pressure is relieved gradually.
7. One final time, the dimensions of the cylinder are measured, in the same manner as at step 1.

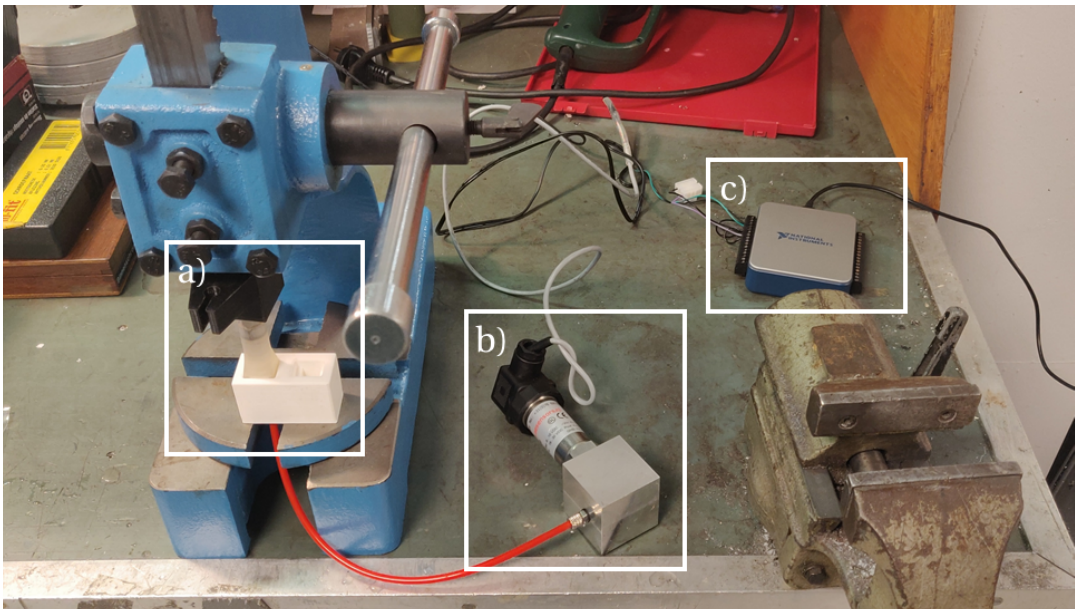

Figure 2.12: Setup of the pressure measurements with: a) the cylinder placed in a vertical press, b) the pressure sensor, c) a data acquisition system. The cable at the right side of the frame, is connected to a laptop running LabView.

2.3.4. Actuator - Friction in the cylinder

Goal The primary goal of this experiment was to compare the friction in cylinders that are printed at a different print angle. Therefore, the friction force on the piston was determined, as it moves through the cylinder. To do this, the pressure was measured during a dynamic operating cycle of the actuator. First the piston was extended to lift a certain weight, then, the piston is retracted partially while still lifting the same weight. The friction force on the piston is always opposite to its movement, the force of the load on the piston is always in the direction of gravity. During the extension phase, the friction force and the load are in the same direction. During retraction, the friction force and the load are in opposite directions. Therefore, the required pressure to carry the load is expected to be different for both phases. The experiment was designed to measure this difference. Secondly, the output force of the actuator at different pressures could be determined. By comparing this to the theoretical force output at that pressure, the hydraulic efficiency could be determined. To limit the number of variables, the measurements were performed on the proximal cylinders, as the same physical principles apply to both the proximal and distal actuator. As discussed in section 2.2.3, two types of the proximal cylinder were used: printed at 90 degrees and 45 degrees with respect to the build plate. As such, the friction force could be compared for these different print orientations. The two cylinders that were used, and their design parameters, can be found in Table 2.4, using cylinder codes: 3A45 and 5B90.

Setup The lead cylinder that was used to pressurise the system, was placed in a vertical press. A 4x2.5 polyamide tube was connected to the tube connector of the lead cylinder. The other and of the tube was connected to the cylinder of the actuator. The cylinder base of the actuator was clamped vertically in a vice using a FDM printed clamping attachment. A second attachment was mounted on the piston with a cable connected to it. The cable can be used to suspend weights from the piston. In between the cylinders, using a T-connector, a pressure sensor was placed that measures up to 10 MPa (ATM/Ex Analog Pressure Transmitter, STS Sensor Technik). To collect the data, a data acquisition system (USB-6002 12-Bit DAQ, National Instruments) connected the sensor to a laptop that runs LabVIEW 2018. A schematic overview of this setup is depicted in Figure 2.13. An image of the setup is shown in Figure 2.16.

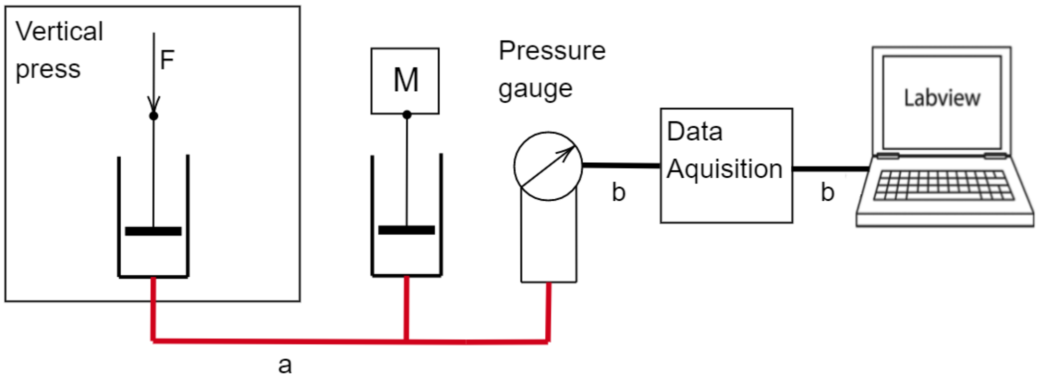

Figure 2.13: Schematic test setup of the friction measurements. The tubes are denoted with an a, the wires with b.

Protocol

1. Initially, the lead piston is extended and the actuator piston is retracted, with an initial system pressure of zero. A weight of 6.49 kg is suspended on the actuator piston. The handle of the vertical press is turned to compress the lead cylinder; the actuator piston extends to about 16 mm and lifts the weights.

2. After a minimum of 2 seconds, the handle of the vertical press is turned back and the actuator piston retracts 8 mm.

3. After a minimum of 2 seconds, the piston is extended back to about 16 mm.

4. Finally, after a minimum of 2 seconds the pressure is relieved and the system pressure is back to zero.

These steps were repeated five times per cylinder.

2.3.5. Prototype - Pinch force

Goal In this experiment, the pinch force of one of the fingers of the prosthesis was determined. The required pinch force of 30 N was used to calculate the operating pressure of the actuators. However, in these calculations, a simplified model of the hand was used in which the phalanges were considered rigid. Also, the joints and the piston were assumed frictionless. Insight in the actual losses due to friction and elastic deformation can be gained by comparing the theoretical pressure force relation with an experimentally determined pressure force characteristic. To gain insight in the pressure force relation, the pinch force was measured at different pressures. Using this data, the force efficiency can be calculated. It was assumed that the force efficiency of one finger is representative of that of the other fingers, therefore, the experiment was conducted with the prototype consisting of one finger together with part of the palm with thumb.

Setup For this experiment, measurements were performed on the prototype. The base of the prototype was placed in a vice. A 4x2.5 polyamide tube connected the actuators to the pump. The pump was controlled using a potentiometer connected to an Arduino. Using a clamp stand, a load cell was positioned at the thumb at the place of contact with the fingertip (Figure 2.17). The load cell is 19 mm wide in the pinched direction and measures up to 45 N (Futek Advanced Sensor Technology Inc.). A pressure sensor was connected to the hydraulic circuit, using a T-connector, that measures up to 10 MPa (ATM/Ex Analog Pressure Transmitter, STS Sensor Technik). A data acquisition system (USB-6002 12-Bit DAQ, National Instruments) connected the sensor to a laptop that runs LabVIEW 2018. The setup was depicted schematically in Figure 2.14. Figure 2.15 shows the hydraulic and electric circuits. Hydraulic oil was used as the working fluid.

Protocol

1. Initially, the finger is extended at 0 degrees flexion and the pistons of both actuators are retracted. The pump is used to flex the finger. The fingertip makes contact with the object.

2. The pressure is increased until the measured force is about 15 N.

3. The power to the pump is set to 0. After about one second, the direction of the pump is reversed.

4. The finger is opened by turning on the pump, until the finger is at 0 degrees flexion.

These steps were repeated 6 times, first with a pinch force of around15 N, then 23 N, and finally 30 N.

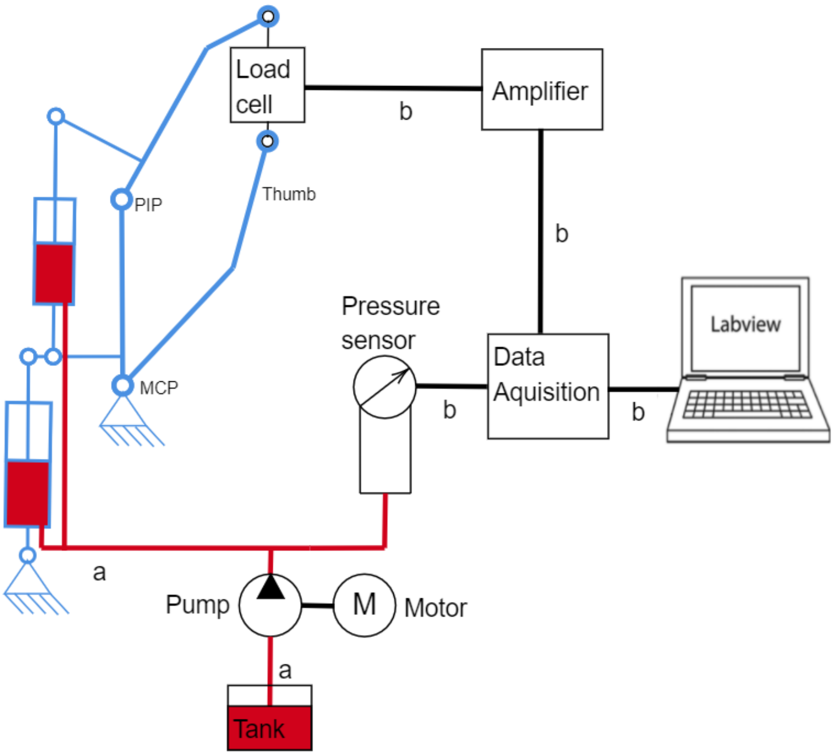

Figure 2.14: Schematic test setup of the pinch force measurements.The tubes are denoted with an a, the wires with b.

.

2.3.6. Prototype - Closing time

Goal The prosthetic hand should have a closing time of 0.25–1.0 seconds, as described in section 2.1.1. The goal of this experiment was to determine the closing time of a single finger. Using this, the closing time of the hand with four fingers can be estimated. The closing time depends on the performance of the pump. Therefore, for this experiment the pump was used as the pressure source. The closing and opening time was determined based on both a video recording and a measurement of the pressure over time.

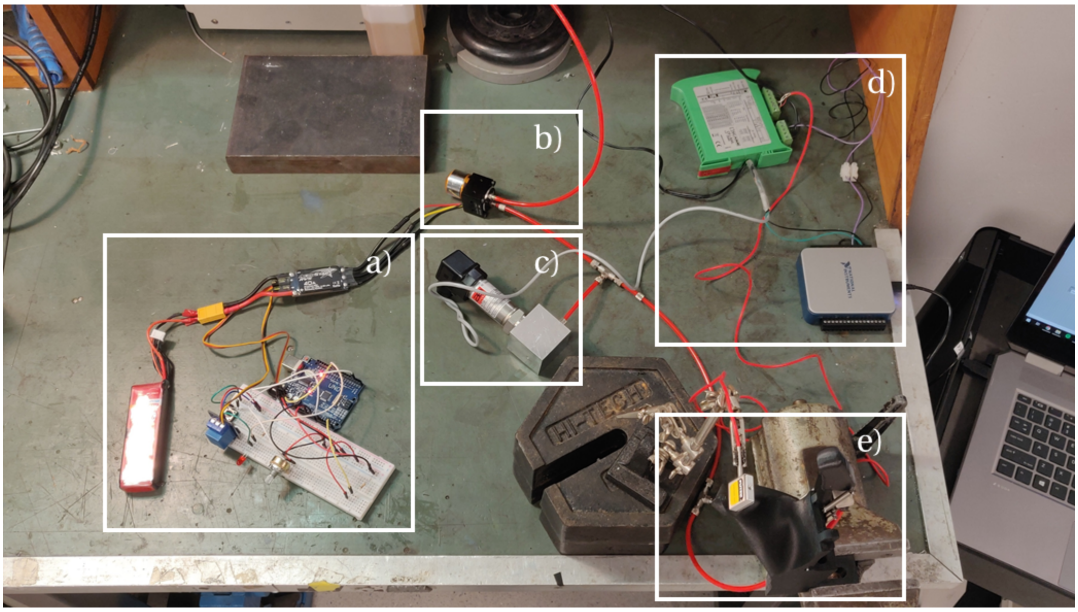

Figure 2.15: Setup of the pinch force measurements. Here, a) is the electric circuit with from left to right: the battery, the breadboard with potentiometer and Arduino Uno, and the ESC. Then, b) is the motor and pump, c) the pressure sensor, d) the amplifier and the data acquisition system, and e) the prototype with the load cell. The cable at the right side of the frame, is connected to a laptop running LabView.

Setup The prototype consisting of one finger connected to a cutout of the palm was used for this experiment. The cutout was placed in a vice. The actuators are connected to the pump with a 4x2.5 mm polyamide tube. A pressure sensor was connected between the pump and the actuators, using a T-connector. The sensor measures up to 10 MPa (ATM/Ex Analog Pressure Transmitter, STS Sensor Technik). A data acquisition system (USB-6002 12-Bit DAQ, National Instruments) connected the sensor to a laptop that runs LabVIEW 2018. A phone placed in a tripod was used to capture the finger on video. Hydraulic oil was used as the working fluid.

Protocol

1. Initially the finger is at 0 degrees flexion. Then, the pump is turned on to ~ 50% power.
2. After the finger touches the thumb, the pump is turned off and finger is kept in a pinching configuration for approximately 1 second.
3. The pump is reversed.
4. The pump is turned on and the finger opens. As the finger reaches 0 degrees flexion again, the power is turned off.

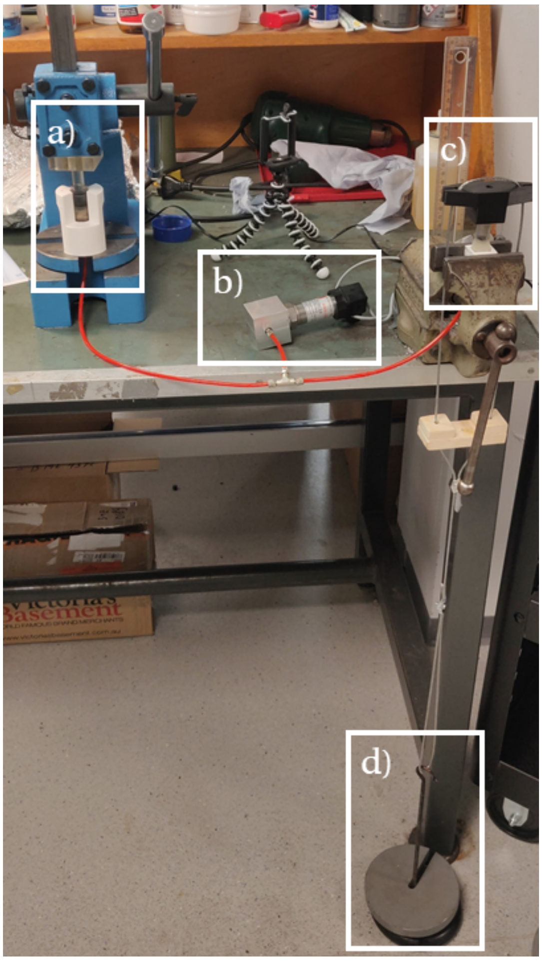

Figure 2.16: Setup of the friction measurements, where a) is the lead cylinder placed within a vertical press, b) is the pressure sensor, c) is the cylinder of which the friction force is to be determined, together with a cable suspension system, and d) is the mass attached to the cable.

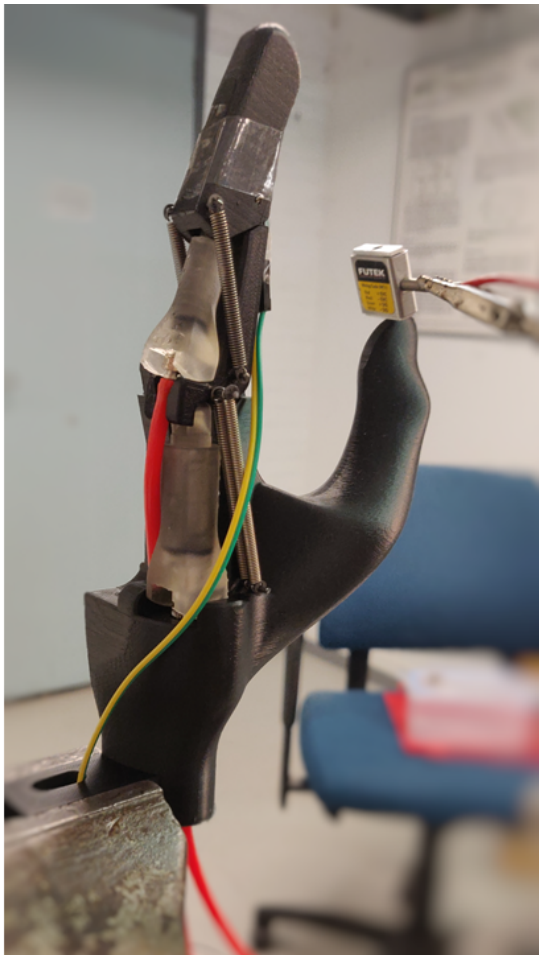

Figure 2.17: Prototype of the one of the fingers of the prosthesis. This was part of the setup used for the pinch force measurements. On the right side of the image, a lead cell is visible.

3 Results

3.1. Design and fabrication results

3.1.1. Hand design

Dimensions phalanges The average human hand length of a Dutch male is 196 mm, based on the anthropomorphic database DINED. The average index finger length is 78 mm. A silicone cosmetic hand was selected from Regal Prosthetics LTD. The model that matches the aforementioned dimensions most closely, is the 101L XL1 Male glove. It has similar dimensions as commercially available prosthetic hands of size M. The dimensions of this glove as defined by the manufacturer, are shown in Figure 3.2. The dimensions of individual hand segments were determined using their relative dimensions with respect to the entire finger. This proportionality was extracted from a paper by Buryanov [13]. The notation that is used for the metacarpals and phalanges, is shown in Figure 3.1. The length of each finger segment as a percentage of finger length, is shown in Table 3.1. The length of the phalanges in the mechanism was calculated by multiplying its portion of the total finger, with the finger length of the glove for the respective digit. The results are described in Table 3.2. As mentioned in section 2.2.1, the phalanxes were designed to have a high bending stiffness. The phalanges are fabricated through FDM. During FDM printing, a solid perimeter of multiple layers was formed and the space in between is filled according to an infill pattern that has an infill density that is less than 100% [3]. Therefore, the phalanx could be compared to a hollow beam: an elongated structure with a low density centre and solid perimeter. In the design, the material was placed towards a perimeter that is as wide as the dimensions of the silicone glove allow.

Table 3.1: Length of finger segments as a percentage of total finger length. The data in the first and second column is adopted from Buryanov [13].

	tip + pd [%]	pm [%]	pp [%]
Index finger	0.28	0.31	0.41
Middle finger	0.26	0.33	0.41
Ring finger	0.28	0.34	0.38
Little finger	0.34	0.32	0.34
Thumb	0.49	-	0.51

Moment arm and cylinder dimensions Recall that the transmission ratio between the middle-distal phalanx and the proximal phalanx can be calculated using equation 2.7 from section 2.2.1, and that for the hand to achieve both a stable pinch grip and a power grip, the transmission ratio should comply with the following constraint:

$$\frac{2\left(M-L_0^2\right)\left(M+(L_0-L_1)^2\right)}{4M\left(L_0^2+M\right)} \leq R \leq \frac{(L_0-L_1)\left(M+(L_0-L_1)^2\right)}{M(L_0-2L_1)+L_0(L_0-L_1)^2} \tag{2.4}$$

Figure 3.1: Notation of hand segments as used by Buryanov [13]. I–V – finger index numbers; tip – soft tissues of the finger tip; pd – distal phalanx; pm – medial phalanx; pp – proximal phalanx; m – metacarpal; pp* – web height from metacarpophalangeal joint; d – the entire length of the finger skeleton from metacarpophalangeal joint to the tip of the distal phalanx bone; de – the entire finger length from the web space to the very tip of the finger including the soft tissues of the tip.

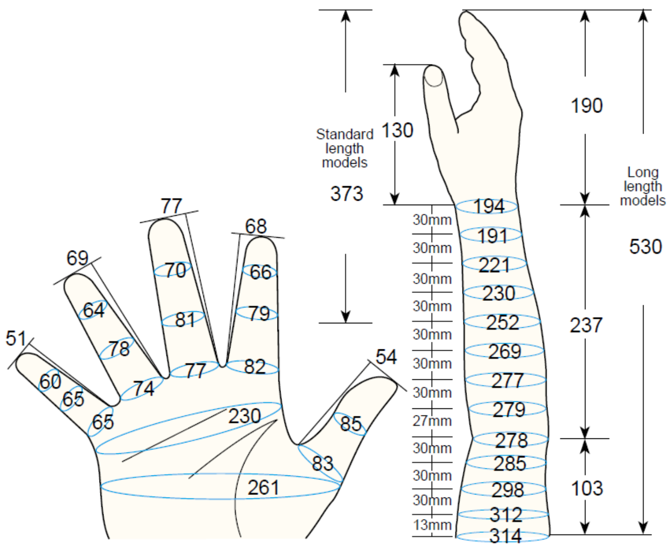

Figure 3.2: Dimensions of the selected silicone cosmetic glove (101L XL1 Male glove, Regal Prosthetics LTD.).

Table 3.2: Length of the designed components. The total finger length is based on the dimensions of the cosmetic glove. The tip dimension is based on the thickness of the glove.

	tip [mm]	pd [mm]	pm [mm]	pp+pp* [mm]	Total finger [mm]
Index finger	2.0	16.9	21.0	39.4	68.0
Middle finger	2.0	18.3	25.5	42.5	77.0
Ring finger	2.0	17.5	23.2	37.6	69.0
Little finger	2.0	15.3	16.3	28.6	51.0
Thumb	2.0	26.7	-	27.3	54.0

In equation 2.4, the first term is considered to be R_{min} and the second term is R_{max}. The values for R_{min} and R_{max} were evaluated using the dimensions of the phalanges of the index finger as defined in Table 3.2. L_0 was approximated to be $0.5 \cdot L_1$. This results in the following plot shown in Figure 3.3, showing the constraints on the transmission ratio versus the diameter of the object being pinched. If the transmission ratio $R = 0.41$, the index finger can achieve a stable pinching grip for objects up to a diameter of 85 mm. The torque delivered by the actuators scales with the radius squared, based on equation 2.6. To maximize the torque delivered by the actuators around the MCP and PIP joints, the radius of the cylinders was maximized. The radius of the cylinders are constraint by the silicone glove. The inner radii of the index finger of the silicone glove are shown in Table 3.3. In Appendix D, both the phalanges and the actuators are shown within the perimeter of the silicone glove. The internal diameter of both cylinders and the moment arm of both actuators are shown in Table 3.4. The dimensions of the actuators were determined based on the parameters of the index finger. First the parameters of the proximal actuator were determined, then the parameters for the distal actuator, using the relation for the transmission ratio given in equation 2.7. For the proximal cylinder, this is the largest, round numbered internal diameter such that the mechanism fits within the glove as the finger flexes. Some assumptions on the geometry were made in determining this. The most notable assumptions are that the cylinder wall is less than 2 mm thick, and that the phalanx is sufficiently stiff with a width of 5 mm. The cylinder wall thickness is addressed in section 3.1.2. Substituting the dimensions from Table 3.4 in equation 2.7, gives the transmission ratio without springs. The transmission ratio is 0.43, which is similar to that of the Delft Cylinder Hand [64]. With a transmission ratio of 0.43, the finger can achieve a stable pinch grip on objects with a diameter of 78 mm.

Table 3.3: Inside diameter of the index finger of the silicone glove. The dimensions are calculated at the joints, assuming that the cross section of the finger is a circle, using data provided by the manufacturer (Regal Prosthetics LTD.).

Joint	$P_{outside}$ [mm]	$D_{internal}$ [mm]
MCP	82	22.1
PIP	79	21.1
DIP	66	17.0

Table 3.4: Cylinder radius and moment arm of the proximal and distal actuator.

	$r_{cylinder}$ [mm]	$a_{actuator}$ [mm]
Proximal	5	8
Distal	3.5	7

Springs The spring characteristics of the chosen springs are shown in Table 3.5. The points of engagement can be seen in Figure 3.5a and 3.6a, being the hole in the lower left corner of each phalanx. Through these holes, an axle is placed. On both sides of the phalanx, the springs are mounted on this axle, secured by a circlip. The actual driveback force $F_{driveback,springs}$ was calculated for the proximal actuator, and depends on the spring characteristics, the geometry and the angle of the MCP joint. During pinching, the average driveback force is 25.5 N. This is larger than the estimated friction force in the cylinder (10-20 N). Finally, the transmission ratio should still comply with the constraints set out by equation 2.4. Using the spring characteristics and equation 2.10, the average transmission ratio during a pinch manoeuvre was determined to be $R_{average} = 0.44$. This is close to the designed transmission ratio without springs, $R = 0.41$. Moreover, a stable

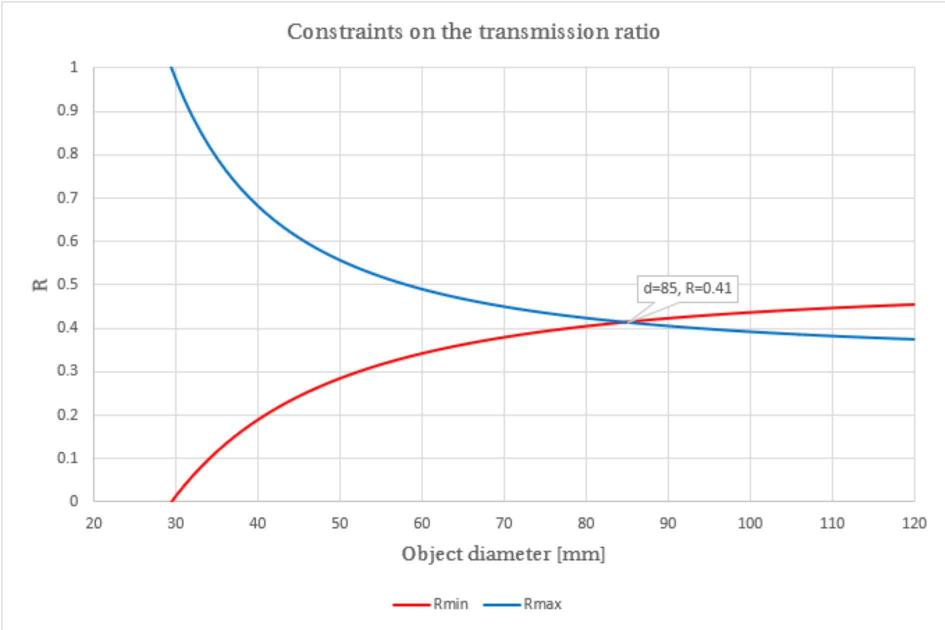

Figure 3.3: Minimum and maximum value of the transmission ratio R, as calculated using equation 2.4 and the dimensions of the phalanges.

pinch grip can be achieved on objects with a diameter of 72 mm, which is the maximum opening distance between the index finger and the thumb.

Table 3.5: Spring characteristics of the springs used to open the hand. Each spring is used in pairs.

	Springs proximal	Springs distal
c_{spring}	1.87 N/mm	0.37 N/mm
F_0	6.81 N	1.94 N
L_0	46.1 mm	31.8 mm
D_{out}	3.5 mm	3.7 mm

Joints In this paragraph, the result of the design method for the joints is discussed. The joints in the mechanism were divided into three groups, per group a joint type is chosen. For Group 1, the MCP and PIP joint, it was decided to use a sliding hinged joint with a steel axle. Using a steel axle instead of printing the entire joint, allows for a much smaller axle diameter and thus a smaller friction torque, based on equation 2.11. Moreover, using a metal axle allows the joint to be considerably smaller than a fully 3D printed joint would be. A spring steel wire iss used for the axle, with a diameter of 1.5 mm. The ROM of both the MCP and PIP joint is constraint to be 0 to 90 degrees flexion. For Group 2, the joints at the piston, a sliding curved joint was chosen. As the joints are only loaded under compression, there is an opportunity to minimize the number of parts and assembly steps. This was given priority over minimizing the friction. There are some transversal forces on the joint, therefore the rolling friction joint was not selected, for the risk of slip and break away. A toothed rolling joint was not used at is deemed unfit due to the challenging fabrication of the toothed structure and the risk of fracture. The radius of the curved surface of the sliding joint is a compromise between minimizing the friction torque and minimizing the risk of plastic deformation of either of the two surfaces. Plastic deformation leads to immense energy loss or failure. Two small knobs are added at both sides of the joint at the distal piston, to prevent the piston from dislocating. The knobs are placed in two small notches in the middle-distal phalanx, see Figure 3.5b. Similarly, the joint at the proximal piston has a notch that prevents the piston from moving outside of the plane in which the finger flexes (Figure 3.6b). The joints at the cylinder, Group 3, are executed as rolling friction joints. The risk of slip or break away are less than for the joints at the piston as the transversal forces on the joint are limited and the ROM is just 5 degrees. The friction in this joint is rolling friction and driven by the normal load. As the surface area and radius have a minimal influence on the friction, the surface area was maximized to evade the risk of plastic deformation. The rounded surface of the cylinder rolls on the flat surface of the proximal phalanx. When the finger is extended at 0 degrees flexion, the rounded surface of the cylinder is lined up with the curvature of the proximal phalanx. This joint can be assembled in a single step and does not require any extra parts.

Detailed design The final design for the prosthesis is shown in Figure 3.4. The detailed design of both phalanges are shown in Figures 3.5 and 3.6. Technical drawings of all individual parts are listed in Appendix D. Figure 3.7 shows a cross section of the mechanism in both extended and pinched configuration.

3.1.2. Actuator design

Force and pressure To determine the required operating pressure P_{work} for the finger to pinch with 30 N, the proximal actuator is considered. The equilibrium equation around the MCP joint is evaluated, following equation 2.14:

$$-T_{actuator} + T_{springs} + T_{pinch} = 0 \tag{2.14}$$

Counter clockwise rotation was defined as positive. First, the reaction torque of the object that is pinched was calculated:

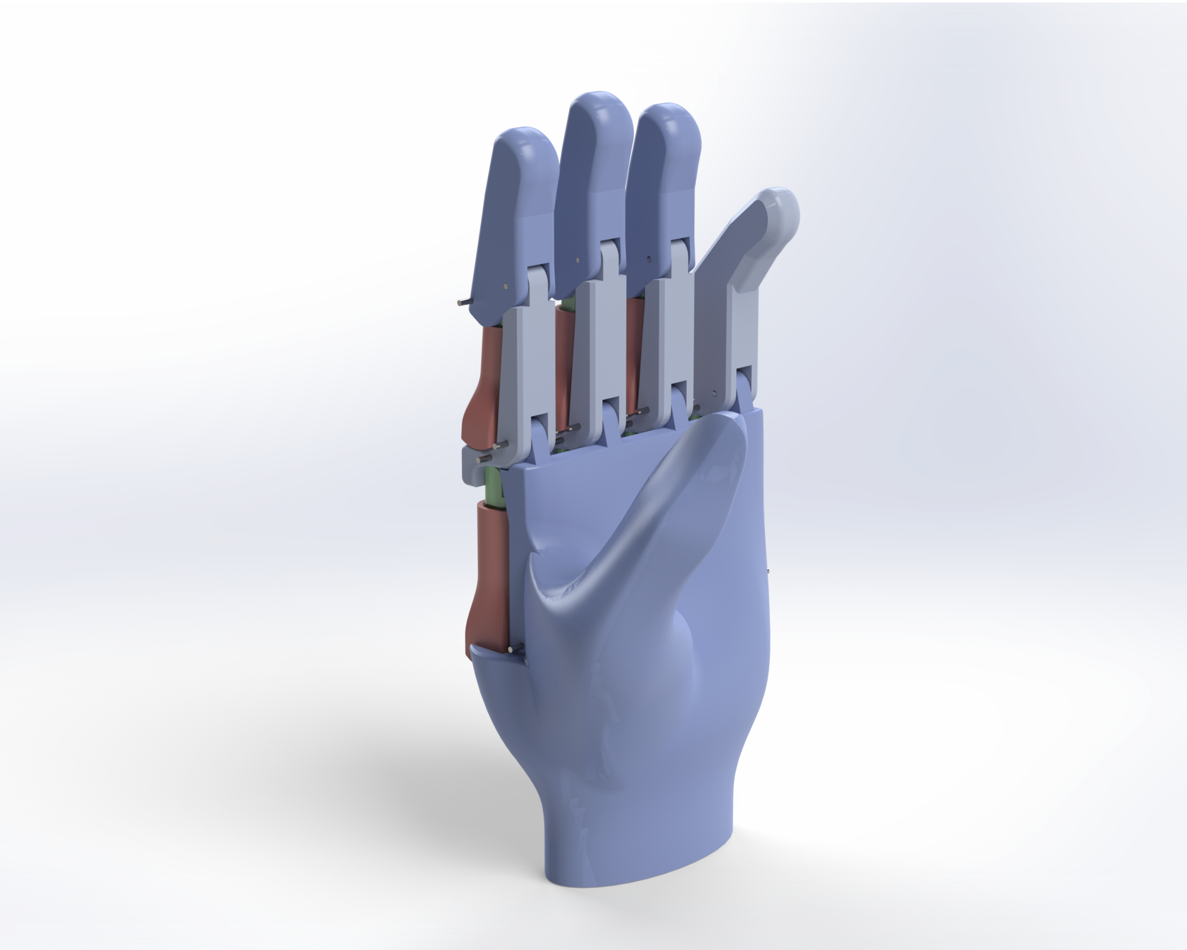

Figure 3.4: Rendered image of the final design for the prosthesis. The structural elements are shown in light and darker blue, the cylinders in red and the pistons in green.

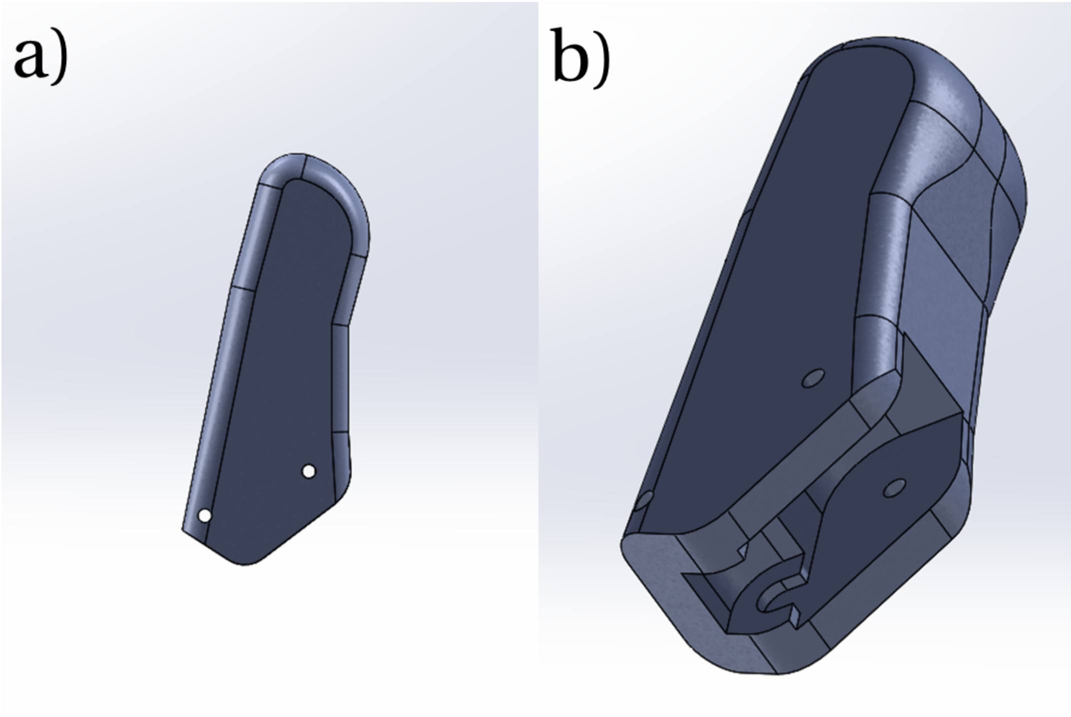

Figure 3.5: Final design of the middle-distal phalanx. Here, a) is a side view of the phalanx, and b) shows the joint cavity of both the PIP joint and the joint of the distal piston. The technical drawings of this part can be found in Appendix D.

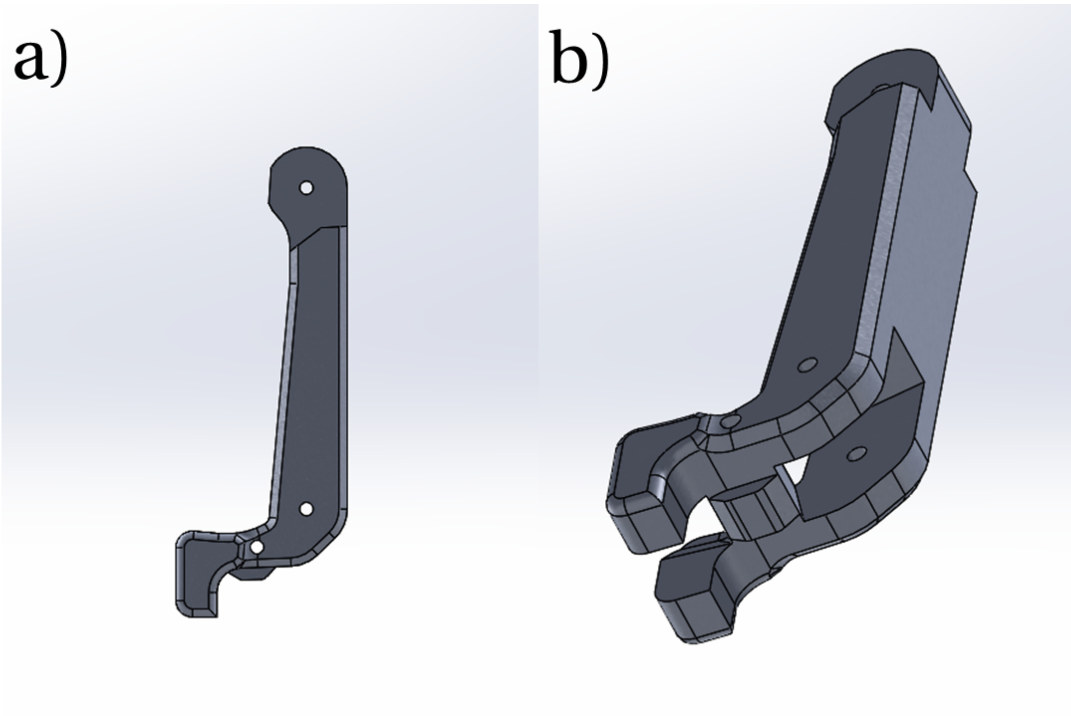

Figure 3.6: Final design of the proximal phalanx. Here, a) is a side view of the phalanx, and b) shows the joint cavity of the MCP joint and the contact surface of the proximal phalanx with the proximal piston. The technical drawings of this part can be found in Appendix D.

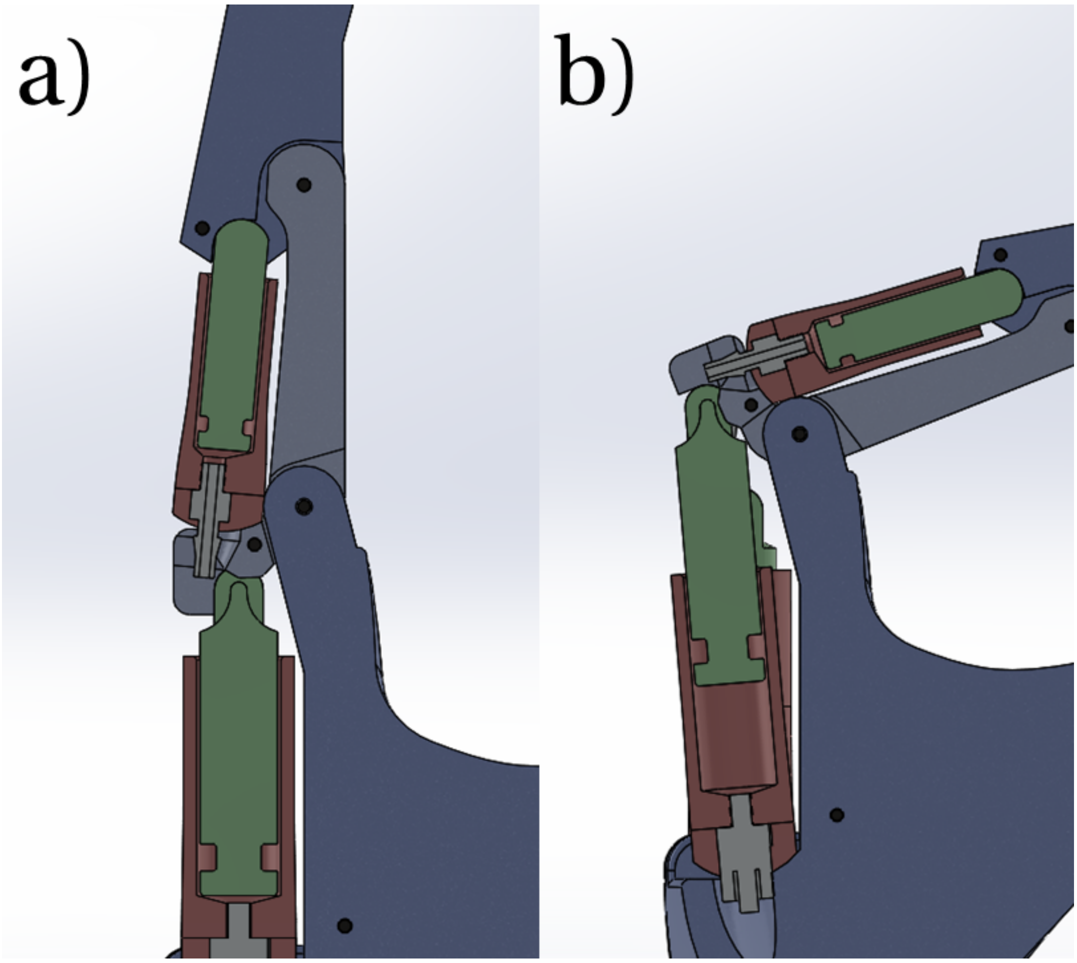

Figure 3.7: Cross section of the mechanism in both a) extended and b) pinched configuration.

$$\begin{aligned} T_{pinch} &= F_{pinch} \cdot a_{pinch} \\ &= F_{pinch} \cdot (L_{dist} + (L_{mid} + L_{prox}) \cdot cos(\theta)) \\ &= 30\,\mathrm{N} \cdot (0.0168\,\mathrm{m} + (0.0210\,\mathrm{m} + 0.0394\,\mathrm{m}) \cdot cos(15°) \\ &= 2.257\,\mathrm{Nm} \end{aligned} \tag{3.1}$$

Note that θ is the angle of the fixated DIP joint. Both F_{spring} and a_{spring} depend on the angle of flexion of the proximal phalanx, ϕ. As discussed in section 2.2.2, it was assumed that the object that is pinched, has a negligible thickness. The angle of flexion of the MCP joint in this configuration was determined to be $\phi = 68.35°$, based on the detailed design. Evaluating $\Delta L(\phi)$ and $a_{spring}(\phi)$, yields: $dL(68.35°) = 0.0092\,\mathrm{m}$ and $a_{spring}(68.35°) = 0.0055\,\mathrm{m}$. Substituting eq. 2.16 in eq. 2.15 and filling in all parameters for $\phi = 68.35°$, gives:

$$\begin{aligned} T_{spring} &= 2 \cdot (c_{spring} \cdot \Delta L(68.35°) + F_0) \cdot a_{spring}(68.35°) \\ &= 2 \cdot (1870\,\mathrm{N/m} \cdot 0.0092m + 6.81\,\mathrm{N}) \cdot 0.0055\,\mathrm{m} \\ &= 0.3183\,\mathrm{Nm} \end{aligned} \tag{3.2}$$

Then, $T_{actuator}$ can be calculated by rewriting and evaluating the equilibrium equation:

$$\begin{aligned} T_{actuator} &= T_{pinch} + T_{spring} \\ &= 2.257\,\mathrm{Nm} + 0.3183\,\mathrm{Nm} = 2.576\,\mathrm{Nm} \end{aligned} \tag{3.3}$$

Now, the actuator force can be calculated:

$$
\begin{aligned}
F_{actuator} &= \frac{T_{actuator}}{a_{actuator}} \\
&= \frac{2.576\,\mathrm{Nm}}{0.0125\,\mathrm{m}} \\
&= 206.6\,\mathrm{N}
\end{aligned}
\tag{3.4}
$$

Finally, the required operating pressure in the cylinders to achieve a pinch force of 30 N is:

$$
\begin{aligned}
P_{work} &= \frac{F_{actuator}}{A_{actuator}} \\
&= \frac{206.6\,\mathrm{N}}{7.840 \cdot 10^{-5}\mathrm{m}} \\
&= 2.6\,\mathrm{MPa}
\end{aligned}
\tag{3.5}
$$

Recall that this is an estimation as friction and other losses are not taken into account in this calculation. It was assumed that during pinching, the middle distal phalanx is pressed against the extension stop and the flexion angle of the PIP joint is 0 degrees. To test if this assumption is correct, the equilibrium equations were evaluated around the PIP joint. Evaluating the different torques acting around the PIP joint, gives the following reaction torque:

$$
\begin{aligned}
T_{result} &= -T_{actuator,distal} + T_{pinch,distal} + T_{spring,distal} \\
&= 0.5203\,\mathrm{Nm}
\end{aligned}
\tag{3.6}
$$

As the resulting torque is positive, the phalanx has the tendency to rotate counter clockwise. Therefore, the phalanx is pressed against the extension stop that exerts a clockwise torque such that the system is in equilibrium. This confirms the assumption that the PIP joint remains at 0 degrees flexion during pinching.

Cylinder dimensions In section 2.2.2 the cylinder ability to withstand internal pressure is discussed, among other properties. In this section, the results of the calculations on minimum wall thickness is discussed. Recall that the minimum wall thickness of the cylinder can be calculated using equation 2.21 [73]:

$$
s = r_i \left(\sqrt{\frac{\sigma_w + p_i}{\sigma_w - p_i}} - 1 \right) \tag{2.21}
$$

Here, σ_a is the tensile strength at yield. The Formlabs Clear resin that is used for the actuators, has a tensile stress at yield of 38 to 65 MPa as shown in Table 2.3. To calculate the minimum wall thickness, σ_a= 38 MPa was used. The yield strength is only 65 MPa if the parts are cured at 60° Celsius for 1 hour. The cylinders are designed to have a safety factor of 4, therefore the following pressure was used in calculating the wall thickness:

$$
\begin{aligned}
P_{Sf=4} &= 4 \cdot P_{work} \\
&= 4 \cdot 2.63\,\mathrm{MPa} \\
&= 10.53\,\mathrm{MPa}
\end{aligned}
\tag{3.7}
$$

Substituting the values for the yield strength and pressure into equation 2.21, yields:

$$\begin{aligned}
Proximal: \quad s_p &= 5.0 \cdot \left(\sqrt{\frac{38\,\mathrm{MPa} + 10.53\,\mathrm{MPa}}{38\,\mathrm{MPa} - 10.53\,\mathrm{MPa}}} - 1 \right) = 1.64\,\mathrm{mm} \\
Distal: \quad s_d &= 3.5 \cdot \left(\sqrt{\frac{38\,\mathrm{MPa} + 10.53\,\mathrm{MPa}}{38\,\mathrm{MPa} - 10.53\,\mathrm{MPa}}} - 1 \right) = 1.15\,\mathrm{mm}
\end{aligned} \tag{3.8}$$

In calculating the minimum wall thickness, the assumption was made that the cylinders are thick walled. Using the calculated values of the wall thickness, the criterion for thin walled cylinders can be evaluated:

$$\begin{aligned}
Proximal: \quad \frac{s_p}{d_i} &= \frac{1.64\,\mathrm{mm}}{10\,\mathrm{mm}} = 0.164 \not< \frac{1}{20} \\
Distal: \quad \frac{s_d}{d_i} &= \frac{1.15\,\mathrm{mm}}{7\,\mathrm{mm}} = 0.164 \not< \frac{1}{20}
\end{aligned} \tag{3.9}$$

This shows that the assumption that the cylinders can not be considered thin walled, is correct. Finally, in section 2.2.1, the assumption was used that $s_p < 2\,\mathrm{mm}$; this is also confirmed.

Piston and sealing In this section, the result of the seal design is discussed. For both the cylinder sizes, the selected O-ring size and material, and gland dimensions are elaborated on. First for the proximal actuator, then for the distal cylinder, respectively.

Proximal

The selected O-ring has an outer diameter $D_{out} = 10\,\mathrm{mm}$, equal to the cylinder bore. The selected cross section is $D_{cross} = 2.5\,\mathrm{mm}$, as recommended for a seal with this diameter [53]. The piston groove diameter PGD that is required to achieve the desired squeeze ratio $r_{sq} = 10\%$, were determined using equations 2.23 and 2.24 discussed in section 2.2.2. First, the squeezed cross section $D_{cross,squeezed}$ was calculated:

$$\begin{aligned}
D_{cross,squeezed} &= (1 - r_{sq}) \cdot D_{cross} \\
&= (1 - 0.1) \cdot 2.5\,\mathrm{mm} \\
&= 2.25\,\mathrm{mm}
\end{aligned} \tag{3.10}$$

Then the piston groove diameter is:

$$\begin{aligned}
PGD_{proximal} &= D_{out} - 2 \cdot D_{cross} \\
&= 10 - 2 \cdot 2.25\,\mathrm{mm} \\
&= 5.5\,\mathrm{mm}
\end{aligned} \tag{3.11}$$

Distal

The O-ring in the distal actuator has an outer diameter $D_{out} = 7\,\mathrm{mm}$. Its cross section is $D_{cross} = 1.5\,\mathrm{mm}$. The squeezed cross section and the piston groove diameter were calculated as follows:

$$\begin{aligned}
D_{cross,squeezed} &= (1 - r_{sq}) \cdot D_{cross} \\
&= (1 - 0.1) \cdot 1.5\,\mathrm{mm} \\
&= 1.35\,\mathrm{mm}
\end{aligned} \tag{3.12}$$

$$
\begin{aligned}
PGD_{distal} &= D_{out} - 2 \cdot D_{cross} \\
&= 7 - 2 \cdot 1.35\,\mathrm{mm} \\
&= 4.3\,\mathrm{mm}
\end{aligned} \tag{3.13}
$$

A complete list of all dimensions of the O-ring seal for both the proximal and distal actuator, is shown in Table 3.6. The meaning of the parameters are illustrated in Figure 2.7. The selected O-rings are made from nitrile butadiene rubber (NBR). According to Eriks technical handbook on O-rings, NBR has a high wear resistance and performs well compared to other elastomers [25]. Importantly, it is compatible with hydraulic oils. Alternative O-ring materials are ethylene propylene diene monomer (EPDM) and VQM silicone. However, the former is not compatible with hydraulic oils and the latter has a relatively low tensile strength and wear resistance [25].

Table 3.6: Symbols and value of the design parameters for the cylinder and O-ring seal for both the proximal and distal actuator.

	Symbol	Proximal [mm]	Distal [mm]
Cylinder bore diameter	$D_{cylinder}$	10	7
O-ring outer diameter	D_{out}	10	7
O-ring cross section	D_{cross}	2.5	1.5
Piston outer diameter	D_{piston}	9.5	7.5
Piston groove diameter	PGD	5.5	4.3
Piston groove width	PGW	3.3	1.9

Tubing and connectors The type of tube that was selected has a 4 mm outside diameter and a 2.5 mm inside diameter (4x2.5). This tube is compatible with the tube connectors that are mounted on the pump that was selected as discussed in section 2.2.2. Secondly, the material of the tube was selected. The working pressure of the tube varies largely with the material. Table 3.8 shows a list of the most common used materials for high pressure, flexible tubing and their recommended working pressure. Based on this data, a polyamide tube was chosen as it has the largest allowable pressure. The tube connectors that are used for the actuators, are the same as those mounted on the motor. For the proximal actuator, there is enough room for a connector with a locking sleeve. At the distal cylinder, there is no room for a sleeve; a more simple connector is used, without a sleeve. There are no specifications available on the maximum pressure of the connectors. Therefore, the pressure at which the connectors fail was determined experimentally. The results are discussed in section 2.3.3. The tube connectors are mounted on the cylinders using a threaded connection. For this purpose, a thread was tapped in the hole at the bottom of the cylinder. The failure mode of this connection, was assumed to be thread stripping, as discussed in section 2.2.2. Here, the pressure at which the threaded connection fails was calculated. The parameters of the connection that are used in this calculation, are listed in Table 3.7. First, the length of engagement of the connection:

$$
\begin{aligned}
L_e &= n_{threads} \cdot ph \\
&= 4 \cdot 0.5\,\mathrm{mm} \\
&= 2.0\,\mathrm{mm}
\end{aligned} \tag{3.14}
$$

Then, the shear area was calculated using equation 2.26:

$$
\begin{aligned}
A_{th} &= 0.5 \cdot \pi \cdot d_{pitch} \cdot L_e \\
&= 0.5 \cdot \pi \cdot 2.675\,\mathrm{mm} \cdot 2.0\,\mathrm{mm} \\
&= 8.4\,\mathrm{mm}^2
\end{aligned} \tag{3.15}
$$

The shear strength of the material was approximated using the following relation:

$$
\begin{aligned}
\sigma_{shear} &= 0.577 \cdot \sigma_{tensile} \\
&= 0.577 \cdot 38\,\mathrm{MPa} \\
&= 21.9\,\mathrm{MPa}
\end{aligned} \tag{3.16}
$$

Then, the force at failure is:

$$\begin{aligned} F_{fail} &= \sigma_{shear} \cdot A_{th} \\ &= 21.9\,\text{MPa} \cdot 8.4\,\text{mm} \\ &= 184\,\text{N} \end{aligned} \tag{3.17}$$

To calculate the pressure at which the force on the tube connector is F_{fail}, the area at the top of the connector was calculated:

$$\begin{aligned} A_{connector} &= \frac{1}{4} \cdot \pi \cdot (d_{pitch}^2 - d_{hole}^2) \\ &= \frac{1}{4} \cdot \pi \cdot ((2.675\,\text{mm})^2 - (1.2\,\text{mm})^2) \\ &= 4.5 \cdot 10^{-6}\text{m}^2 \end{aligned} \tag{3.18}$$

Finally, the estimated pressure at which the threaded connection would fail through thread stripping is:

$$\begin{aligned} P_{fail} &= \frac{F_{fail}}{A_{connector}} \\ &= \frac{184\,\text{N}}{4.5 \cdot 10^{-6}\text{m}^2} \\ &= 41\,\text{MPa} \end{aligned} \tag{3.19}$$

Table 3.7: Parameters of the threaded connection between the tube connectors and the cylinder. The number of effectively engaged threads is calculated as $n_{threads} = 80\% \cdot n_{threads,total}$.

Parameters of threaded connection	Symbol	Value
Number of threads engaged	$n_{threads}$	4
Pitch	ph	0.5 mm
Pitch diameter	d_{pitch}	2.675 mm
Hole diameter in connector	d_{hole}	1.2 mm

Table 3.8: Tube materials and their recommended working pressure. To calculate burst pressure, the values in this table can be multiplied by 3.

	Size	Working pressure [Mpa]
Polyurethane (PU)	4x2.5	1.0 [52]
Polyamide (PA)	4x2.5	3.1 [52]
Polytetrafluoroethylene (PTFE)	4x2.5	2.0 [2]
Polyethylene (PE)	4x2.5	1.6 [52]

Detailed design The final design for the actuators and their place in the prosthesis is shown in Figure 3.8. The detailed design of both pistons is shown in Figure 3.9. The cylinders are shown in Figure 3.10. Technical drawings of the parts of the actuators are listed in Appendix D.

3.1.3. Fabrication of the prototype

Actuators The actuators were printed using an SLA printer, the Form 2 (Formlabs) [27]. The material that was used, is Clear Resin 03 [28]. The cylinders that were printed at 90 degrees from the build plate, were printed directly on the surface of the plate, without any support material. In the final design, there are small notches at the brim of the cylinders to allow airflow into the cylinders during printing (see Appendix D). This allows the resin to flow out of the partially printed cylinders during printing, preventing a small under pressure each time the build plate is lifted to print a new layer. The cylinders that were printed at a 45 degree angle, were printed with support material. There was also a test print that included cylinders printed horizontally, at a 0 degree angle from the build plate. This resulted in cylinders that were not fully round, with a flattening at one side due to leftover resin that could not drain away. The setup of virtual environment of the SLA printer can be seen in Figure C.3. The layer thickness that was used is 0.025 mm. A full list with technical specifications of the printer can be found in Appendix C. The print time per cylinder was approximately 100 minutes. The pistons were both printed vertically, with the end that holds the O-ring, directly on the build plate. After printing, the parts were removed from the print bed using a putty knife. Then, the parts were rinsed in ethanol to remove any uncured resin. The parts were cured with an ultra violet lamp for 40 minutes at room temperature. After curing and drying, the support material was trimmed off and the outside brim of the cylinders was smoothed using sandpaper (P240). The most demanding step in manufacturing the actuators, was tapping the thread in the holes in the cylinder bottom. This was done with a low cost tap and die set. The tap could be turned by hand without much resistance, while the cylinders were placed in a vice. In Table 3.9 the actual dimensions of the actuators are listed, when using the cylinders printed at different printing angles.

Structural elements The structural elements of the prototype are the middle-distal phalanx, proximal phalanx and the cutout of the palm. They were fabricated through FDM printing with an Ultimaker 3 (Ultimaker B.V.). The material that was used, is Ultimaker Tough PLA. It has an ultimate yield strength that is similar to regular PLA (37 MPa compared to 35 MPa) but is less brittle [70]. The settings recommended for the printer

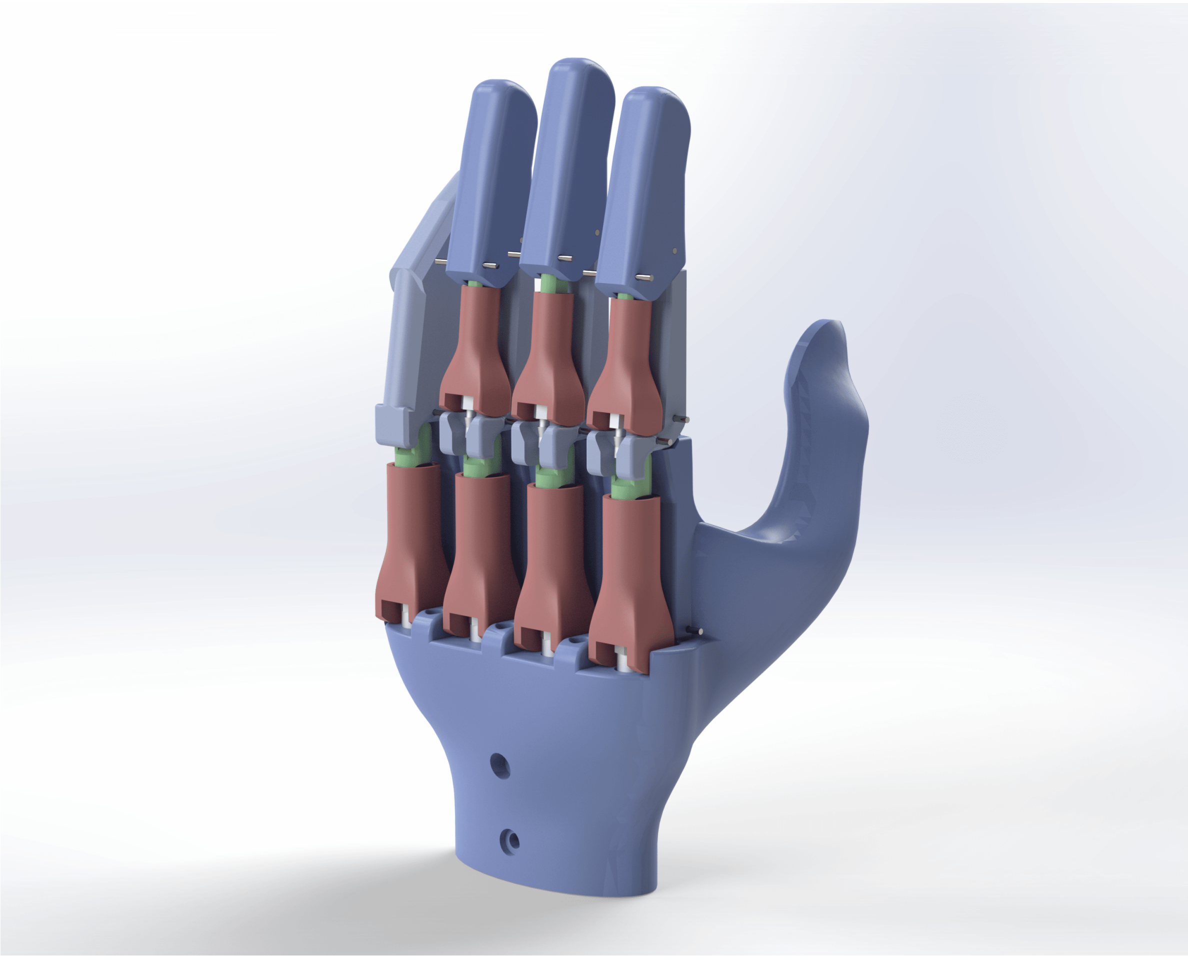

Figure 3.8: Rendered image of the final design for the prosthesis. The structural elements are shown in light and darker blue, the cylinders in red and the pistons in green. The holes that can be seen on the dorsal side of the hand and wrist, can be used to fixate a rod that can be inserted through the wrist, parallel to the fingers.

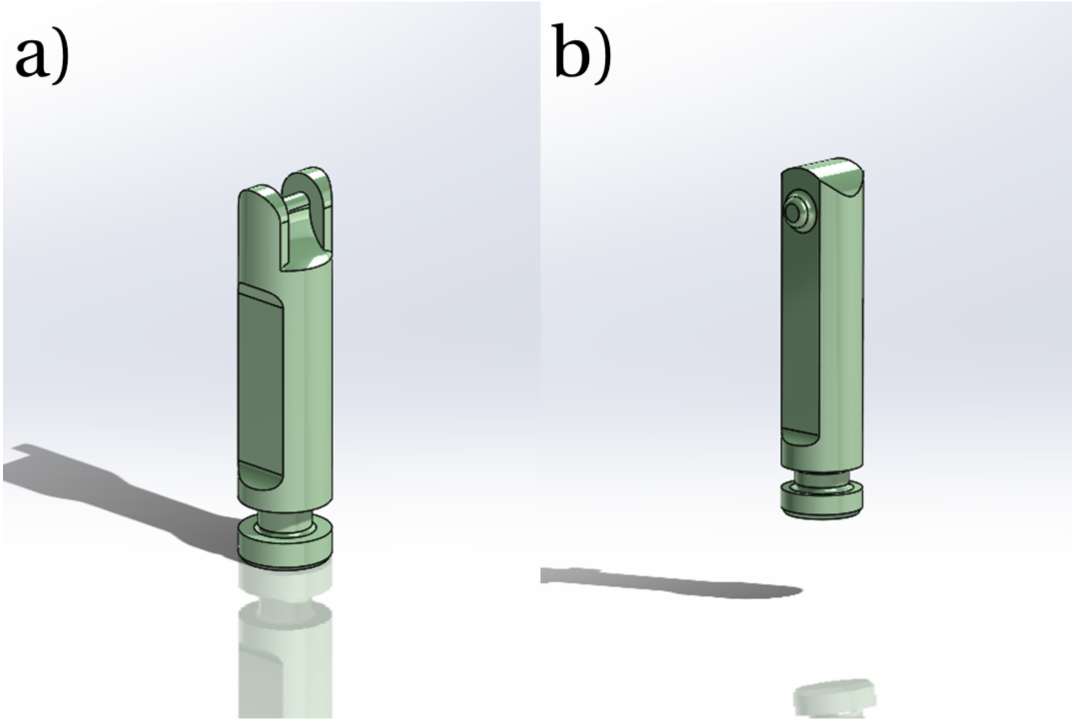

Figure 3.9: Final design of the pistons. Here, a) is the proximal piston. The groove at the top fits over a ridge on the proximal phalanx (Figure 3.6b), such that the piston is constraint in the sagittal plane of the finger. b) is the distal phalanx. The nobs at the top of the piston fit loosely in the grooves of the PIP joint of the middle-distal phalanx (Figure 3.5b). The technical drawings of both parts can be found in Appendix D.

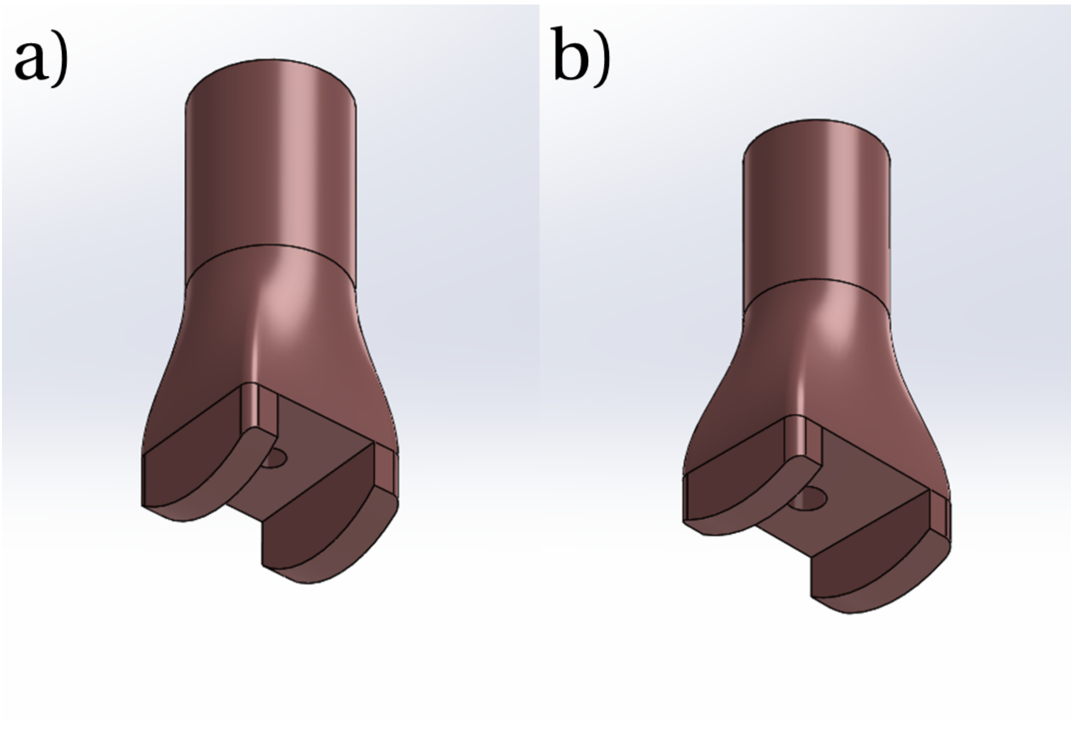

Figure 3.10: Final design of both a) the proximal cylinder and b) the distal cylinder. The technical drawings of both parts can be found in Appendix D.

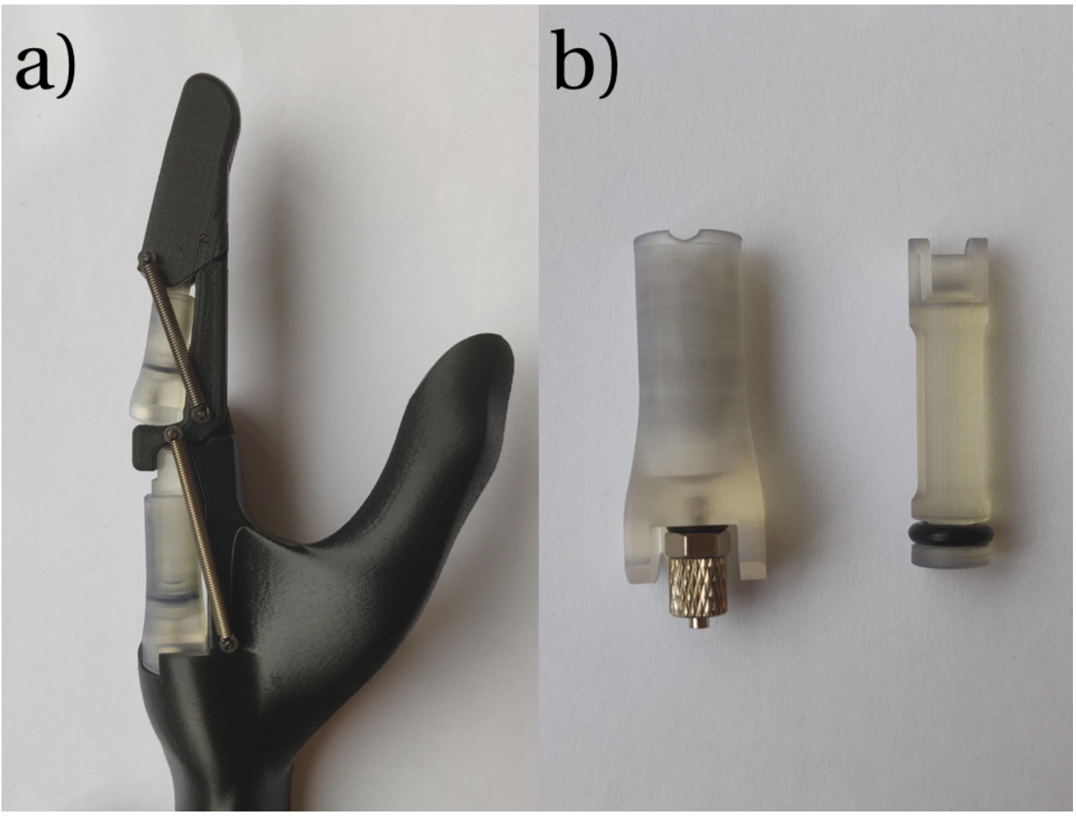

Figure 3.11: a) Side view of the assembled prototype, without tubes. b) Proximal actuator including tube connector and O-ring.

were used, with a layer thickness of 0.1 mm. The parts were printed with a variable infill percentage. The areas near the joints were printed at 100%, the rest of the part at 30% infill. A complete list with technical specifications of the printer can be found in Appendix C. The total print time was approximately 18 hours. Few post processing steps were needed before the parts were ready to be assembled. First, the parts were removed from the build plate and the excess material at the brim was removed using a utility knife. Second, the axle holes of the phalanxes were made a little wider using a 1.5 mm drill.

Assembly First the structural part of the prototype were assembled, then, the actuators could be placed inside the device. The axles of the pin joints are made from a spring steel wire, with an outside diameter of 1.5 mm. For the single finger, five pieces are required that were cut to the correct size using a wire cutter. Using pliers, the axles were placed trough the holes, connecting the phalanges to each other and the palm. The springs were mounted on the mechanism and are kept in place using axle circlips. The springs intended to be used as proximal spring in the prosthesis, was unavailable. Therefore, for the prototype, two springs with a lower stiffness were used that have the desired stiffness when used in parallel. To assemble the actuators, first the O-ring was slid over the piston and placed in the groove. This was done by hand as not to damage the rubber with tools with sharp edges. The tube connectors were secured in the holes using a small piece of PTFE tape as a thread seal, to prevent leakage. Finally, the tubes were slid through the tube channels and connected to the cylinders. With the pistons put in the cylinders, the actuators were placed in the mechanism and the prototype was finished. The result is shown in Figures 3.11 and 3.12.

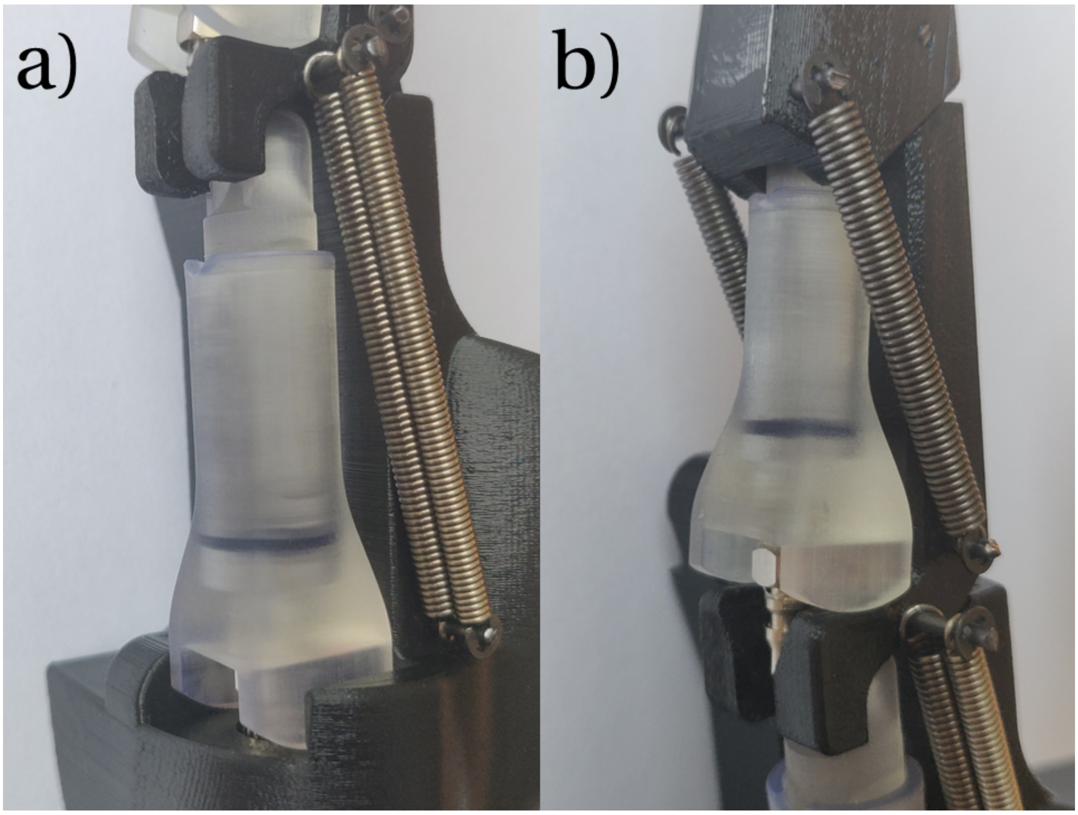

Figure 3.12: a) Close-up of the proximal cylinder placed in the prototype. For the prototype, two springs in parallel were used, resulting in a similar stiffness as the springs of the design. b) Close-up of the distal cylinder within the prototype.

Table 3.9: Actual dimensions regarding the proximal and distal actuators. The fifth column denotes the values for the cylinders printed at 90 degrees, the sixth the values for the cylinders printed at 45 degrees.

Actuator		Designed	Actual (90°)	Actual (45°)
Proximal	$D_{cylinder}$	10.00	10.27	10.18
	D_{piston}	9.50	9.71	9.71
	Clearance	0.25	0.28	0.24
	PGD	5.50	5.63	5.63
	Squeeze ratio	10.0%	7.2%	9.0%
Distal	$D_{cylinder}$	7.00	7.22	7.11
	D_{piston}	6.50	6.79	6.79
	Clearance	0.25	0.22	0.16
	PGD	4.30	4.43	4.43
	Squeeze ratio	10.0%	7.0%	10.7%

3.2. Evaluation results

3.2.1. Actuator - Geometrical accuracy

Following the protocol as described in section 2.3.2, a total of 96 measured values were collected. Halfway down the cylinder, a set of four measurements were performed. The actual inside diameter D_{in} is defined as the average of these four measurements. The wall thickness was computed using the inside and outside diameter. The dimensions of the evaluated cylinders are shown in Table 3.10, together with their design parameters. A visual representation of the data is given through a set of box plots. For the proximal cylinders, the results are shown in Figures 3.13 and 3.14. The results for the distal cylinders can be found in Appendix B. The distribution of the values measured for a single cylinder, can give an indication of the roundness of the part. Ideally, the cylinder is perfectly round and the measured values for D_{in} have a small spread.

Table 3.10: Designed and measured dimensions of the proximal and distal cylinders. The 'actual' values are an average of the measured values halfway down the cylinder.

	Cylinder code	Print angle [deg]	Inner diameter [mm] Designed	Actual	Wall thickness [mm] Designed	Actual
Proximal	1A90	90	10.3	10.25	1.65	1.77
	2A90	90	10.3	10.22	1.65	1.78
	3A45	45	10.3	10.18	1.65	1.81
	4A45	45	10.3	10.18	1.65	1.84
	5B90	90	10.3	10.27	1.18	1.26
	6C90	90	10.3	10.36	0.75	0.80
Distal	7D90	90	7.3	7.22	1.16	1.27
	8D45	45	7.3	7.11	1.16	1.38

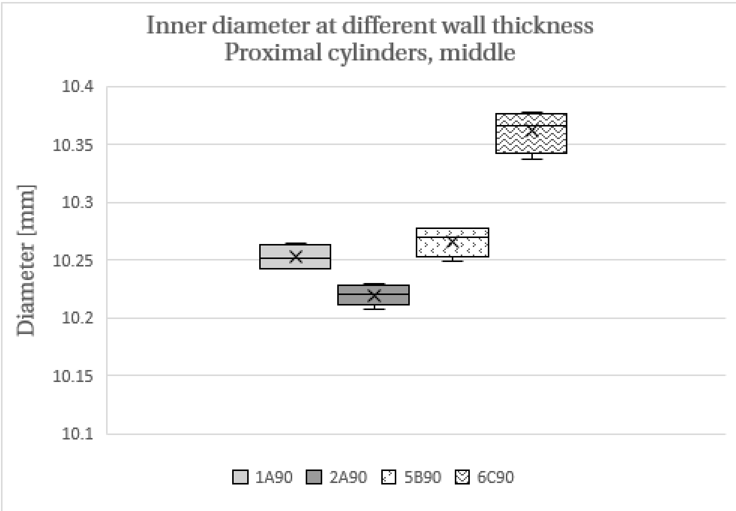

Figure 3.13: Measured values for D_{in} of four proximal cylinders. Three different wall thicknesses were used. The measurement was performed halfway down the cylinder.

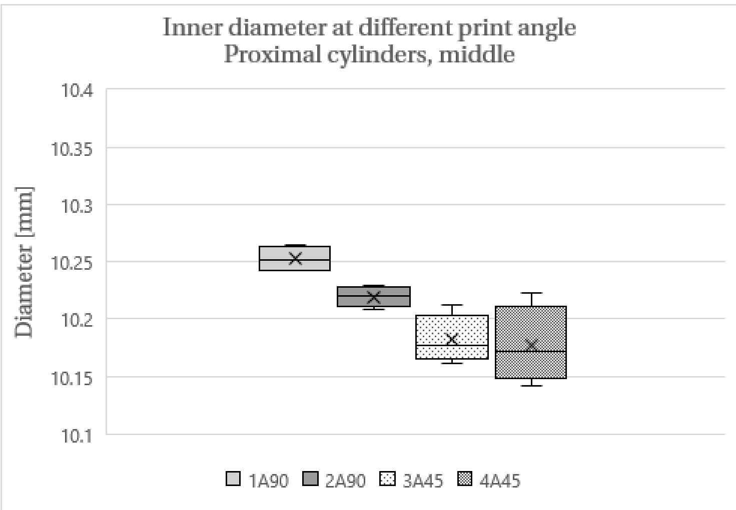

Figure 3.14: Measured D_{in} of four proximal cylinders. The first two cylinders are printed at a 90° angle from the build plate, the last two cylinders with an angle of 45°. The measurement was performed halfway down the cylinder.

3.2.2. Actuator - Static pressure

Three proximal cylinders, each with a different wall thickness, were loaded under internal pressure, according to the protocol set out in section 2.3.3. After each pressurization step, the inner diameter in the middle of the cylinder was measured. The resulting values are shown in a set of three box plots in Figure 3.15. Notably, the cylinder with wall thickness $s = 0.80\,\text{mm}$ fractured during the measurement. As the inner diameter was determined near the brim of the cylinder, the part cracked, starting at the top. This was likely the result of the force exerted by the three point internal micrometer on the cylinder wall.

Additionally, measurements were performed on the maximum pressure of the tube connectors. The tube connector with the locked sleeve did not fail at pressures as high as 6.0 MPa. The simple one part tube connector, without sleeve, dislodged at an average pressure of 5.9 MPa. This is well above the estimated operating pressure $P_{work} = 2.6\,\text{MPa}$.

3.2.3. Actuator - Friction in the cylinder

For each of the cylinders, one of the five trials is shown in a pressure versus time graph (Figure 3.16 and Figure 3.17). First the weight is lifted and the pressure increases. At 16 mm lift, the weight is held steady and the pressure graph flattens, resulting in the first plateau, Π_1. As the weight is lowered, pressure drops. As the retraction of the piston stops and is held steady, a second plateau Π_2 is visible. During these plateau's, the actuator exerts the same force at a different pressure. This pressure difference can be explained by the friction in the cylinder, as the friction on the piston is always opposite to its movement. The magnitude of the friction force on the piston can be calculated using this pressure difference and the following equation:

$$F_{friction} = \Delta P \cdot A_{piston} \tag{3.20}$$

The pressure P_{force} that actually contributes to the force exerted by the piston, is the average of the two plateau's. The pressure difference ΔP due to friction iss calculated as:

$$\Delta P = P_{plateau} - P_{force} \tag{3.21}$$

To calculate the friction, the pressure $P_{plateau}$ at Π_1 and Π_2 was determined. For the high pressure at Π_1, this was done by taking the average pressure that was measured during the 5 seconds before the graph starts to decline significantly. For the lower pressure at Π_2, first the middle of the plateau was determined. Then, 5 seconds around this time step was used to calculate the average measured pressure. The range that was used to calculate the pressure at the plateau's, is marked with red lines in Figure 3.16 and 3.17. The dashed line marks the average between them; P_{force}. For the second plateau in Figure 3.16, the pressure during 6 seconds instead of 5 was used to determine $P_{plateau}$. This interval was regarded to give a more accurate reflection of the pressure of the plateau. Finally, the hydraulic efficiency of the actuators can be determined. This is the ratio between the actual P_{force}, representing the pressure in the cylinder that contributes to lifting the weight, and the theoretical pressure needed to lift the weight. The only external force acting on the actuator is caused by the supported weight, therefore, the theoretical pressure P_{theory} can be calculated as follows:

$$\begin{aligned} P_{theory} &= \frac{F_{theory}}{A_{piston}} \\ &= \frac{m \cdot a}{A_{piston}} \end{aligned} \tag{3.22}$$

Here, m is the mass of the supported weight and a is the gravitational acceleration, $9.81\,\text{m/s}^2$. The average plateau pressures, friction force and hydraulic efficiency, for both the tested cylinders, are calculated using equations 3.20 through 3.22. The results are shown in Table 3.11. Finally, some visual observations were made during the friction measurements. Both cylinders showed signs of leakage between the piston and the cylinder. This was in the form of droplets forming at the brim of the cylinder. The leakage at the first cylinder, A345, with a print angle of 45° degrees, seemed more significant than for the second one, 5B90, with a print

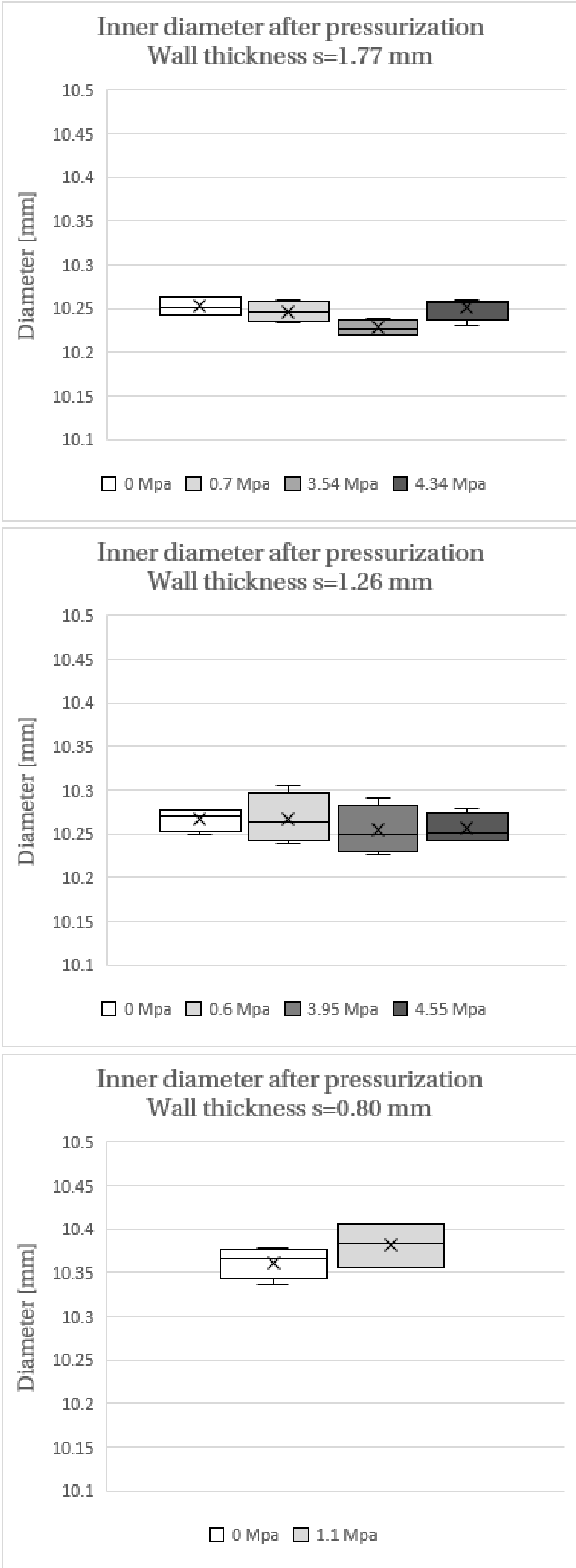

Figure 3.15: Inner diameter of proximal cylinders 1A90, 5B90 and 6C90, after being loaded under different internal pressures. Each cylinder has a different wall thickness.

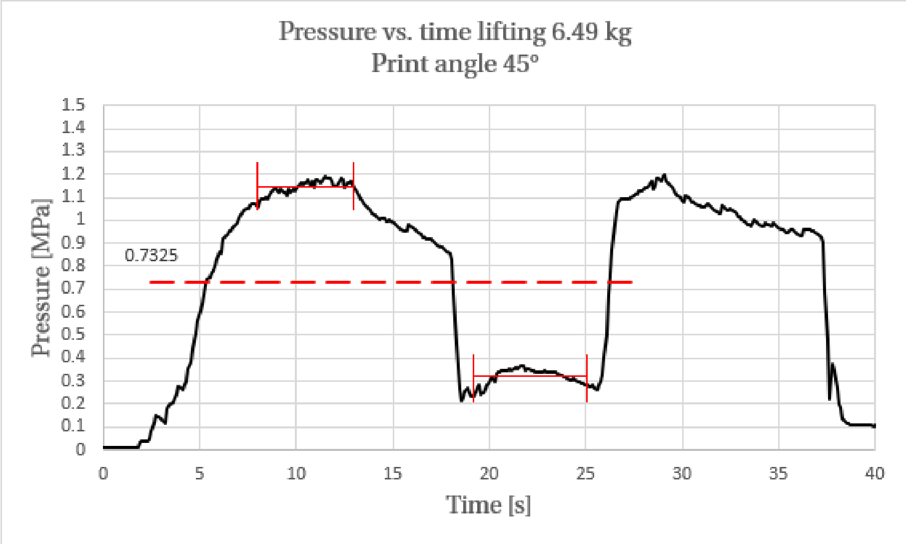

Figure 3.16: Pressure versus time graph as the proximal actuator is used to lift a mass of 6.49 kg. The cylinder was printed at a 45° angle form the build plate. The marked parts of the graph are used to determine the average pressure at both the low and high plateau. The dashed line notes the average pressure between the two plateau's.

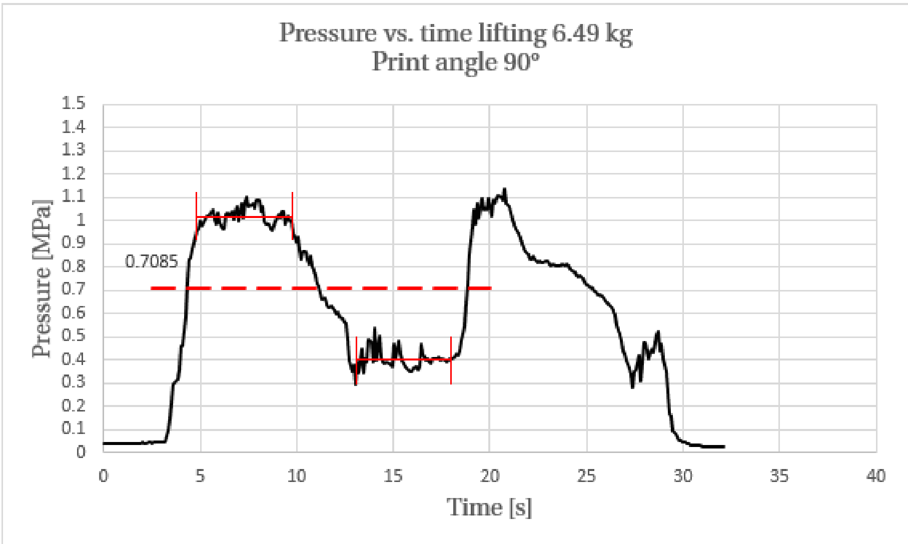

Figure 3.17: Pressure versus time graph as the proximal actuator is used to lift a mass of 6.49 kg. The cylinder was printed at a 90° angle form the build plate. The marked parts of the graph are used to determine the average pressure at both the low and high plateau. The dashed line notes the average pressure between the two plateau's.

angle of 45° degrees. However, this was not quantified. Also, at some instances, the piston was observed to misalign with with the cylinder as the weight was lifted.

Table 3.11: Results of the measurements on friction in the cylinder. Π_1 and Π_2 are the first and second stable region in each pressure graph, respectively.

Print angle	Pressure at Π_1	Pressure at Π_2	P_{force}	$F_{friction}$	Hydraulic efficiency
45°	1.15 MPa	0.32 MPa	0.73 MPa	34.2 N	93%
90°	1.02 MPa	0.4 MPa	0.71 MPa	25.7 N	92%

3.2.4. Prototype - Pinch force

The goal of this experiment was to determine the pinch force of the prosthesis and gain insight in the pressure-force relationship of the device. The cylinders that were used are the 5B90 for the proximal actuator and the 8D45 for the distal actuator. In total, 23 trials were performed in which the finger was flexed according to the protocol set out in section 2.3.5. Four trials were aborted during or dismissed after the measurement, due to issues regarding either the hydraulic circuit or the electrical components. A total of 19 trials were used for the analysis of the pinch force. These consist 3 times 6 trials that aimed for a pinch force of around 15, 23 and 30 N, respectively, and one outlier in which a pinch force of 41 N was achieved. For each trial, the time was determined at which the maximum pinch force was recorded. At this time step, the pressure and pinch force were noted. These data points were plotted in a pinch force versus pressure graph, see Figure 3.18. The dashed line is a trendline based on the method of the least squares. A second line, in solid blue, was added to show the theoretical pressure-force relation. This was calculated using a model of the hand in which all friction is assumed zero and the parts have an infinite stiffness, similar to equation 2.14. Using this, the force efficiency of the prototype can be determined. First, for the six trials in which the aim was to pinch 30 N, the average pinch force and average pressure was calculated. Then, the theoretical pinch force at this pressure was calculated using the model. The force efficiency is defined as:

$$\eta_{force} = \frac{F_{pinch,measured}}{F_{pinch,model}} \tag{3.23}$$

The results are listed in Table 3.12. The development of the pressure and the pinch force over time, throughout the maneuver, is shown in Figure 3.19. The peak shows the moment at which the pinch force was maximal, at that time the power to the pump was switched of. The steep decline to zero, at $t \approx 8.5$ s, is the moment at which the pump is reversed. Some challenges arose during the pinch force measurements. Most significant, at peak pressures during pinching, there was leakage visible between the piston and the cylinder. Also, during 6 trials, the pump did not reverse properly when attempting to extend the finger. This problem was determined to originate in the ESC, with no clear cause.

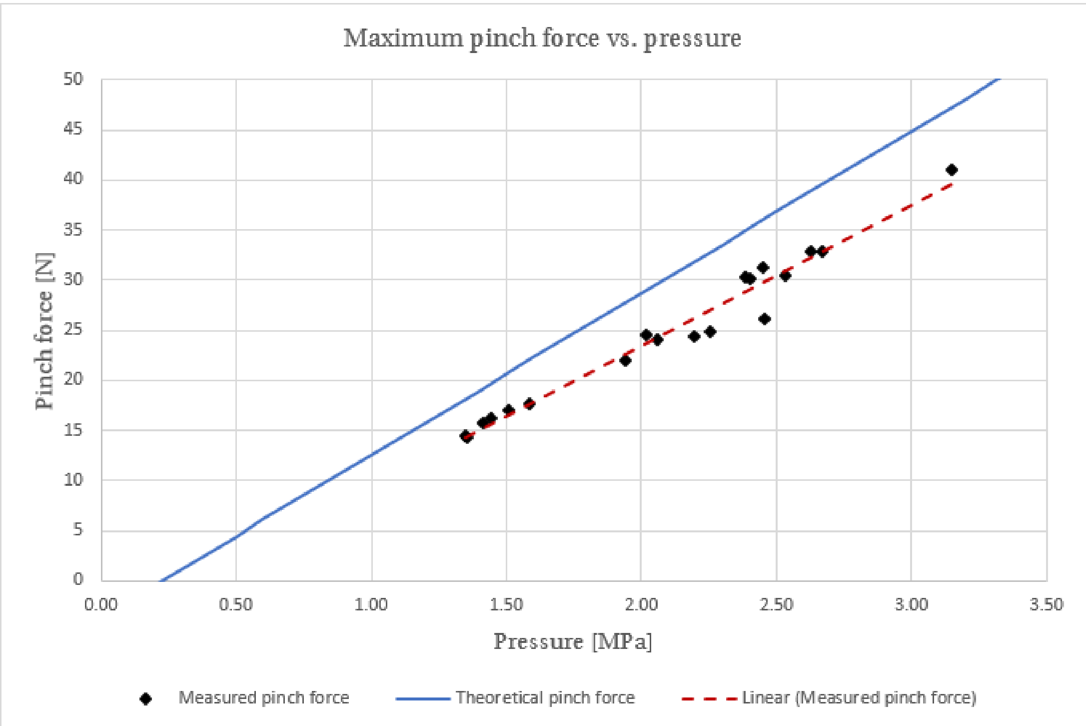

Figure 3.18: Pinch force versus pressure of the maximum recorded pinch force during 19 trials using the prototype. The pinched object has a width of 19 mm. The solid line represents the theoretical pinch force, calculated with a model that omits friction and elasticity. The dotted line is a trendline computed using the least squares method.

Table 3.12: Mean pressure and force of the measurements with the aim to pinch 30 N. The model used to calculate the theoretical values, omits friction and elasticity.

	Measured (mean)	Model
Pressure	2.51	2.51
Force	31.29	36.95
Force efficiency η_{force}	84.7%	100%
F/P	12.5	14.7

3.2.5. Prototype - Closing time

Several close and open cycles were performed with the prototype, according to the protocol described in section 2.3.6. The recorded pressure data during the closing of the hand, did not conclusively show the moment when the fingers made contact. Therefore, the video material was used to determine the close and open time. For each maneuver, the number of frames was determined within a video editing software program. The audio was used to determine the moment that the motor started. For the opening of the finger, the moment the finger is opened at ≈ 90% was considered the end of the maneuver. The resulting average closing time is 0.53 s and the opening time is 0.75 s. Note that this is the closing and opening time of the prototype with one finger. For the entire hand, the closing time is estimated based on these measurements.

3.2.6. Weight

The weight of the actuators and the prototype are of interest for the evaluation of the prosthesis. The weight was determined using a scale with a resolution of 1 g. The results are shown in Table 3.13. The independent actuators consist of the piston, O-ring, cylinder and tube connector. The mechanism concerns the prototype without any components of the hydraulic circuit. The prototype was weighed both with and without oil in the hydraulic system. The weight of the oil was determined to be 3 g.

Table 3.13: Weight of the components of the prototype. The distal and proximal tube connectors were determined to weigh 1 g and 2 g, respectively. The hydraulic oil contributes 3 g to the total weight of the prototype.

	Weight [g]
Actuator distal	4
Actuator proximal	9
Mechanism without actuators	95
Prototype with oil and tubing	136

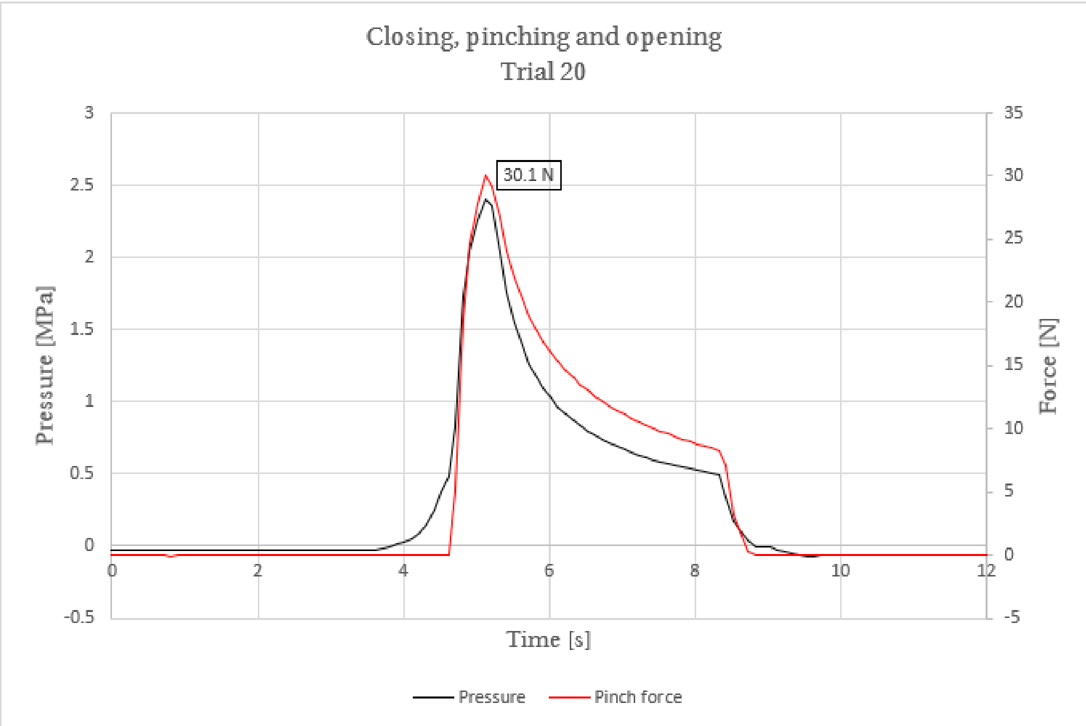

Figure 3.19: Pinch force and pressure recorded over time during trial 20.

4
Discussion

4.1. Remarks on the fabrication and assembly

Fabrication of the actuators In this section, the fabrication process and the resulting part quality are reflected on. The actuators were designed to fabricated without extensive post processing. All SLA printed parts required rinsing and curing. The pistons and the cylinders that were printed at a 90 degrees angle from the build plate, only required some sanding at the bottom edge. The cylinders printed at 45 degrees additionally required removal of the support material, which was done using pliers and was finished in a few minutes. This leads to the conclusion that easy fabrication was achieved. The surface quality of the SLA printed parts seems high, based on a visual inspection. The actual dimensions of the actuator differs from the designed dimensions. Table 3.9 shows the designed actuator parameters compared to that of the actually fabricated actuators. Most notable is the inner diameter of the proximal cylinders, which was designed to be 10 mm. To achieve this, the .stl file that was used to print the cylinders had a cylinder diameter of 10.3 mm. This dimension was based on a few iterations of printing cylinders with different wall thicknesses. However, the resulting parts still had a cylinder diameter that is larger than 10 mm. The unexpected difference could be the result of inaccurate measurements on the early iterations (performed using an ordinary micrometer) or the influence of a different wall thickness. Secondly, the squeeze ratio of the O-ring is smaller than designed. Although this parameter is essential for proper operation of the seal, the designed squeeze ratio of 10% is based on rule of thumb [53]. Therefore, it is reasonable to expect proper operation from a seal with a squeeze ratio of 7%. The difference in squeeze ratio between the actuators printed at different angles, is significant. There is a trade off in increasing the squeeze ratio, as it decreases leakage but increases friction [53]. Finally, tapping the treads in the holes at the bottom of the cylinder, was the most demanding part of the fabrication of the actuators. The process demands some caution and patience from the person who performs it. It does not require training and can be carried out using a low cost tap and die set.

Fabrication of the structural elements The printing time of the structural elements was considerable ($> 18\,h$). However, the post processing time was minimal. The excess material that is deposited at the build plate to prevent warping and allow for better adhesion, was easily removed using a utility knife. Some om the holes for the axles needed to be drilled out. This was done in a few minutes. However, the designed dimensions of the holes were changed, such that this should not be required. The parts were printed with a layer thickness of 0.1 mm. This could be increased to 0.15 mm to reduce the print time significantly (from 18 hours to 10 hours). The small layer thickness did result a smooth surface finish.

Assembly steps and difficulty The entire hand consists of 95 parts (see Appendix A). Of these parts, 30 are the circlips used to secure the springs (14 parts) on the axles (15 parts). The hand can be assembled in 42 steps (see Appendix A). In this case, placing the spring around an axle and securing it with a circlip is considered to be one step. This has to be done a total of 21 times. Therefore, the number of assembly steps could be reduced significantly if less springs are used, or if they would be secured differently. The assembly of the prototype could be carried out with a set of pliers and took about 30-60 minutes. The assembly of the prosthesis does not require any training and could be explained using a simple manual.

4.2. Verification of the design

Required actuator pressure In this section, the design is reflected on by discussing some of the steps that were taken and assumptions that were made in the design. The first two paragraphs consider the actuation system of the prosthesis, the final paragraph discusses the design of the phalanges. The operating pressure of the actuators P_{work} was determined by calculating the pressure required to pinch 30 N. In this calculation, the point of application of the pinch force was chosen to be the most distal point on the centreline of the distal phalanx. As expected, the actual point of application is closer to the PIP joint, therefore, the reaction torque of the pinch force is smaller and the required actuator torque is smaller. The actual required theoretical operating pressure can be calculated using the dimensions of the detailed design. This would result in a P_{work} of 2.2 MPa. If this lower pressure was used to design the actuators, the wall thickness could have been smaller. However, the calculation for P_{work} omits losses due to friction. From the measurements follows that the larger P_{work} of 2.6 MPa that was used for the design, actually came close to the real pressure required to pinch 30 N.

Maximum pressure of hydraulic components The components of the hydraulic system that are first to fail due to high pressures, are the tube connectors without sleeve, at the distal phalanx. The average measured pressure at which the tube dislodged, was 5.9 MPa. Therefore, the maximum pressure of the hydraulic circuit is approximately 5.9 MPa. This is similar to that of the Delft Cylinder Hand (6 MPa) [64], and significantly higher than that of the hydraulically actuated hand developed by Kargov et al. [39]. The maximum pressure that the pump can generate, according to the manufacturer, is 4.5 MPa. This means that the theoretical maximum pinch force is 68 N, assuming that there is no friction and that the structural elements do not fracture. Additionally, that the hydraulic circuit fails at 5.9 MPa, means that the cylinders are overdimensioned. With a safety factor $sf = 4$, the cylinders withstand a pressure of over 10 MPa. A safety factor 2.5 would suffice for the cylinders not to be the weakest link in the hydraulic circuit. However, there are some comments to be made on the calculations that were used to determine the wall thickness. First of all, it was assumed that the material is homogeneous. As the cylinders are printed in layers, through SLA printing, it is questionable to what extend the structure is isotropic. There has been little research on the dependence of mechanical properties on print direction of SLA printed structures. One recent paper by Saini et al. concluded that the print orientation does play a significant role in the mechanical behaviour [59]. Multiple specimen, printed at different angles were loaded under tension and compression. It was observed that the material fractures differently at different angles. Specimen printed at 22.5 and 67.5 degrees, took the highest loads. However, the measured ultimate tensile strength of the specimen printed at 45 degrees was only 1% higher than that of the ones printed at 0 degrees. Moreover, an ultimate yield strength of 38 MPa was used to calculate the wall thickness. This is as described by the manufacturer for uncured parts. According to the manufacturer, the material has an ultimate yield strength of 65 MPa if the parts are cured with UV light at 100° C for 1 hour [28]. Sani et al. have measured a yield strength of 60-69 MPa for parts that were cured only at 60° C for 30 minutes. The parts of the prototype are cured at room temperature for 45 minutes. This leads to the conclusion that the ultimate yield strength of the cylinders of the prototype, is probably higher than 38 MPa. Finally, some remarks are to be made on the calculation of the maximum pressure the threaded connection of the tube connector can withstand. The shear strength that is used, is estimated on the yield strength. As mentioned, the actual yield strength is probably higher than the 38 MPa that was used. Moreover, the formulae used to calculate the shear area, are based on an approximation of the actual shear area and length of engagement [20, 23]. The calculated pressure at which thread stripping occurs, was an estimate. This estimated pressure of 41 MPa is high enough to assume that at high pressures, failure of the cylinder wall would occur first. Overall, the calculations of the maximum pressure of each component of the hydraulic circuit, were sufficient to determine an appropriate cylinder wall thickness and indicate which component would be the first to fail.

Design of the phalanges and joints The working principle of the prosthesis is essentially the same as that of the DCH. Although the placement of the actuators at the back of the hand seems to be the optimal placement, exploring different possibilities could be interesting. Perhaps the cylinders could be integrated into the phalanges. The finger mechanism consists of two four-bar linkages that are connected to each other. Therefore, it was not possible to reduce the number of parts while maintaining the same degrees of freedom. The desired transmission ratio R was calculated meticulously. The constraints on R are based on equations derived for a gripper with two opposing, mirrored fingers. Hence, some assumptions are made in using these equations. Moreover, for small objects, the transmission ratio can be in a broad range to still achieve a stable pinch grip. Larger objects are likely to be grabbed with a power grip. In conclusion, the desired transmission ratio could have been estimated or calculated at a lower significance. In the design of the phalanges, the moment arm of the actuators was rounded of. Although convenient, this is not necessary. The shape of the phalanxes might suggest that they were designed to be fabricated through conventional methods such as milling. This is evidently not the case and fabricating the parts through milling would be challenging to achieve. The rectangular shapes are the result of the objective to design parts that are easily 3D printed and of the design approach. The design of the phalanxes was approached by considering the constraints on the dimensions, in each of the three principle planes of the phalanx. The added design freedom that is offered by using 3D printing could have been explored more. Possibilities were missed to adapt the cross sectional shape of the phalanges to the cosmetic glove and the actuators. The design considerations regarding the joints were discussed comprehensively. However, the prioritization of reducing the number of assembly steps could be questioned, especially at the sliding curved joints at the piston. The friction torque in the fully 3D printed piston joints, is significantly higher than in the hinged joints with a steel axle. This is the result of the larger radius of the sliding surface. As shown in equation 2.11, the friction force depends on the friction coefficient, the force on the axle and the radius of the sliding surface. The radius of the proximal piston joint is 3 mm and of the distal piston joint 3.5 mm. The axle of the hinged joints is 0.75 mm. If the friction coefficient for both joint types would be equal, the friction torque in the sliding joint is $\frac{3}{0.75} = 4$ times (proximal) and $\frac{3.5}{0.75} = 4.7$ times (distal) as high as for the hinged joints, based on equation 2.11. Summarizing, the choice was made between a friction torque that is ≥ 4 times higher and reducing the number of assembly steps. Choosing for a lower friction over less assembly effort, would also be defensible. Using a sliding hinged joint would have increased the assembly effort, but reduced friction. Also, the axle could be used as an attachment point for the springs.

4.3. Discussion of measurement results

4.3.1. Actuator measurements

Geometric accuracy The goal of the first experiment was to determine the dimensions of a set of SLA printed cylinders and determine the influence of the print angle and wall thickness of the accuracy of the printed parts. First, the inner diameter at different wall thicknesses is considered, shown in a box plot in Figure 3.13. The measured diameter of the cylinder with a thickness of 0.8 mm, is significantly larger than that of the other specimen. The inner diameters of the cylinders with a wall thickness of 1.8 mm and 1.3 mm are not significantly different from each other. When measuring with the micrometre, the device exerts a force on the cylinder wall. It is possible that this lead to deformation of the specimen. This deformation would depend on the wall thickness. This could be the reason that the diameter of the cylinder with the thinnest wall, was measured to be 0.1 mm larger than that of the other ones. The diameter of cylinders 1A90, 2A90 and 5B90 are similar and there were possible limitations to measuring the diameter of the thin walled cylinder. Therefore a definite conclusion cannot be drawn on the influence of the designed wall thickness on the accuracy of the cylinder diameter. Secondly, the comparison was made between the cylinders printed at different angles, based on the measurement results shown in Figure 3.14. Recall that the cylinder diameter of the files delivered to the printer, was 10.3 mm. The dimensions of the parts printed at 90 degrees were closer to that of the original file used for printing. Shown in the box diagram, the spread of the measurements is larger for the cylinders printed at 45 degrees, than for the ones printed at 90 degrees. This indicates that the former have a higher roundness. A limitation of this experiment is that the cylinders are possibly deformed by the micrometre during the measurement. Nonetheless, the dimensions of the cylinders could still be compared as all measurements were performed the same way. The results indicate that the cylinders printed at 90 degrees, have a more precise diameter and have a higher roundness, than the cylinders printed at 45 degrees.

Static pressure The goal of this experiment was to determine what internal pressure the cylinders can withstand and if such pressure would lead to plastic deformation. Based on the results displayed in Figure 3.15, pressurization of up to 4.3 MPa did not lead to plastic deformation of the cylinders with a wall thickness of 1.8 mm and 1.3 mm. As expected, the mean values of the measurement sets after each pressurization step, are close and within 0.02 mm of each other. The pressure at which the cylinders were tested did not approach the maximum pressure that the cylinders are designed to withstand. Therefore, it could not be confirmed that the wall has the desired safety factor. There is no conclusion possible on plastic deformation of the cylinder with a wall thickness of 0.8 mm as it fractured during the measurements. However, in more general sense, it can be concluded that this cylinder, with a designed safety factor $sf = 2$, was not robust as it fractured at the force exerted by an internal micrometre. Moreover, the experiment showed that there was no plastic deformation at a pressure of ≥ 4.3 MPa.

Friction in the cylinder The goal of this experiment was to compare the friction on the piston for cylinders printed at two different angles. The cylinders with the following codes were used: 3A45 and 5B90. With a print angle of 90 degrees, the layers are perpendicular to the movement of the piston. This could results in a different friction force than for the cylinders that were printed at an angle. The friction in force in the cylinders was calculated for two trials, shown in Figures 3.16 and 3.17. The friction in cylinder 3A45 was 34.2 N and in cylinder 5B90, 25.7 N. However, this difference can not be explained by the difference in surface texture. The difference in diameter of the two cylinders, is 0.11 mm. The surface texture due to the layers is assumed to be in the order of magnitude of the layer thickness, which is 0.025 mm. As this is smaller that the difference in diameter, the influence of surface texture of the difference in friction could not be established based on this experiment. The hydraulic efficiency of the cylinders that were tested is similar, 92% and 93%, although lower than expected. Martinez recorded a hydraulic efficiency of 96% for a 3D printed cylinder [50]. This could be the result from the leakage that was observed. The measured friction was also significantly higher than the friction force that Martinez recorded for an unreamed SLA printed cylinder, at similar pressures. This could be the result from differences in dimensions. Also, the misalignment of the piston and the cylinder could have resulted in a higher friction as the piston slid directly against the brim of the cylinder. Limitations of this experiment include that only two trials were used to compare the friction. As there was leakage, many of the trials did not show a clear plateau as the weight was held at a constant height. Therefore, two trials were used that showed the most steady behaviour. Also, water was used as a working fluid. This allowed for a comparison between the cylinders and between the results from Martinez, this study also used water. However, the measured friction does not predict the friction of the actuators when applied in the hand, when oil is used. In conclusion, although the effect of wall texture on cylinder friction could not be determined, the experiment allowed for the comparison between two of the printed cylinders. The experiment had limitations, but the order of magnitude of the friction and the hydraulic efficiency were determined.

4.3.2. Prototype measurements

Pinch force The goal of the pinch force experiment was to determine the pinch force of the prototype and gain insight in the pressure-force relationship of the device. The results in Figure 3.2.3 show than a pinch force of >30 N could be achieved consistently. The highest pinch force that was measured was 41 N, which shows the potential of the finger to pinch at a higher force without failure. The theoretical maximum pinch force of the finger is 68 N at >4.5 MPa. The maximum pinch force was not approached to prevent the risk fracture of the mechanical parts of the prototype. The force efficiency of the prototype was 85% at an average pinch force of 31 N. This means that 15% of the theoretical force input due to pressure in the actuators, is dissipated due to friction in the cylinder and in the joints, elastic deformation of the structural parts and losses due viscosity of the fluid. This seems reasonable. Figure 3.2.3 shows the theoretical pressure force relation and the data points that were actually measured. The difference between the trend line trough the measured data and the theoretical force pressure graph, can be explained by the friction and deformation losses. The difference between the theoretical pinch force and the actual pinch force at 2.5 MPa, could be dissolved by adding a cylinder friction force of 29 N to the model of the finger. This is not the actual friction force as there are more losses to account for, however it does indicate that the actual friction has the same order of magnitude as the friction that was measured in section 3.2.3. This also means that the losses due elastic deformation and friction in the joints, are low compared to the friction loss in the cylinder. Overall, it can be concluded that the prototype can deliver a pinch force that is similar to that of the Delft Cylinder Hand (over 30 N) [64]. The hand developed by Kargov et al., one of the few hydraulic hand prostheses in current literature, has a "holding force" of 110 N. Limitations of this experiment include that the object that was pinched was not varied in size. Also, the maximum pinch force was not determined. The goal of measuring the pinch force and gaining insight in the pressure force relation, was achieved.

Closing time This experiment was executed to determine the closing time of a single finger of the prosthesis. Although the method of using the pressure sensor to determine the beginning and the end of the closing manoeuvre did not work, the closing time was successfully determined using the video footage. The average closing time was measured to be 0.53 s, opening the finger to 90% took 0.75 s. An estimation of the closing time of the prototype $t_{close,p}$ can be calculated using the following formula:

$$t_{close,p} = \frac{V_p}{Q_p} \tag{4.1}$$

Here, V_p is the volume of oil that has to be displaced to close the prototype. Q_p is the flow rate through the hydraulic circuit of the prototype. To estimate the closing time of the entire prosthetic hand, the volume V_h and flow rate Q_h were approximated. As the prototype has 2 cylinders and the prosthesis has 7, V_p was estimated to be $3.5 \cdot V_p$. The motor power was approximately 50% for the prototype. Assuming that the motor operates at 100%, the flow rate for the prosthesis can be estimated to be $2 \cdot Q_p$. Similar to equation 4.1, the closing time of the entire hand $t_{close,h}$ can be estimated as:

$$\begin{aligned} t_{close,h} &= \frac{V_h}{Q_h} \\ &= \frac{3.5 \cdot V_p}{1.75 \cdot Q_p} \\ &= 0.93\,\mathrm{s} \end{aligned} \tag{4.2}$$

This is a rough estimation but it shows that it is likely that the prosthesis is able to close within 1 s.

4.4. Evaluation of requirements

4.4.1. Actuator requirements

Working principle In this section it is evaluated to what extend the prosthesis meets the requirements. First for the actuator, then for the entire prosthesis. The first requirement for the actuator was that it should be hydraulic, meaning that is uses a liquid as its working fluid. The prosthesis was designed to operate with hydraulic oil as its working fluid, as was also used in the prototype. Thereby, this requirement was met.

Force and pressure The actuator is able to generate enough force for the finger to pinch with 30 N. In the design phase, the required operating pressure was approximated to be 2.6 MPa, omitting friction. The actual working pressure at which an average pinch force of 30 N was achieved, was 2.5 MPa. This is larger than the 1.4 MPa that was set out in the objective, based on the need for small hydraulic components that operate at high pressures [74]. The cylinders are designed to withstand a pressure of up to four times the operating pressure. The weakest link in the hydraulic system is the small tube connector at the distal actuator, at 5.9 MPa. However, the maximum pressure that the pump can generate is 4.5 MPa, according to the manufacturer. Overall, the requirement for operating pressure and sufficient force output were fully met.

Dimensions The goal is met for the actuators to fit within the dimensions of the selected cosmetic glove. The cylinder diameter was also limited by the moment arm of the actuator. Both are constraint by the geometry of the glove. The cylinder diameter could be increased if the safety factor of the cylinder wall is reduced. This could result in a higher pinch force at a lower pressure. The length of the phalanges allowed for a stroke of the piston such that a range of motion of 90 degrees flexion is realised.

Fabrication Both the pistons and the cylinders were largely fabricated through single step fabrication. Some post processing was required. The actuators were required to be fabricated without extensive post processing such as using a reamer. This requirement is met. The actuators consist of 4 parts each, resulting in a minimal number of assembly steps. Achieving sufficient geometrical accuracy was a challenge. More iterations steps are required to achieve a level of accuracy that is satisfactory. Using a print angle of 90 degrees, a sufficient level of roundness is achieved (four 3-point measurements within 0.028 mm).

Sealing The ability of the seal to contain the working fluid was not sufficient to prevent contamination of the actuators environment. At high pressures, some leakage was observed along the the O-ring gland. This is possibly caused by the squeeze ratio of the O-ring. This was designed to be 10%, while the squeeze ratio of the prototype is 7%. Unfortunately there is a trade-off between the squeeze ratio and the friction in the cylinder, which is also measured to be higher than expected. Other ways to reduce the leakage could be to reduce the clearance between the piston and the cylinder wall. The leakage did not limit the actuators' ability to deliver the required force.

4.4.2. Prototype requirements

Mass Increasing the comfort through weight improvement, is of the highest importance according to individuals using a prosthesis [7]. The goal was to design the prosthesis such that is weighs less than a human hand (426 ± 63 g). This is lighter than most current 3D printed prostheses. The total estimated mass of the hand is 286 g. Extended effort to reduce the mass have a high potential. Especially when focused on the palm. Together with the motor and the pump, the device weighs 402 g. The mass of the battery is not taken into account as it could be placed somewhere else on the body without major design implications, for example in the socket of the prosthesis.

Functionality With the prototype of one finger, both a pinch grip and a power grip have been established. This demonstrates that the prosthesis is able to perform the two grip types that are used most frequently, which make it useful for activities of daily living [58]. The hand is multi articulate and underactuated, such that a power grip can be achieved, with the fingers adapting to the shape of the object. A stable pinch grip can be achieved on objects as large as the opening diameter of the hand (78 mm). In reducing the complexity of the design, a two point pinch grip was opted for. A three point grip would offer several benefits. Such as a more stable grip on cylinder shaped objects, such as a pen. Moreover a higher total pinch force could be achieved. With one finger, a pinching force as high as 41 N was established. Pinching over 30 N was proven to be reliably possible. The closing time of the prototype is 0.53 s, well within the target range (0.25-1 s) and competitive with commercially available hands [51, 63]. The estimated closing time of the entire hand is 0.93 s.

Cosmesis The designed prosthesis is to be covered with a cosmetic glove. This cosmetic glove is designed to appear like a human hand. The mechanism is designed according to the shape of a human hand. All parts of the mechanism are dimensioned such that they fit within the glove. Thereby, excellent cosmesis is achieved when the glove is used over the hand. For this study, the selected model of the glove was unavailable. Therefore, the hand was designed to have a basic level of anthropomorphism.

Fabrication The structural parts of the prosthesis were all fabricated through FDM printing. The extended design freedom offered by 3D printing, was used in the anthropomorphic design of the palm. The design of the phalanges include basic geometrical shapes to allow for single step printing without using support material. The hand is completely modular and the total number of assembly steps is 42. Half of those steps are the placing and securing of the springs. Assembly efforts were reduced as the actuators can be placed directly in the mechanism in a single step. The prosthesis can be assembled within 30-60 minutes, requiring a set of pliers. The assembly does not require any training and could be explained using a simple manual.

4.5. Recommendations

4.5.1. Improvements on the design

Introduction In this section, recommendations for further research are presented. First, improvements on the current design are suggested. Second, suggestions for future research are discussed. The design can be improve upon in multiple ways. A selection of suggested improvements is categorised in four groups, as follows.

Improved gripping The gripping ability of the hand can be improved by realising a three point grip. With two fingers and the thumb, a higher force can be used than with a two point pinch grip. This also allows the hand to be used to grip a wider range of objects. Secondly, the shape of the thumb is more suited for pinching than for a power grip around an object. A redesign of the thumb could allow the hand to grasp objects like larger coffee cups. Moreover, the thumb could be designed such that the thumb can be passively controlled. A hook grip with four fingers could be realised this way.

Integration of components Since the parts are 3D printed, there is a large design freedom for the shapes of the structural parts. Designing the hand such that the actuators and tubing are integrated with the phalanges, could lead to higher cosmesis. This could be an alternative for using a cosmetic glove, which adds to the total mass of the hand. Furthermore, the design should be developed further, including the integration of the pump and electrical components in a socket.

Reduced weight The weight of the hand can be reduced significantly. This was not prioritized in the design of the palm. The mass of the palm accounts for approximately 46% of the mass of the hand (without pump, etc.). It can be reduced by replacing it with a hollow structure that has a similar shape and mechanical properties.

Actuator performance Finally, the actuator performance should be improved. Two aspects of the actuators that were unsatisfactory, were the seal performance and the friction in the cylinder. The performance of the seal should be enhanced to reliably prevent the leakage of the working fluid. This is challenging as a tighter seal results in increased friction. The friction that was measured according to section 3.2.3, was 29% of the theoretical force output of the proximal actuator. Besides the limitations of the experiment, e.g. the occasional tilting of the piston within the cylinder, the high friction could have several causes. The dimensions of the cylinder are crucial for a properly operating seal, such as diameter and roundness. Also, the surface roughness of the cylinders contributes to the friction. Both the geometry and the surface quality could be improved upon by post processing or optimizing the print settings for printing a hydraulic cylinder. Using a different printing technique is also an option, although the layer height of SLA printing (0.025 mm) leaves little room for improvement.

4.5.2. Future research

Several options for future research are recommended. Most relevant is the further development of the 3D printed hydraulic actuators, as little to nothing is present in current literature. Starting with the challenges encountered in this study, the geometric accuracy and surface quality of different printing techniques could be investigated. This could include optimization of certain print parameters, such as layer thickness. Complementary to this, the influence of surface texture on seal friction could be determined. Improving the surface quality and accuracy of the 3D printed cylinders could be pursued by reviewing different print techniques and post processing steps. If successful, the sealing and friction can be improved upon. There are several relevant research directions to further advance the possibilities of 3D printed hydraulic actuators. It is essential is to test them in multiple applications, starting by designing an actuator that has joint connections that are compatible with conventional mechanical parts. Different operating principles can also be tested, such as a double acting piston cylinder system. The scalability of hydraulic actuators offers also an interesting research perspective. An elaborate performance review is necessary of 3D printed actuators to allow for a comparison with conventional hydraulic actuators. This includes gaining insight in the durability of the actuator, especially the sealing.

5 Conclusion

This study presents the first hydraulic actuation system that was fabricated entirely with 3D printing. It was designed to be applied in a multi-articulate hand prosthesis that meets the essential user requirements. A prototype was built to demonstrate that the hand is able to produce a pinch force of > 40 N, showing that it can compete with similar prosthetic devices. Its mass (0.35 kg without pump and battery) is less than that of a human hand. The actuators were tested at an operating pressure of 3.2 MPa and have a theoretical maximum pressure of up to 5.9 MPa, showing that with a compact design, high pressures can be achieved. The cylinders were fabricated in a single step using SLA printing, requiring only cleaning and curing as post processing steps. The cylinder friction in the prototype was measured to be 25.7 N, significantly higher than expected, at a pressure of around 1 MPa. Measurements were performed to investigate a possible dependence of the friction on the surface texture of the cylinder wall, due to a different print angle. It was not possible to draw a valid conclusion as the difference in cylinder diameter was larger than the layer thickness (0.085 mm versus 0.025 mm), an indicator for the order of magnitude of the surface texture. Finally, when operating at high pressures, leakage through the piston O-ring seal was observed and has not been prevented. This speaks to the general issue of geometrical accuracy in 3D printing hydraulic cylinders. The entire hand with four articulating fingers and seven actuators, can be assembled in 42 steps (21 steps for placing and securing the springs). This makes the prosthesis widely accessible as it can be fabricated through 3D printing and assembled with a few basic tools, without requiring any training. This study has proven the feasibility of small scale hydraulic actuation systems that are fabricated through additive manufacturing. Controlling friction and leakage remains a serious concern due to the geometrical accuracy of 3D printing. However, by applying the actuation system in a wearable device, it was shown that it can compete with similar conventional devices. Recommendations for subsequent research include increasing the effectiveness of the seal and determining the scalability of 3D printed hydrailic cylinders. Future possibilities are increased customization and reduced fabrication cost of hydraulically actuated mechanical systems.

A

Appendix A: Assembly

Table A.1: Total number of parts of the entire prosthesis

	Number of parts
Palm	1
Phalanxes	7
Axles	15
Circlips	30
Springs	14
Cylinders	7
Pistons	7
O-rings	7
Tube connectors	7
Total	95

Table A.2: Total number of assembly steps to assemble the hand.

	Assemly steps
Assemble joints	7
Place and lock springs	21
Connect tubes to actuators	7
Place actuators in mechanism	7
Total	42

B

Appendix B: Other Results

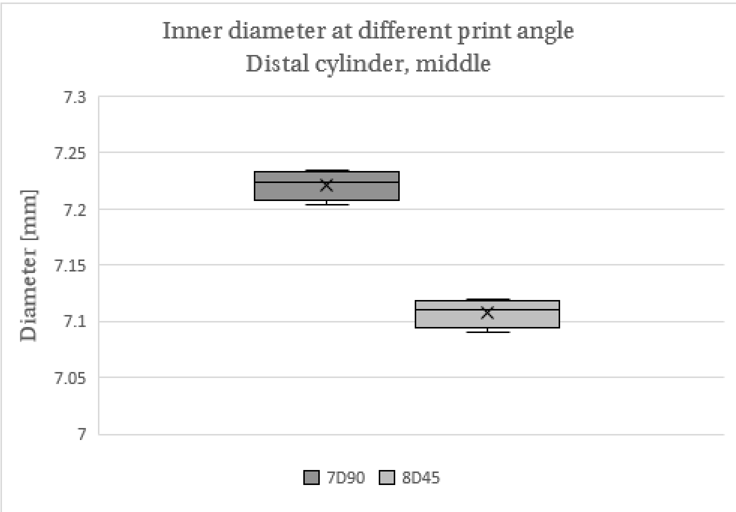

Figure B.1: Measured D_{in} of two distal cylinders. Both are printed at a different angle from the build plate. The measurement was performed halfway down the cylinder.

C

Appendix C: Printer specifications

Ultimaker 3 series specifications

Printer and printing properties	Technology	Fused filament fabrication (FFF)	
	Print head	Dual extrusion print head with a unique auto-nozzle lifting system and swappable print cores	
	Build volume (XYZ)	**Ultimaker 3** Single extrusion: 215 x 215 x 200 mm (8.5 x 8.5 x 7.9 in) Dual extrusion: 197 x 215 x 200 mm (7.8 x 8.5 x 7.9 in)	**Ultimaker 3 Extended** Single extrusion: 215 x 215 x 300 mm (8.5 x 8.5 x 11.8 in) Dual extrusion: 197 x 215 x 300 mm (7.8 x 8.5 x 11.8 in)
	Layer resolution	0.25 mm nozzle: 150 - 60 micron 0.4 mm nozzle: 200 - 20 micron 0.8 mm nozzle: 600 - 20 micron	
	XYZ resolution	12.5, 12.5, 2.5 micron	
	Build speed	< 24 mm^3/s	
	Build plate	Heated glass build plate (20 - 100 °C)	
	Nozzle diameter	0.4 mm (included) 0.25 mm, 0.8 mm (sold seperately)	
	Operating sound	< 50 dBA	
	Connectivity	Wi-Fi, LAN, USB port	
Physical dimensions	Dimensions (with Bowden tubes and spool holder)	**Ultimaker 3** 342 x 505 x 588 mm (13.5 x 19.9 x 23.1 in)	**Ultimaker 3 Extended** 342 x 505 x 688 mm (13.5 x 19.9 x 27.1 in)
	Net weight	**Ultimaker 3** 10.6 kg (23.4 lbs)	**Ultimaker 3 Extended** 11.3 kg (24.9 lbs)
Software	Supplied software	Ultimaker Cura, our free print preparation software Ultimaker Connect, our free printer management solution Ultimaker Cloud, enables remote printing	
	Supported OS	Windows, MacOS, Linux	

Figure C.1: Specifications of the printer that was used for the parts that were printed using Fused Deposition Modeling (FDM).

Technical Specifications

PRINTER

Price	
Dimensions	35 × 33 × 52 cm 13.5 × 13 × 20.5 in
Weight	13 kg / 28.5 lbs
Operating Temperature	Autoheats to 35° C or 95° F Self-heating Resin Tank
Power Requirements	100–240 V 1.5 A 50/60 Hz 65 W
Laser Specifications	EN 60825-1:2007 certified Class 1 laser product 405 nm violet laser 250 mW laser
Connectivity	Wi-Fi, Ethernet, and USB
Printer Control	Interactive touch screen

PREFORM SOFTWARE

System Requirements	Windows 7 and up Mac OS X 10.7 and up
File Type	.STL or .OBJ

PRINTING PROPERTIES

Technology	Stereolithography (SLA)
Peel Mechanism	Sliding peel process with wiper
Resin Fill System	Automated cartridge system
Build Volume	145 × 145 × 175 mm 5.7 × 5.7 × 6.9 in
Layer Thickness (Axis Resolution)	25, 50, 100, 200 microns 0.001, 0.002, 0.004, 0.008 in.
Laser Spot Size (FWHM)	140 microns 0.0055 inches
Supports	Auto-generated Easily removable

FINISHING KIT

Includes

- Finishing tray
- Scraper
- Pre and post-rinse tubs
- Rinse basket
- Squeeze bottle
- Flush cutters
- Tweezers
- Disposable Nitrile gloves
- Removal tool
- Removal jig

Figure C.2: Specifications of the printer that was used for the parts that were printed using Stereolithography (SLA).

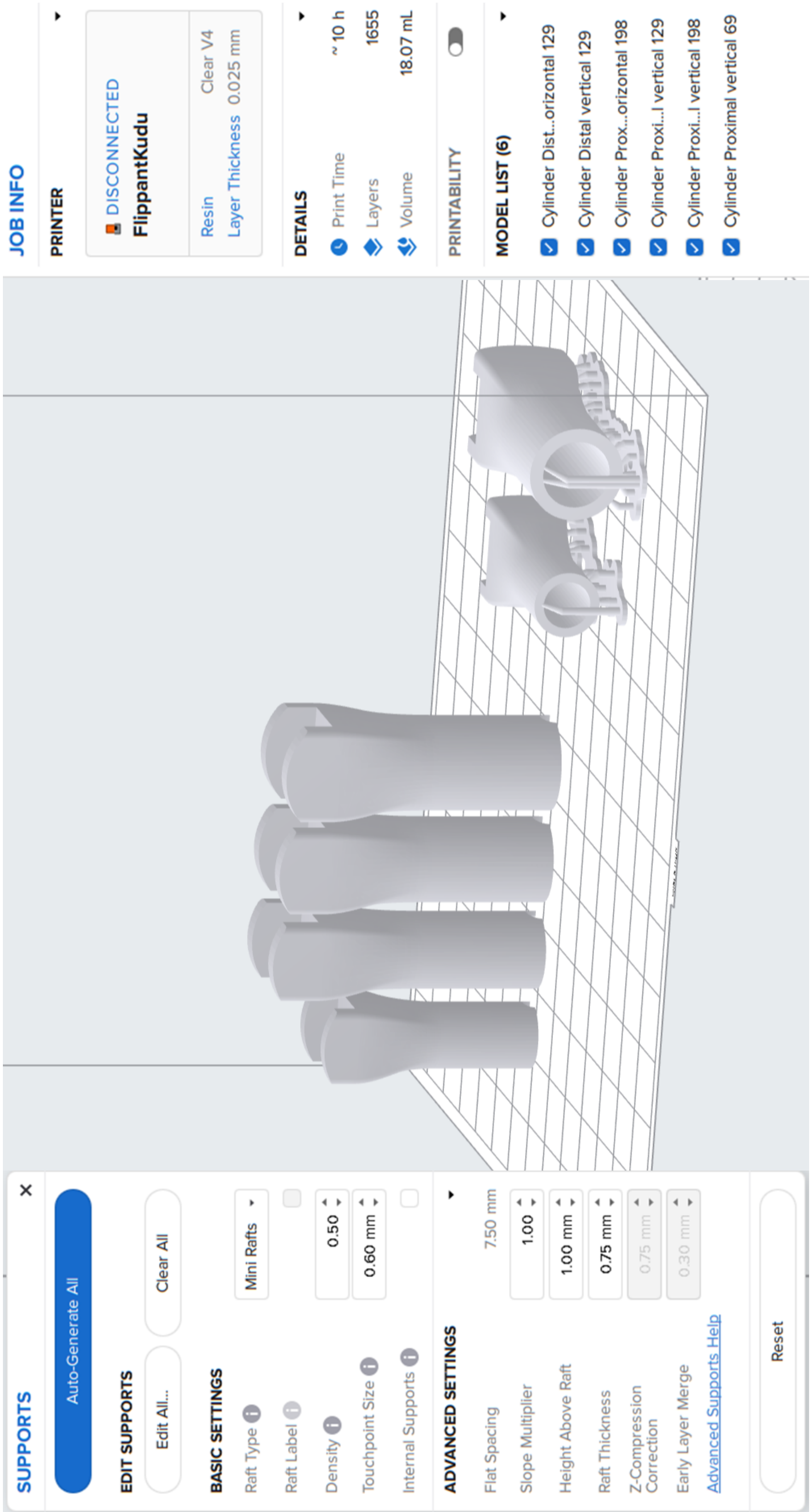

Figure C.3: Screenshot of setting up the Form 2 SLA printer. Note: The two cylinders on the right were used to test if printing at 0 degrees with respect to the build plate was possible. This led to cylinders that were not fully round due to leftover resin in the cylinder.

D

Appendix D: Detailed Design

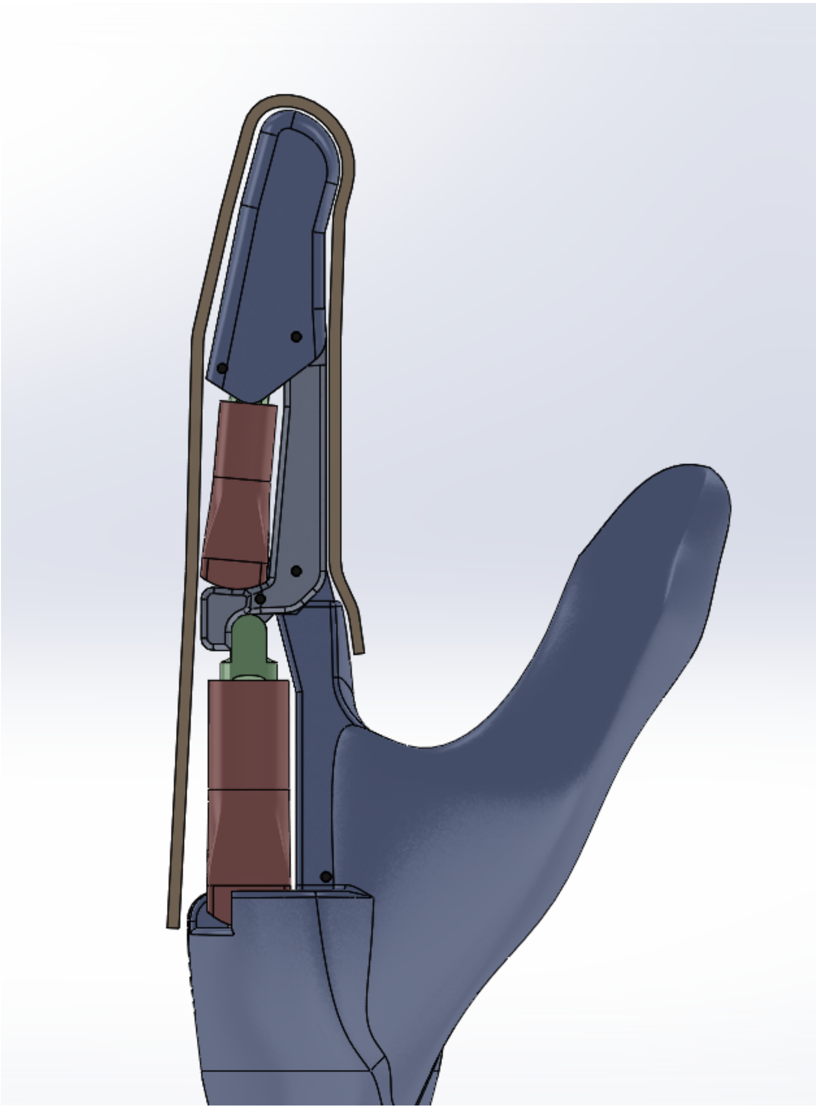

Figure D.1: Side view of the designed index finger withing the glove. A cutout of the glove is portrayed that is consistent with the dimensions as described by the manufacturer (101L XL1Male glove, Regal Prosthetics LTD.).

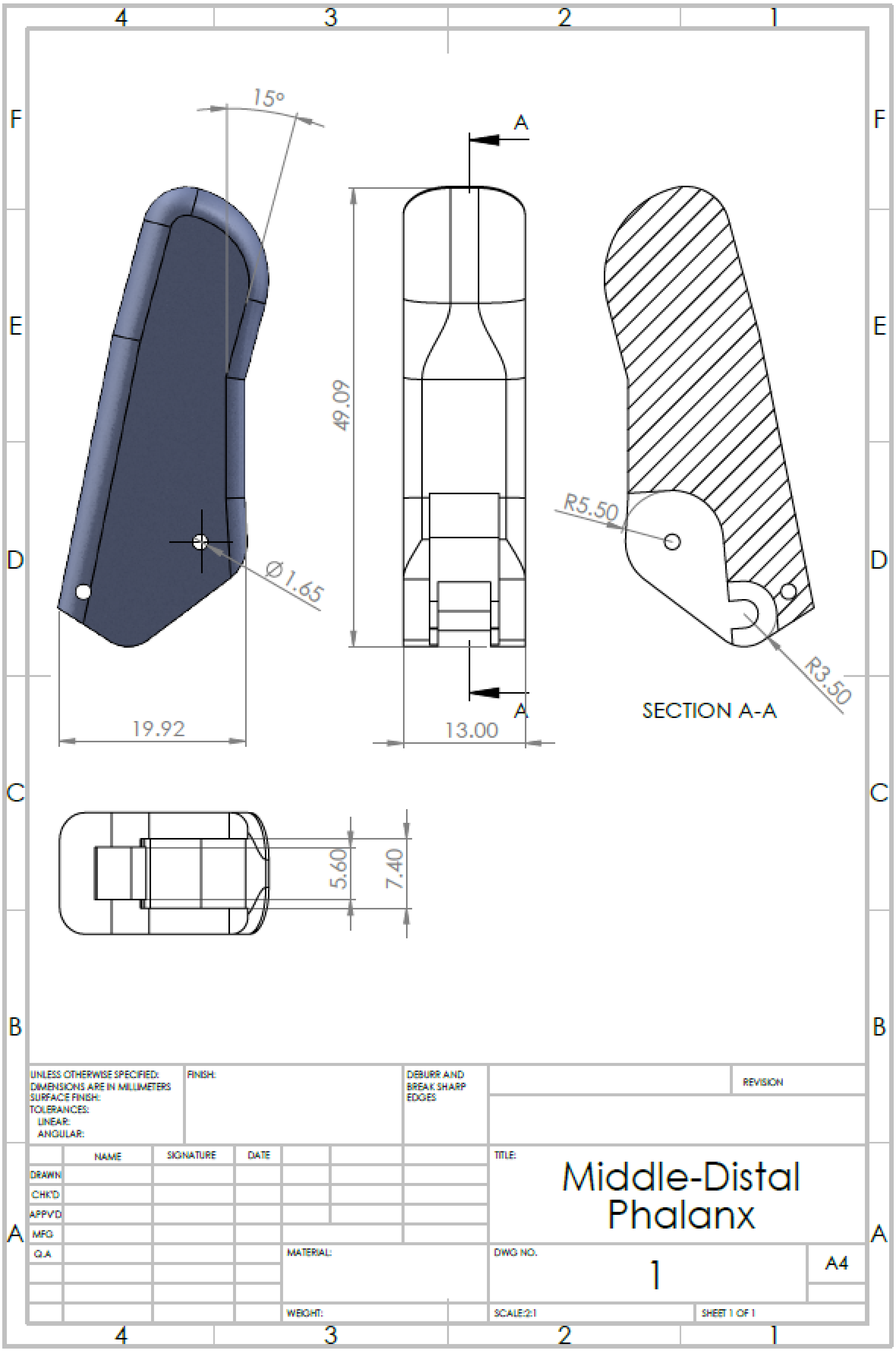

Figure D.2: Technical drawing of the middle-distal phalanx.

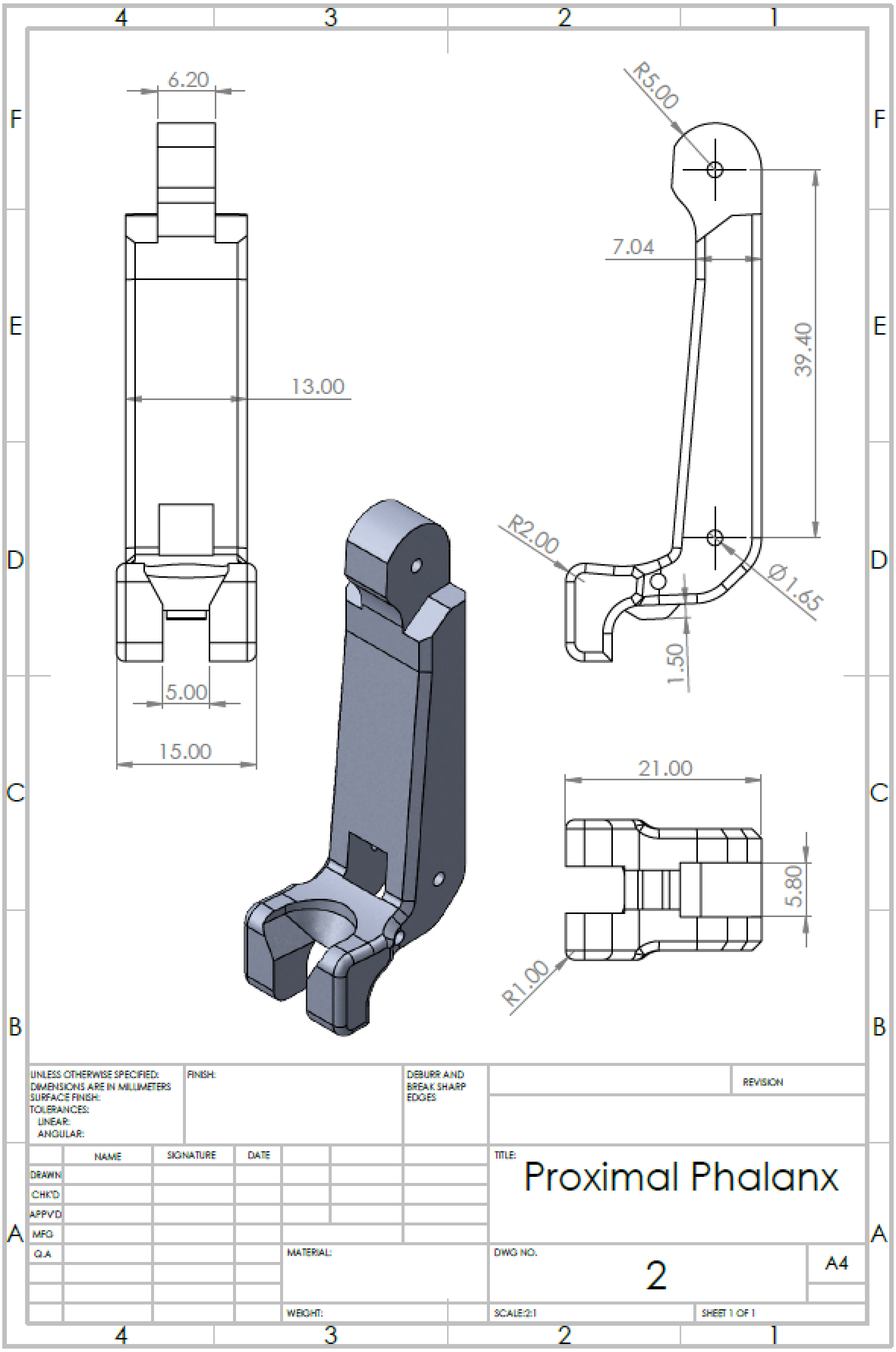

Figure D.3: Technical drawing of the proximal phalanx.

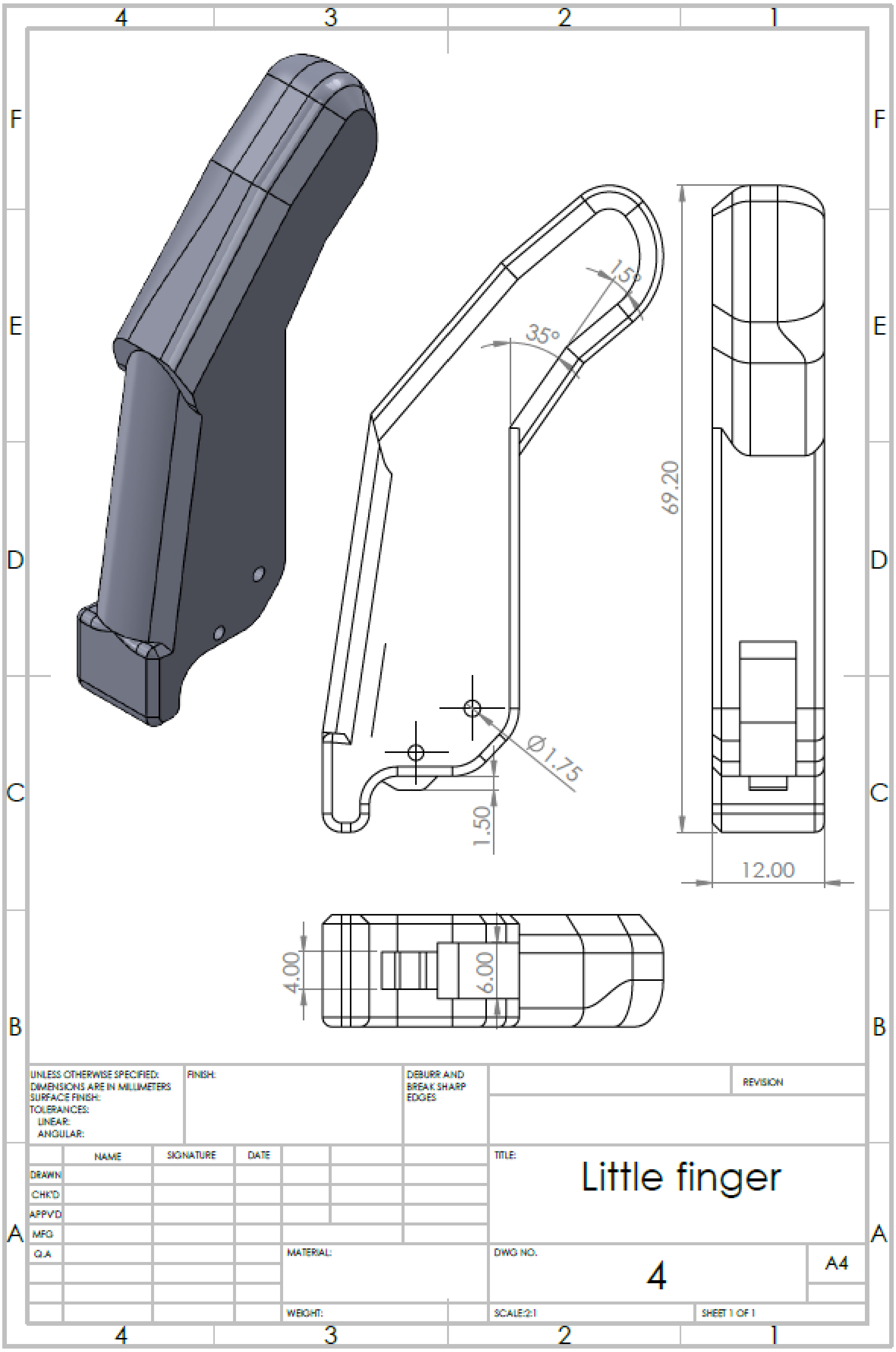

Figure D.4: Technical drawing of the little finger.

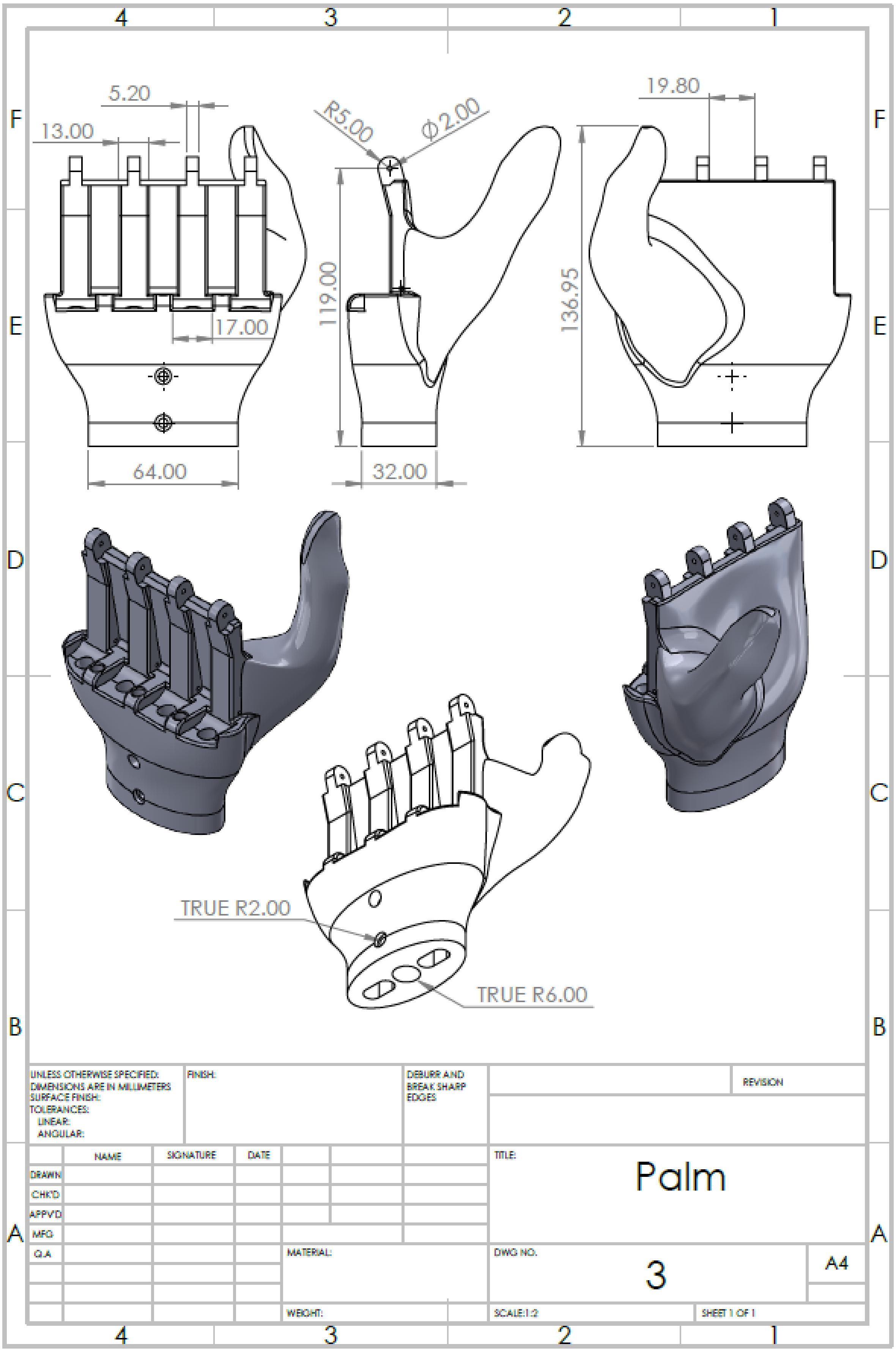

Figure D.5: Technical drawing of the palm. The scale is half of that of the other technical drawings.

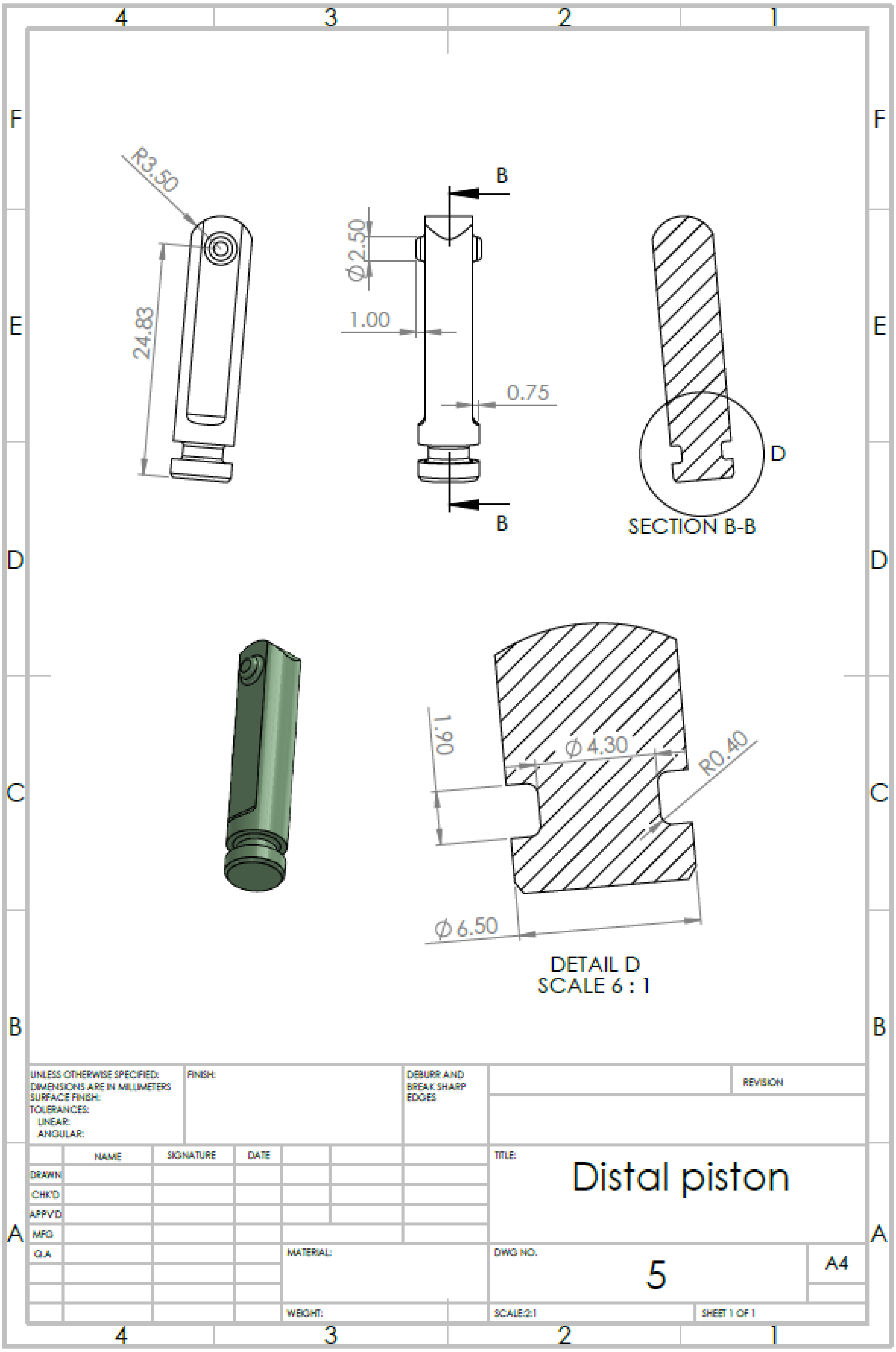

Figure D.6: Technical drawing of the distal piston.

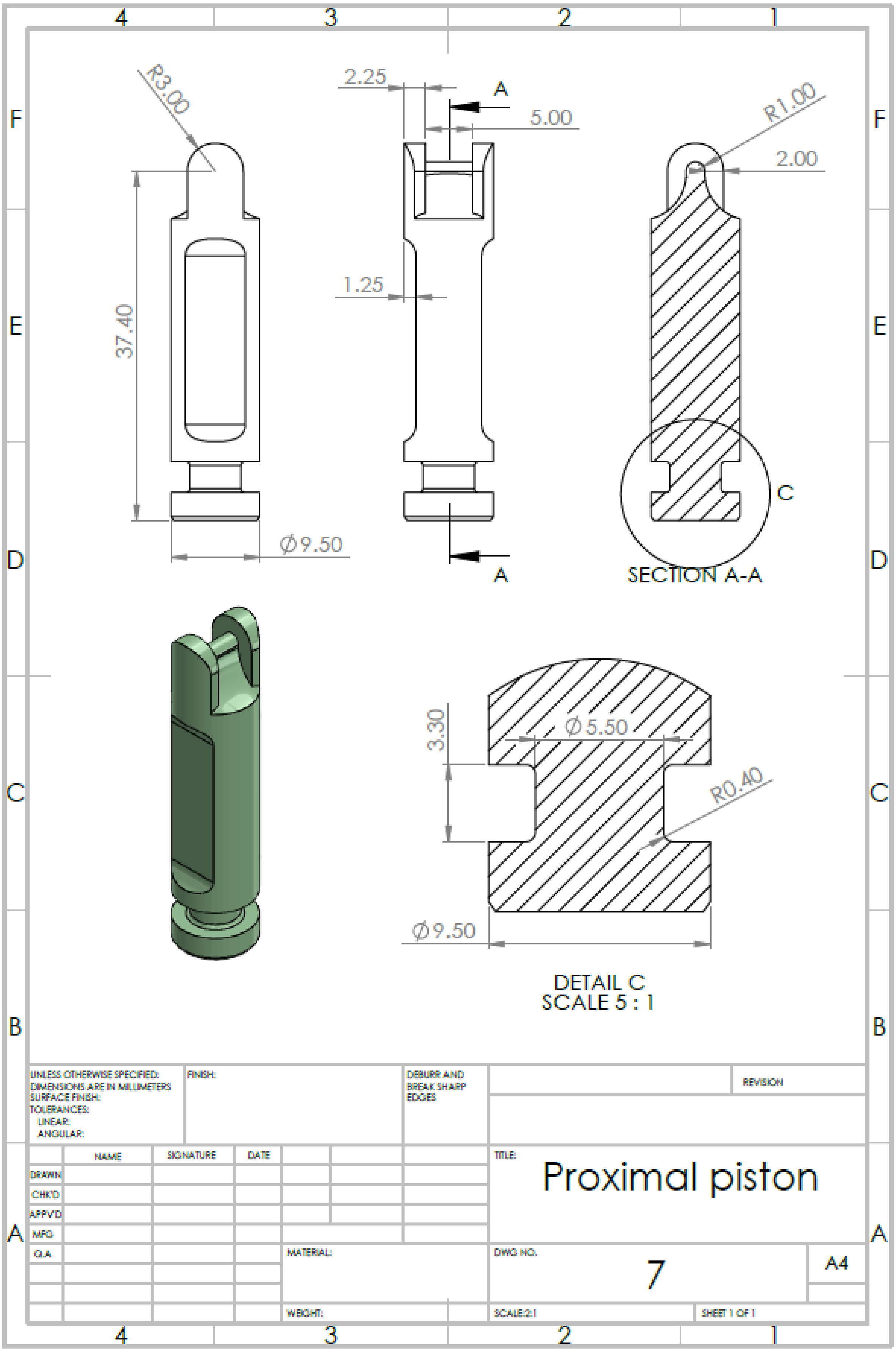

Figure D.7: Technical drawing of the proximal piston.

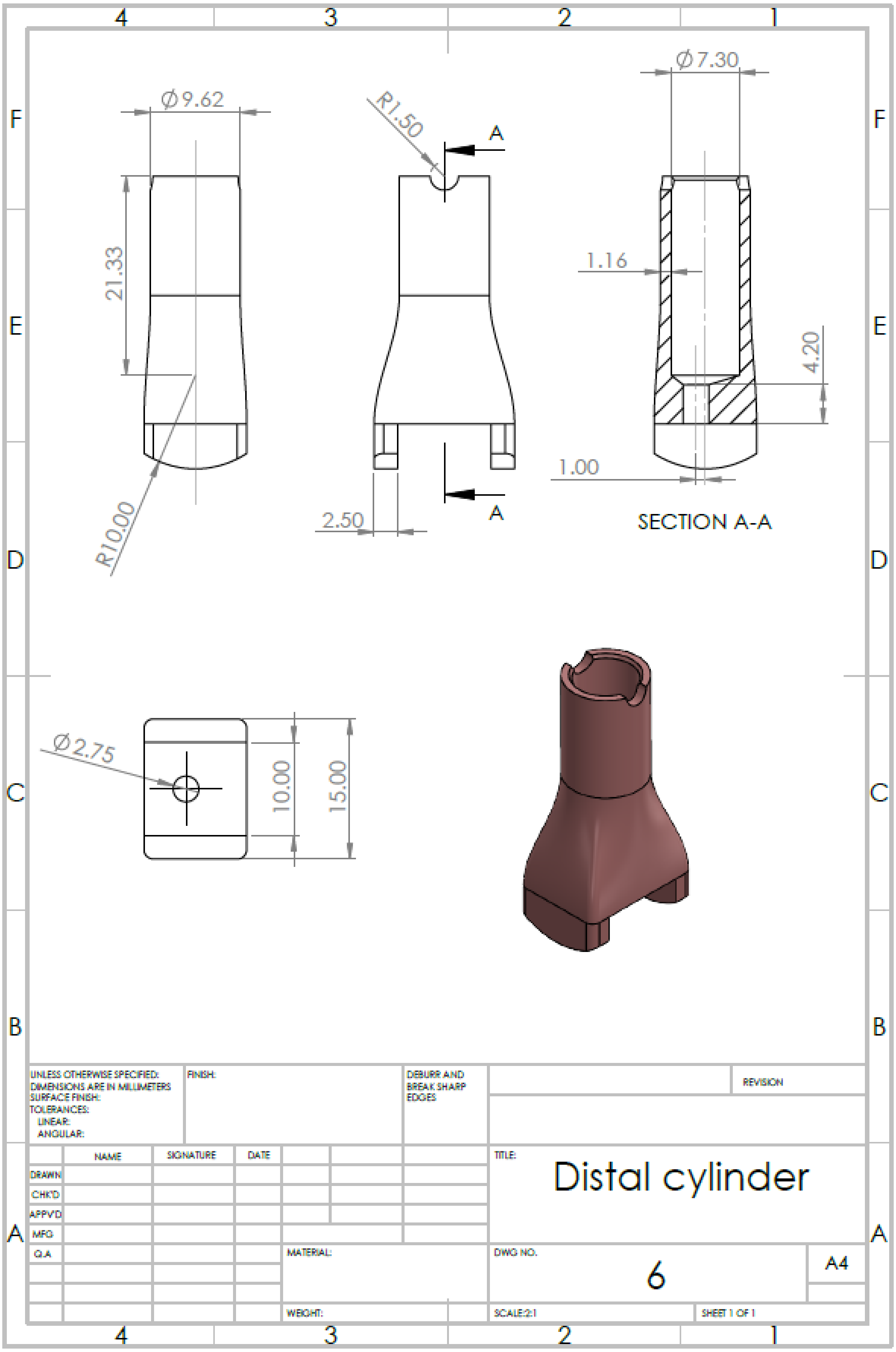

Figure D.8: Technical drawing of the distal cylinder.

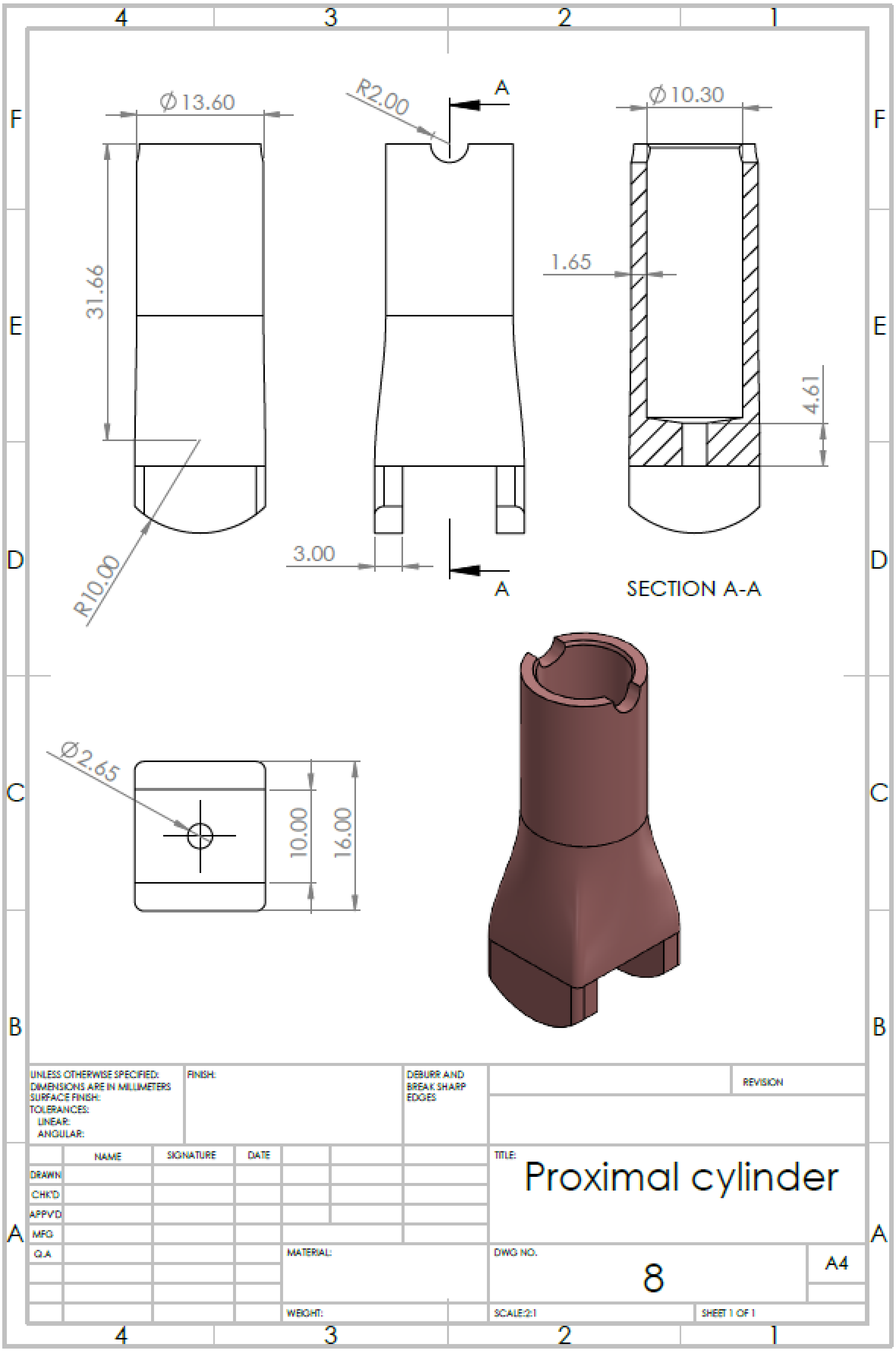

Figure D.9: Technical drawing of the proximal cylinder

Bibliography

[1] 123-3D.nl. 123-3D Filament zwart 1,75 mm PLA 1 kg (Jupiter serie). URL https://www.123-3d.nl/123-3D-Filament-zwart-1-75-mm-PLA-1-kg-Jupiter-serie-i1800-t7316.html?mkwid=sAj30GflU_dc%7Cpcrid%7C445479947650%7Cpkw%7C%7Cpmt%7C%7Cslid%7C%7Cprid%7CPF_DFP11000_8718237049205_&pgrid=101846517005&ptaid=pla-928234287019&gclid=Cj0KCQjwx.

[2] Advanced Technology Products. PTFE04MANA (4mm x 2.5mm x 100 PTFE Tubing). URL https://www.atp4pneumatics.com/product/ptfe04mana/.

[3] Liseli Baich, Guha Manogharan, and Hazel Marie. Study of infill print design on production cost-time of 3D printed ABS parts. *International Journal of Rapid Manufacturing*, 5(3/4):308, 2015. ISSN 1757-8817. doi: 10.1504/ijrapidm.2015.074809.

[4] G. I. Bain, N. Polites, B. G. Higgs, R. J. Heptinstall, and A. M. McGrath. The functional range of motion of the finger joints. *Journal of Hand Surgery: European Volume*, 40(4):406–411, 2015. ISSN 20436289. doi: 10.1177/1753193414533754.

[5] Bennett Berger. What Infill Settings Should I Use For My FDM 3D Print?, 2018. URL https://www.sd3d.com/infill-settings-fdm-3d-print/.

[6] Elaine Biddiss and Tom Chau. Upper-limb prosthetics: Critical factors in device abandonment. *American Journal of Physical Medicine and Rehabilitation*, 86(12):977–987, 2007. ISSN 08949115. doi: 10.1097/PHM.0b013e3181587f6c.

[7] Elaine Biddiss, Dorcas Beaton, and Tom Chau. Consumer design priorities for upper limb prosthetics. *Disability and Rehabilitation: Assistive Technology*, 2(6):346–357, 2007. ISSN 17483107. doi: 10.1080/17483100701714733.

[8] Brian L. Boland, Sheng Xu, Bradford Wood, and Zion Tsz Ho Tse. Pneumatic piston stepper motor: An enabler for MRI-guided robotic interventions. In *Frontiers in Biomedical Devices, BIOMED - 2018 Design of Medical Devices Conference, DMD 2018*. American Society of Mechanical Engineers (ASME), 2018. doi: 10.1115/DMD2018-6890.

[9] Alkianos Bournias Varotsis. Introduction to FDM 3D printing, . URL https://www.3dhubs.com/knowledge-base/introduction-sla-3d-printing/.

[10] Alkianos Bournias Varotsis. Introduction to SLA 3D printing, . URL https://www.3dhubs.com/knowledge-base/introduction-sla-3d-printing/.

[11] D. R. Broome, B. L. Davies, and M. Lord. A total hydraulically powered prosthetic arm system. *Engineering in Medicine*, 3(2):8–14, 1974. ISSN 00462039. doi: 10.1243/EMED{_}JOUR{_}1974{_}003{_}014{_}02.

[12] Brush Wellman Inc. Cantilever Beams Part 1 - Beam Stiffness. (20), 2010.

[13] Alexander Buryanov and Viktor Kotiuk. Proportions of Hand Segments. *International Journal of Morphology*, 28(3):755–758, 2010. ISSN 0717-9502. doi: 10.4067/s0717-95022010000300015.

[14] Mike Clark. The 3 Key Aspects of ASME's BPV Code Material Standards, 2018. URL https://info.thinkcei.com/think-tank/asme-standards.

[15] Conrad Electronic. LiPo accupack 11.1 V 1300 mAh. URL https://www.conrad.nl/p/lipo-accupack-111-v-1300-mah-aantal-cellen-3-1344131.

[16] Jan c. Cool. *Werktuigbouwkundge Systemen*. VssD, 3rd editio edition, 2011. ISBN 978-90-407-2451-0.

[17] Juan Sebastian Cuellar, Gerwin Smit, Paul Breedveld, Amir Abbas Zadpoor, and Dick Plettenburg. Functional evaluation of a non-assembly 3D-printed hand prosthesis. *Proceedings of the Institution of Mechanical Engineers, Part H: Journal of Engineering in Medicine*, 233(11):1122–1131, 2018. ISSN 20413033. doi: 10.1177/0954411919874523.

[18] Michaël De Volder and Dominiek Reynaerts. Pneumatic and hydraulic microactuators: A review. *Journal of Micromechanics and Microengineering*, 20(4), 2010. ISSN 09601317. doi: 10.1088/0960-1317/20/4/043001.

[19] William Durfee, Jicheng Xia, and Elizabeth Hsiao-Wecksler. Tiny hydraulics for powered orthotics. *IEEE International Conference on Rehabilitation Robotics*, (1), 2011. ISSN 19457901. doi: 10.1109/ICORR.2011.5975473.

[20] Engineering-abc. Thread Stripping Strenght Calculator. URL `https://www.tribology-abc.com/calculators/e3_6f.htm`.

[21] Engineering ToolBox. Young's Modulus - Tensile and Yield Strength for common Materials. 2003. URL `https://www.engineeringtoolbox.com/young-modulus-d_417.html`.

[22] Engineering ToolBox. Factors of Safety, 2010. URL `https://www.engineeringtoolbox.com/factors-safety-fos-d_1624.html`.

[23] Engineers Edge. Fastener Threaded Shear Area Equation and Calculator ISO 898. URL `https://www.engineersedge.com/thread_strength/thread_bolt_stress_area_iso.htm`.

[24] Epec Engineering Technologies. BATTERY CELL COMPARISON. URL `https://www.epectec.com/batteries/cell-comparison.html`.

[25] Eriks. Sealing Elements - Technical Handbook O-rings. *Eriks*, pages 1–255, 2013. URL `http://o-ring.info/en/o-ring/Oring-Handbook/ERIKS_SealingElements_TechnicalHandbook_O-rings.pdf`.

[26] EuroRC. Differences Between NiMH and LiPo Batteries. URL `https://www.eurorc.com/page/69/differences-between-nimh-and-lipo-batteries`.

[27] Formlabs. Form 2 3D Printer, . URL `https://formlabs.com/3d-printers/form-2/`.

[28] Formlabs. Clear Resin 1 L, . URL `https://formlabs.com/store/clear-resin/`.

[29] Formlabs. 3D Printing Technology Comparison: FDM vs. SLA vs. SLS, . URL `https://formlabs.com/blog/fdm-vs-sla-vs-sls-how-to-choose-the-right-3d-printing-technology/`.

[30] Formlabs. Material Properties Flexible Photopolymer Resin for Form 1+ and Form 2. pages 3–5, 2016.

[31] Formslab. Density engineering resin, 2019. URL `https://forum.formlabs.com/t/density-engineering-resin/24998`.

[32] Emma Frosina, Adolfo Senatore, and Manuel Rigosi. Study of a high-pressure external gear pump with a computational fluid dynamic modeling approach. *Energies*, 10(8), 2017. ISSN 19961073. doi: 10.3390/en10081113.

[33] Jahan Zeb Gul, Memoon Sajid, Muhammad Muqeet Rehman, Ghayas Uddin Siddiqui, Imran Shah, Kyung Hwan Kim, Jae Wook Lee, and Kyung Hyun Choi. 3D printing for soft robotics–a review. *Science and Technology of Advanced Materials*, 19(1):243–262, 2018. ISSN 18785514. doi: 10.1080/14686996.2018.1431862. URL `http://doi.org/10.1080/14686996.2018.1431862`.

[34] Hobby King. Aerostar RVS 40A Electronic Speed Controller w/Reverse Function 3A BEC (2~4S). URL `https://hobbyking.com/en_us/aerostar-rvs-40a-electronic-speed-controller-w-reverse-function-html?___store=en_us`.

[35] IGEM. Comparison of typical 3D printing materials. page 7, 2016. URL `http://2015.igem.org/wiki/images/2/24/CamJIC-Specs-Strength.pdf`.

[36] Helen M.A. Ingoe, Jonathan F. O'Hare, and Alan Middleton. A Functional Angle of Up to 35° at the Distal Interphalangeal Joint Can Be Achieved with Headless Compression Screw Fusion. *The journal of hand surgery Asian-Pacific volume*, 23(3):377–381, 2018. ISSN 24248363. doi: 10.1142/S2424835518500406.

[37] Filip Jelínek, Ewout A. Arkenbout, Paul W.J. Henselmans, Rob Pessers, and Paul Breedveld. Classification of joints used in steerable instruments for minimally invasive surgery. *Journal of Medical Devices, Transactions of the ASME*, 8(3):3–4, 2014. ISSN 1932619X. doi: 10.1115/1.4027035.

[38] Hiroshi Kaminaga, Satoshi Otsuki, and Yoshihiko Nakamura. Development of high-power and back-drivable linear electro-hydrostatic actuator. *IEEE-RAS International Conference on Humanoid Robots*, 2015-Febru:973–978, 2015. ISSN 21640580. doi: 10.1109/HUMANOIDS.2014.7041481.

[39] A Kargov, C Pylatiuk, R Oberle, H Klosek, T Werner, W Roessler, and S Schulz. Development of a Multifunctional Cosmetic Prosthetic Hand. 00(c):550–553, 2007.

[40] Artem Kargov, Christian Pylatiuk, Jan Martin, Stefan Schulz, and Leonhard Döderlein. A comparison of the grip force distribution in natural hands and in prosthetic hands. *Disability and Rehabilitation*, 26 (12):705–711, 2004. ISSN 09638288. doi: 10.1080/09638280410001704278.

[41] Tianyi Ko, Hiroshi Kaminaga, and Yoshihiko Nakamura. Underactuated four-fingered hand with five electro hydrostatic actuators in cluster. *Proceedings - IEEE International Conference on Robotics and Automation*, pages 620–625, 2017. ISSN 10504729. doi: 10.1109/ICRA.2017.7989077.

[42] Gert Kragten, Frans Van der Helm, and Just Herder. Underactuated Robotic Hands for Grasping in Warehouses. *Automation in Warehouse Development*, pages 1–241, 2012. doi: 10.1007/978-0-85729-968-0.

[43] Gert A. Kragten, Frans C.T. Van Der Helm, and Just L. Herder. A planar geometric design approach for a large grasp range in underactuated hands. *Mechanism and Machine Theory*, 46(8):1121–1136, 2011. ISSN 0094114X. doi: 10.1016/j.mechmachtheory.2011.03.004.

[44] Jeremy Krause and Pranav Bhounsule. A 3D printed linear pneumatic actuator for position, force and impedance control. *Actuators*, 7(2), 5 2018. ISSN 20760825. doi: 10.3390/act7020024.

[45] John Peter Kuntz. *Rolling Link Mechanisms*. PhD thesis, Delft University of Technology, 1995.

[46] Magnus Landberg, Martin Hochwallner, and Petter Krus. NOVEL LINEAR HYDRAULIC ACTUATOR. pages 1–9, 2016.

[47] Soojun Lee and Yong-kwun Lee. Development of Micro Hydraulic Actuator for Force Assistive Wearable Robot. 2013.

[48] Magom HCR. Locking sleeve for connectors, . URL `https://www.magomhrc.com/en/for-3-mm-hose/228-locking-sleeve-for-connectors-3mm.html`.

[49] Magom HCR. Mini Hydraulic brushless pump M3 with motor, . URL `https://www.magomhrc.com/en/brushless-hydraulic-pump-without-tank/486-mini-hydraulic-brushless-pump-m3-with-motor.html`.

[50] Ion Martinez. Development of a 3D printed hydraulic piston-cylinder system ME-51032. Technical report, Delft University of Technology, 2019.

[51] Otto Bock HealthCare LP. Ottobock Bebionic User Guide. Technical report, Otto Bock HealthCare LP, 2018. URL `https://www.ottobock.ca/media/local-media/prosthetics/upper-limb/files/15667-bebionic-user-guide.pdf`.

[52] Parker. Parker Legris Technical Tubing & Hose. 2014.

[53] Parker Hannifin Corporation. *Parker O-Ring Handbook*. 2018.

[54] Dick H. Plettenburg. Basic requirements for upper extremity prostheses: The Wilmer approach. *Annual International Conference of the IEEE Engineering in Medicine and Biology - Proceedings*, 5(5):2276–2281, 1998. ISSN 05891019. doi: 10.1109/iembs.1998.744691.

[55] Christian Pylatiuk, Stefan Schulz, Artem Kargov, and Georg Bretthauer. Two multiarticulated hydraulic hand prostheses. *Artificial Organs*, 28(11):980–986, 2004. ISSN 0160564X. doi: 10.1111/j.1525-1594.2004.00014.x.

[56] Xiaolei Xiong Qicai Zhou, Jiong Zhao and Haiyan He. *Design of New Hydraulic Pushing Device*, volume 286. 2015. ISBN 978-3-662-44673-7. doi: 10.1007/978-3-662-44674-4. URL `http://www.scopus.com/inward/record.url?eid=2-s2.0-84921868332&partnerID=tZOtx3y1`.

[57] Regal Prosthetics LTD. Regal Silicone Prostheses Brochure. 2008.

[58] Linda Resnik, Frantzy Acluche, and Matthew Borgia. The DEKA hand: A multifunction prosthetic terminal device—patterns of grip usage at home. *Prosthetics and Orthotics International*, 42(4):446–454, 8 2018. ISSN 17461553. doi: 10.1177/0309364617728117.

[59] J. S. Saini, Luke Dowling, John Kennedy, and Daniel Trimble. Investigations of the mechanical properties on different print orientations in SLA 3D printed resin. *Proceedings of the Institution of Mechanical Engineers, Part C: Journal of Mechanical Engineering Science*, 234(11):2279–2293, 2020. ISSN 20412983. doi: 10.1177/0954406220904106.

[60] François Schmitt, Olivier Piccin, Laurent Barbé, and Bernard Bayle. Soft robots manufacturing: A review, 2018. ISSN 22969144.

[61] Brian Schneider. A Guide to Understanding LiPo Batteries. URL `https://rogershobbycenter.com/lipoguide`.

[62] Gerwin Smit and Dick H. Plettenburg. Comparison of mechanical properties of silicone and PVC (polyvinylchloride) cosmetic gloves for articulating hand prostheses. *Journal of Rehabilitation Research and Development*, 50(5):723–732, 2013. ISSN 07487711. doi: 10.1682/JRRD.2011.12.0238.

[63] Gerwin Smit, Dick H. Plettenburg, and Frans C.T. van der Helm. Design and evaluation of two different finger concepts for body-powered prosthetic hand. *Journal of Rehabilitation Research and Development*, 50(9):1253–1266, 2013. ISSN 07487711. doi: 10.1682/JRRD.2012.12.0223.

[64] Gerwin Smit, Dick H. Plettenburg, and Frans C.T. Van Der Helm. The lightweight Delft Cylinder hand: First multi-articulating hand that meets the basic user requirements. *IEEE Transactions on Neural Systems and Rehabilitation Engineering*, 23(3):431–440, 2015. ISSN 15344320. doi: 10.1109/TNSRE.2014.2342158.

[65] Luigi Solazzi. Design and experimental tests on hydraulic actuator made of composite material. *Composite Structures*, 232(October 2019):111544, 2020. ISSN 02638223. doi: 10.1016/j.compstruct.2019.111544. URL `https://doi.org/10.1016/j.compstruct.2019.111544`.

[66] Top-Gun RC Store. Mini Hydraulische Olie Pomp Met Borstelloze Motor Voor 1/12 Rc Graafmachine Bulldozer Trailer Auto Onderdelen. URL `https://nl.aliexpress.com/item/4000643654854.html?spm=a2g0o.detail.1000014.11.130c7925cbG8Ol&gps-id=pcDetailBottomMoreOtherSeller&scm=1007.14976.157518.0&scm_id=1007.14976.157518.0&scm-url=1007.14976.157518.0&pvid=f7d4af8a-246a-48e1-a9e6-7efff6c36a8e&_t=g`.

[67] Piotr Stryczek. Design and research on a hydraulic cylinder with plastic components. In *Symposium on Fluid Power*, pages 1–8, 2016.

[68] Piotr Stryczek, Franciszek Przystupa, and Michal Banas. Research on series of hydraulic cylinders made of plastics. *2018 Global Fluid Power Society PhD Symposium (GFPS)*, pages 1–7, 2018.

[69] Jelle ten Kate, Gerwin Smit, and Paul Breedveld. 3D-printed upper limb prostheses: a review. *Disability and Rehabilitation: Assistive Technology*, 12(3):300–314, 2017. ISSN 17483115. doi: 10.1080/17483107.2016.1253117.

[70] Ultimaker B.V. Ultimaker Tough PLA. URL `https://ultimaker.com/nl/materials/tough-pla`.

[71] A. Van Beek. *Advanced Engineering Design*. 2015. ISBN ISBN 978 90 810406.

[72] Mark Van Dort. Creating a Miniature Hydraulic System to Power the Delft Cylinder Hand. 2019.

[73] Vincenzo Vullo. *Circular Cylinders and Pressure Vessels*. Springer International Publishing, 2014. ISBN 9783319006895. doi: DOI10.1007/978-3-319-00690-1.

[74] Jicheng Xia and William K. Durfee. Analysis of small-scale hydraulic actuation systems. *Journal of Mechanical Design, Transactions of the ASME*, 135(9):1–11, 2013. ISSN 10500472. doi: 10.1115/1.4024730.

[75] Jicheng Xia and William K. Durfee. Experimentally validated models of O-ring seals for tiny hydraulic cylinders. *ASME/BATH 2014 Symposium on Fluid Power and Motion Control, FPMC 2014*, (1):1–6, 2014. doi: 10.1115/FPMC2014-7825.

[76] Xue Yong, Junhong Yang, Jianzhong Shang, and Huixiang Xie. Design and optimization of a new kind of hydraulic cylinder for mobile robots. *Proceedings of the Institution of Mechanical Engineers, Part C: Journal of Mechanical Engineering Science*, 229(18):3459–3472, 2015. ISSN 20412983. doi: 10.1177/0954406215570106.

[77] Ye Zhang, Ken Mao, Simon Leigh, Akeel Shah, Zhiming Chao, and Guotao Ma. A parametric study of 3D printed polymer gears. *International Journal of Advanced Manufacturing Technology*, 107(11-12):4481–4492, 2020. ISSN 14333015. doi: 10.1007/s00170-020-05270-5.

[78] Chen Zheng, Peter Hehenberger, Julien Le Duigou, Matthieu Bricogne, and Benoît Eynard. Multidisciplinary design methodology for mechatronic systems based on interface model. *Research in Engineering Design*, 28(3):333–356, 2017. ISSN 14356066. doi: 10.1007/s00163-016-0243-2.